Chemical and Physical Determinants of Cell Migration

Chemical and Physical Determinants of Cell Migration

A dissertation presented

by

Harrison Valentine Prentice Mott

to

The Harvard School of Engineering and Applied Sciences

in partial fulfillment of the requirements

for the degree of

Doctor of Philosophy

in the subject of

Applied Physics

Harvard University

Cambridge, Massachusetts

April 2014

Dissertation Advisor: Professor Jagesh Shah Harrison Valentine Prentice Mott

Chemical and Physical Determinants of Cell Migration

Abstract

The phenomenon of directed cell motion in response to external directional cues has drawn significant interest for more than a century, with the first recorded observations of bacterial chemotaxis at the end of the 19th century. Furthermore, movies generated by David Rogers while at Vanderbilt University of a peripheral blood neutrophil tracking a bacterium are a staple of any college biology class to demonstrate the phenomenon of eukaryotic chemotaxis. In just the last decade, our understanding of the biochemical mechanisms underlying the process of directed eukaryotic cell migration. As a result, several generalized processes have been identified, connecting multiple phenomena from cancer metastasis to axon guidance. Making further sense of the complex biochemical pathways requires both quantitative mathematical models and fine control over the external cellular environment. To this end, microfluidics has proven extremely useful, allowing for precise quantification of both the external environment and the cellular response.

This dissertation presents new experimental studies of neutrophil migration in confining microchannels exposed to both physical and chemical directional cues. First, through the fabrication of asymmetric bifurcating microchannels, a novel form of cellular directional sensing is identified, namely the ability of asymmetric hydraulic resistances to direct cell motion. Furthermore, it is also shown that the directional cue from hydraulic resistance can overcome a strong chemical directional cue. Next, straight, confining microchannels are used to investigate the response of cells to various chemical

environments. Through the generation of static chemical concentration differences across a cell, it is shown that chemotactic signals of varying strength affect cell migration by modulating cellular persistence. It is subsequently shown that cells exposed to a uniform concentration of chemokine exhibit a strong directional bias of re-polarization. Through the dynamic variation of the uniform chemical environment, this is further identified as a directional memory capable of biasing the direction of polarization, the strength of which decays over time. Finally, molecular perturbations of cytoskeletal elements identify microtubules and moesin as components of this memory. The identification of these novel phenomena provides new information about how cells might incorporate and interpret directional cues from multiple sources to navigate complex environments.

Table of Contents

List of Figures:

Citations to Previous Published Work

Chapter 2, in its entirety was published under the following title:

> Prentice-Mott, H.V., et al., *Biased migration of confined neutrophil-like cells in asymmetric hydraulic environments.* Proc Natl Acad Sci USA, 2013. **110**(52): p. 21006-11.

Attributions:

Chapter 2:

> Measurements of beads in microchannels and subsequent STICS analysis and measurements of cell directional decisions in the 8x and 32x resistance channels was performed by Chi-Han Chang. Otherwise all reagent generation, experimental measurements and analysis were conducted by the author

Acknowledgements

I could not have completed this work without the support of many people that gave me the strength and courage to continue on when I was not sure I could.

First, to my best friend and the love of my life, my wife Swetlana Lobachova. Despite the demands of residency, you found the energy and patience to help me through some very difficult times. I cannot thank you enough for your invaluable support. To my wonderful daughter Samantha, thank you for reminding me what I am working for. Your love and joy brought light to even the darkest times.

To my parents, I want to thank you for the numerous lessons you provided while I was growing up, most importantly to have confidence in myself, that I can do anything I can put my mind to and to never give up on my dreams.

To the members of the Shah lab, your guidance and assistance was invaluable. Specifically, to Chi-Han, thank you for your help in both collecting and analyzing data of cells in the high resistance bifurcating channels. To Kelly, thank you for your patience and guidance in teaching me how to perform a Western Blot analysis. To Mikhail and Yinghua, thank you for your unending willingness to help me troubleshoot imaging issues. To Mike Manak, thank you for the numerous discussions of sports and the constant reminder that I was responsible for driving my project. To Peter, thank you for helping me to broaden my knowledge of molecular biology. To Megan, thank you for commiserating on the frustrations we experienced in our projects.

To both Dr. Morrison and Dr. Needleman, thank you for the wonderful opportunities to assist in teaching incredibly fascinating topics.

To members of the BioMEMS Resource Center, specifically, Dr. Mehmet Toner, thank you for the very generous use of the microfabrication facilities to generate my devices. To Bashar and A.J. your continuous assistance in accessing the cleanroom during off-hours was instrumental in me being able to effectively manufacture the microfluidic devices I used.

To the members of my thesis committee, thank you for your thoughtful advice and for helping me to focus my many interests and maintain reasonable goals to finish my Ph.D.

Finally, to my advisor Jagesh, thank you for the countless hours of discussion and brainstorming in your office, which was always open when you were in. I am also extremely grateful for your patience during the entire process. Most of all, your expectations of “great things” were a constant driving force to persevere through the numerous frustrations I encountered.

Chapter 1: Introduction

1.1 Directional Sensing in Eukaryotic Cells

The phenomenon of directional cellular responses as a result of external cues can be found in many instances throughout biology, from the reproduction of single cell organisms to the intricate interactions in tissue formation in complex organisms. There are several model systems that have been studied to understand the processes underlying directional cellular responses. What has been found is that these model systems generally respond to a directional cue by creating a highly polarized internal signaling cascade, which then drives processes such as protrusion formation or migration.

In one example, the budding yeast, *Saccharomyces cerevisiae,* produces a directed protrusion, called a schmoo, in the direction of a gradient of mating pheromone from the opposite mating type [1]. The powerful genetic tools available in this organism have allowed scientists to identify much of the signaling involved in the directional sensing of this pathway. Interestingly, the biochemical pathway of schmoo formation shares many of the features of the pathway regulating formation of a new bud during cell division, the location of which is determined by the location of the bud scar from the previous division [2-4]. Similarly, the single-cell amoeba of the slime mold *Dictyostelium discoideum* respond to the molecule cyclic adenosine monophosphate (cAMP), which is produced by these cells in response to an environment scarce in nutrients [5]. The result is that the cells begin to aggregate to form slugs and eventually a fruiting body, which then produces a spore, beginning the amoeba life cycle over.

Development of the nervous system in humans and other mammals is highly

dependent on accurate responses to directional cues. Proper functioning of the brain relies on the intricate connections formed between tens of billions of neurons. Meanwhile, the motor neurons at the base of the spinal cord extend axons stretching to the tip of the big toe, a distance of roughly 1 m. In both cases, the axons formed by the neurons are guided by a broad array of both attractive and repulsive molecules, such as neuregulins and semaphorins [6]. Meanwhile, fibroblasts respond to gradients of platelet-derived growth factor (PDGF) and migrate into the site of a wound [7]. Once there, these cells promote healing by breaking down the fibrous clot, reforming the extracellular matrix (ECM) to provide a scaffold for new cell growth and to contract the wound.

Another set of processes heavily dependent on directional cell migration is that of the immune system. Cells of the innate immune system, such as neutrophils, macrophages and dendritic cells respond to a variety of chemokines, produced by invading pathogens, damaged tissues or other components of the immune system, in order to migrate to the site of an infection and to locate and phagocytose pathogens. A subset of these cells then leave the infection and migrate to lymph nodes where they can interact with B- and T-cells of the acquired immune system to promote antibody production. In addition, the trafficking of both B- and T-cells of the acquired immune system is highly dependent on directional cues. Both cells are continuously recruited to lymph nodes for the purpose of antigen presentation. In order to ensure that both types of cells are able to sample antigens throughout the entire body, they also respond to chemorepulsive signals after residing for a period of time in the lymph nodes. Finally,

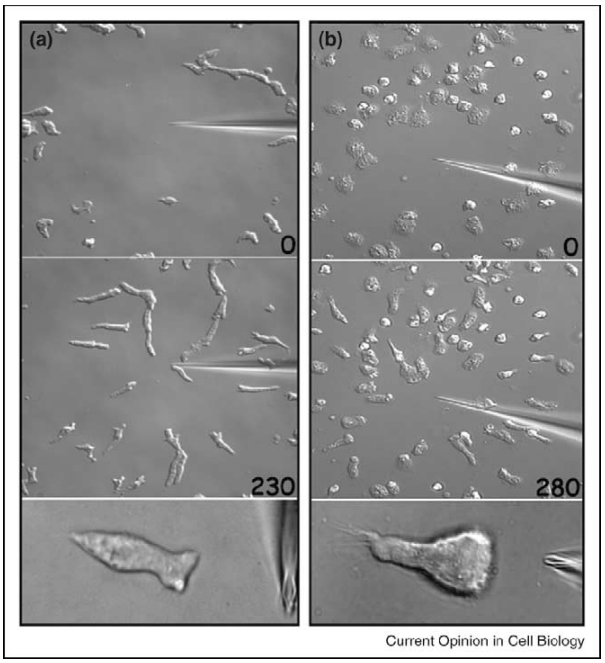

Figure 1-1 l Polarization of eukaryotic cells. **a**) Cells of the slime mold *Dictyostelium discoideum* responding to cAMP micropipette stimulation. Bottom panel shows polarized morphology of migrating cell. **b**) Peripheral blood neutrophils responding to micropipette stimulation with 1 μM fMLF. Bottom panel shows polarized morphology of migrating cell. Both sets of images demonstrate the large speed of these cells, which have moved a distance of several cell lengths over the course of just a few minutes. Reprinted, with permission from **[121]**.

chemotaxis is believed to play a large role in the process of cancer metastasis. There is growing evidence that metastatic cancer cells have somehow hijacked the chemotactic signaling pathway used by other cells to respond to gradients of molecules such as epithelial growth factor (EGF) [8] to migrate out of the tumor, into the blood stream and eventually into other tissues.

I am particularly interested in chemotaxis of highly motile cells, capable of speeds as high as 20 microns/minute [9, 10]. Two heavily studied models of eukaryotic chemotaxis are the slime mold amoeba *Dictyostelium discoideum* and the neutrophil and I will focus on the understanding of the chemotactic signaling processes discovered in these two system. However, as more is discovered regarding the directional responses of “slower” chemotactic cells, such as fibroblasts and neurons, it is becoming clear that many of the mechanisms of chemotaxis are conserved across these systems.

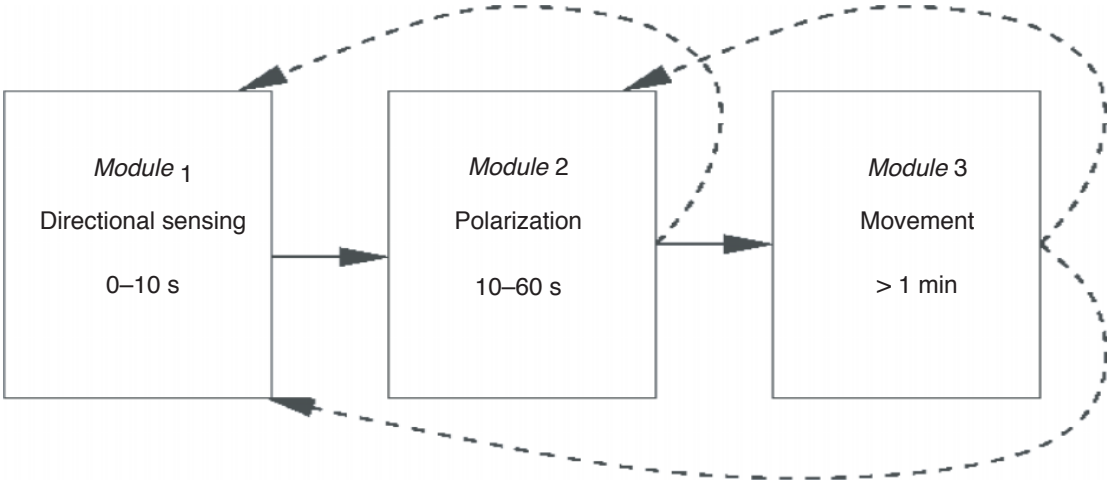

Figure 1-2 | Conceptual model of Chemotaxis. Diagram demonstrates conceptual separation of main processes in eukaryotic chemotaxis. Dashed lines demonstrate potential feedback from the separate modules. Reprinted, with permission from **[11]**

1.2 Chemotactic Signaling and Polarization

The chemotactic biochemical network is extremely complex and, for simplification, is often separated into three modules, namely directional sensing, polarization and motility [11]. The process of directional sensing is usually taken to be the ability of the cell to detect an external asymmetrical chemical signal and produce an asymmetric intracellular distribution of a set of signaling pathways. On the other hand, polarization is generally the process by which the cell generates distinct front and back domains. Given that directional sensing and polarization both result in an asymmetrical spatial distribution of signaling cascades, it is difficult to draw a distinct separation between the two modules. However, it is generally thought that the magnitude internal gradient resulting from purely directional sensing is comparable to that of the external gradient, while the processes involving polarization exhibit a highly amplified separation relative to the external gradient. Furthermore, an external gradient results in a strong coupling between the directional sensing and polarization modules. However, polarization can occur in the absences of an external gradient. Finally, motility refers to

the set of processes which, as a result of the developed polarization of the cell, drive the motion of the cell. At the molecular level, it is not clear where the demarcation between these different modules occur. I will focus primarily on our understanding of the processes of directional sensing and polarization and how it is understood that the two modules connect to each other.

1.2.1 Chemoattractant receptor signaling

As mentioned previously, the slime mold *Dictyostelium discoideum* responds to the chemoattractant cAMP. Meanwhile, neutrophils respond to a variety of signaling molecules. These molecules can generally be separated into two groups, namely molecules produced by a pathogen, or molecules produced by the host in response to the presence of a pathogen. Examples of the former include molecules such as lipopolysaccharide (LPS) or the formylated tripeptide, N-formyl-methionyl-leucyl-phenylalanine (fMLF), both of which are produced by bacteria. Examples of the latter include components of the complement pathway, such as C5a, leukotrienes, such as leukotriene B4 (LTB4) and various other chemokines, most notably CXCL8 (also referred to as IL-8). Despite the wide array of chemokines, chemotactic signaling almost exclusively occurs through the class of receptors known as G-protein coupled receptors (GPCRs). These receptors consist of a seven-transmembrane protein and an associated heterotrimeric G-protein. In the inactivated state, the G-protein consists of a G_α, G_β and G_γ subunit which binds guanosine diphosphate (GDP), and associates with the cytosolic carboxy-tail of the transmembrane receptor. When a ligand binds the receptor, it causes a conformational change in the transmembrane protein, which in turn promotes the guanine nucleotide exchange factor (GEF) activity of the G-protein,

resulting in an exchange of guanosine triphosphate (GTP) for GDP. This causes the G_α subunit to dissociate from the other subunits, allowing for downstream signaling of both G_α and $G_{\beta\gamma}$ subunits.

Genetic screens have identified 11 types of G_α and a single type of $G_{\beta\gamma}$ subunits in *Dictyostelium discoideum* [12-15]. Similarly, human cells also exhibit a wider variety of G_α subunits. In contrast, human cells contain several genes encoding for different types of both G_β and G_γ. It is believed that chemotactic GPCR signal transduction is predominantly through G_α subunit. As a result, this subunit has been more heavily studied and can be separated into four classes: G_s, $G_{i/o}$, $G_{q/11}$, and $G_{12/13}$, each with a different set of downstream effectors. It is believed that the dominant role for $G_{\beta\gamma}$ is to inhibit the G_α subunit, however there is evidence that $G_{\beta\gamma}$ also possesses downstream signaling capabilities [16, 17].

In 1999, Servant et al. used cells expressing a GFP-tagged version of the C5a receptor to visualize the distribution of receptors in polarized neutrophils. They found that even cells with a highly polarized morphology did not exhibit an enrichment of receptors at the leading edge [18]. This strongly suggested that the polarization exhibited by chemotaxing neutrophils is driven by polarization of the internal signaling network. Work done by Henry Bourne at the University of California-San Francisco (UCSF) identified two distinct signaling pathways, which are spatially separated during neutrophil chemotaxis. Bourne termed these two pathways “frontness” and “backness”. Much of the current understanding of chemotactic directional sensing and polarization is shaped by this framework [19].

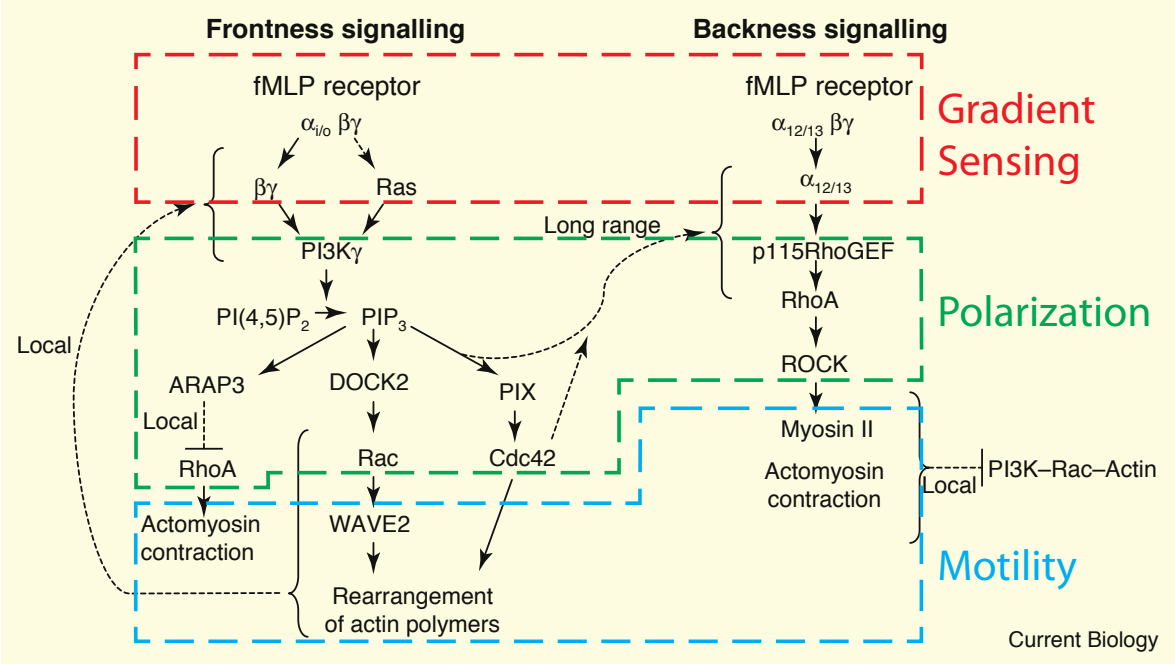

Figure 1-3 I Biochemical pathways in chemotaxis. Simplified diagram of primary biochemical signaling in both frontness and backness signaling pathways. The dashed outlines demonstrate potential separation of the identified pathways into the conceptual model in Figure 1-2. Reprinted, with permission from **[171]**.

1.2.2 "Frontness" in a chemotactic cell

It was found in *Dictyostelium discoideum* that the pleckstrin homology domains of the cytosolic regulator of adenylyl cyclase (CRAC) and AKT protein kinase (protein kinase B) tagged with GFP translocated to the leading edge in cells exposed to a chemoattractant gradient [20]. This response was not dependent on the ability of the cells to migrate, as cells treated with Latrunculin still produced an asymmetric distribution of the fluorescent probe. A similar response was shown by Weiner et al. in neutrophils using a PH-Akt-GFP probe [21]. The authors also showed that the polarized response was abolished when the cells were treated with toxin B from *Clostridium difficile*, which inactivates small GTPases through glycosylation, suggesting that the Rho-family GTPases, which include the Rac, Rho and CDC42 classes, play a strong role in regulating this response.

The pleckstrin homology domain of both proteins used in the studies above were known to have a strong affinity for the membrane phospholipid phosphoinositol-(3,4,5)-trisphosphate (PIP3) [22, 23], which is a product of the phosphoinoside 3-kinase (PI3K), which phosphorylates phosphoinositol-(4,5)-bisphosphate (PIP2). These results inspired a large body of to understand how PI3K is activated by GPCRs as well as the role that PI3K activity plays in determining the direction of cell migration [24-26]. From this work, it is now understood that PIP3 production occurs primarily via the activation of the PI3Kγ isoform in neutrophils. This isoform consists of two subunits, p101 generally thought to be a regulatory subunit and p110γ, the active subunit. The p101 has a membrane targeting domain [27]. In addition, when the complex is bound to the membrane, it exhibits a strong affinity for the membrane-anchored $G_{\beta\gamma}$ subunit of the heterotrimeric G-protein [28]. This interaction helps to stabilize PI3K recruitment to the membrane, where it can then be activated by the small G-protein, Ras, which is itself activated by $G_{\beta\gamma}$ [29, 30]. There is also some evidence that $G_{\beta\gamma}$ itself could activate PI3K [30].

Early on, it was thought that PI3K was an important piece of the cellular compass involved in directional sensing and driving the direction of polarization. Several studies have shown that cellular migration or other measures of polarization are not necessary to achieve a polarized distribution of PI3K activity. In addition, treatment of cells with PI3K inhibitors, such as wortmannin or LY29004, did result in a decreased production of PIP3. However, cells were still able to polarize and migrate, but with a significantly decreased ability orient and persistently migrate in both weak and strong chemotactic gradients. This was determined using assays that measure the number of cells reaching

a destination signaled by a gradient, as well as by tracing the trajectories of individual cells in established gradients. In the latter, cells exhibited trajectories that were significantly more random and less directionally persistent [25]. Despite this strong evidence, it is still not clear whether PI3K is the key regulator of the cellular compass. Studies have shown that a pathway involving phospholipase A2 (PLA2) acts in parallel with PI3K to regulate directionality in chemotactic cells [31, 32]. In addition, cells with impaired CDC42 activity are unable to respond properly to the presence of a gradient, despite no discernible effect on motility[33].

Downstream PIP3 signaling occurs via the recruitment of proteins containing PH domains. Two such molecules that have been identified are the activating guanosine-nucleotide exchange factors (GEFs), DOCK2 and PIXα for the small Rho family GTPases, Rac1 and CDC42, respectively [34, 35], both of which are key regulators of the actin polymerization machinery. Rac1 acts through the SCAR/WAVE2 complexes to activate the actin nucleator Arp2/3, which is believed to be the primary driver of actin nucleation at the leading edge of a chemotactic cell. Similarly, CDC42 activates the Wiskott-Aldrich Syndrome protein (WASp), which can also activate Arp2/3. Interestingly, both WAVE2 and WASp have been shown to be recruited to the membrane in a PIP3-dependent manner [36], potentially providing an increased level of sensitivity to the internal gradient of PIP3 concentration. Finally, recent work by Charras and colleagues has shown that formin-mediated actin polymerization is essential for the generation of leading edge protrusion in confined microchannels, while Arp2/3-mediated polymerization is dispensable [37]. Both Rac1 and CDC42 have been shown to also activate the formin mDia2 in a GTP-dependent manner.

Figure 1-3 shows the set of signaling pathways that have been identified and are believed to part of the “frontness” pathway. Given the complexity of this network, as well as the complicated spatial and temporal relationships between these proteins, there is debate about which parts of the pathway fit into which of the three modules discussed earlier. However, an appealing separation is shown in Figure 1-3 and is described by the following: 1) GPCR and $G_{\alpha}G_{\beta\gamma}$ dissociation constitute the gradient sensing module; 2) the polarization module encompasses the generation of internal gradients of PIP3 production and Rac1 and CDC42 activity; 3) the motility module encompasses the activation of acting regulators, such as WASp and WAVE and the ensuing actin polymerization.

The separation between the gradient sensing, polarization and motility modules is further complicated by the identification of several feedback loops involving Rho GTPases and actin filaments (F-actin). The first such study was performed by Weiner et al. [38], in which they were introduced exogenous PIP3 into the membrane of a cell. This resulted in the translocation of the PIP3 marker PH-Akt-GFP to the plasma membrane. The observed translocation could be abolished by treatment with a PI3K inhibitor, indicating the presence of PIP3 in the membrane can induce the further production of PIP3. Additionally, treatment with toxin B from *Clostridium difficile*, which inhibits Rac, Rho and CDC42 also effectively eliminated the observed translocation response. However, cells still translocated PH-Akt-GFP to the membrane in response to treatment with insulin, which has been shown to induce Rho-GTPase-independent recruitment of PH-Akt-GFP [21].

A second set of feedback loops involving Rac1 have been identified. First,Castro-

Castro et al. [39] showed that the actin binding protein coronin 1a forms an F-actin-dependent complex with the Rac1 GEF ArhGEF7, Pak1 and the Rho GDP dissociation inhibitor RhoGDIα, to promote the release of Rac1 from RhoGDIα, and thus subsequent activation of Rac1. Similarly, Klooster et al. [40, 41] have shown in fibroblasts that the Rac1 GEF, Tiam1, can interact with the Arp2/3 complex, linking the activation of Rac1 to F-actin polymerization.

Finally, Orchard et al. [42] through an impressive set of experiments identified an F-actin-dependent feedback loop involving CDC42 and the CDC42 GEF Map. This feedback resulted in bursts of F-actin polymerization, the location of which could be determined by localized nucleation of actin filaments and was also sufficient to explain the polarization of CDC42 in response to exposure to enteropathogenic *Escherichia coli*.

1.2.3 "Backness" in a chemotactic cell

The most striking evidence for a separate pathway regulating the signaling at the back of the cell came from a set of observations made by Xu et al. [19]. First, the authors showed that treatment with *Pertussis* toxin (PTX) did not lead to a decrease in activity of the Rho GTPase, RhoA, as measured by a RhoA-GTP pull-down assay. PTX treatment causes ADP-ribosylation of the α subunit of the $G_{\alpha i}$ class of heterotrimeric G-proteins [43, 44]. This modification prevents association between the GPCR and G_{α} subunit, and was shown to abrogate all chemotactic responses in neutrophils, including actin polymerization, PIP3 production and activation of Rac and CDC42 [17]. However, Xu et al. [19] observed that when stimulated by a micropipette gradient, cells treated with PTX formed a distinctive uropod-like structure at the edge of the cell closest to the

micropipette. Finally, expression of a GFP-tagged RhoA, showed that RhoA is excluded from pseudopods in polarized neutrophils. Similar results were shown through immunofluorescence staining of RhoA, which also showed that fMLF stimulation led to the recruitment of RhoA to a detergent resistant pool in the cell uropod. In addition, the expression of a dominant-negative version of the G_{12} and G_{13} versions of the G_{α} subunit mirrored the effects of the expression of a dominant-negative version of RhoA on the ability to properly localize F-actin polymerization. This led the authors to propose that fMLF stimulation leads to the polarized activation through the $G_{12/13}$ classes of G-proteins of RhoA to the trailing edge of the cell. Subsequent work performed by Wong et al. [45] using a FRET-based reporter of RhoA activity showed that indeed, RhoA activity is found predominantly the sides and rear of a polarized neutrophil, and can be observed only transiently and infrequently in regions of membrane ruffling, which is an early indicator of leading-edge development.

To date, all the effects of RhoA on chemotaxis have been shown to act through the Rho-associated protein kinase p160-ROCK. Xu et al. [19] treated cells with the p160-ROCK-specific kinase inhibitor and found that cells were unable to properly localize F-actin polymerization and produced multiple pseudopods in response to fMLF stimulation, similar to observations of cells expressing a dominant-negative RhoA mutant. One of the downstream effectors of p160-ROCK is the phosphoinositol phosphatase Phosphatase and tensin homolog (PTEN) [46]. PTEN acts in direct opposition to PI3K, dephosphorylating PIP3 to reform PIP2. In *Dictyostelium discoideum*, PTEN was shown to be excluded from the leading edge of polarized cells [47, 48]. Immunofluorescence in neutrophils has shown similar results [46], however

expression of GFP-tagged PTEN failed to reveal the same polarized localization [19]. Genetic knockout of PTEN in *Dictyostelium discoideum* results in decreased directional persistence during chemotactic migration, as evidenced by frequent directional changes [48]. Similarly, siRNA knockdown of PTEN in neutrophils produced equivalent behavior, which could be partially but reproducibly rescued by expression of wild-type PTEN [46]. It is unclear what precisely is the role of PTEN, but it likely serves to help indirectly accumulate PIP3 at the leading edge.

Another target of p160-ROCK is the non-muscle myosin Myosin II. p160-ROCK has been shown to phosphorylate Myosin Light Chain Kinase (MLCK) [49], which phosphorylates the Myosin Light Chain subunit of the Myosin II complex, a process that is necessary for the ATPase activity of Myosin II involved in the power stroke of the myosin head. In addition, p160-ROCK regulates the activity of Myosin Light Chain Phosphatase (MLCP), further promoting Myosin II activity [49]. Finally, it is important to note that not only is there differential regulation in the activity of Myosin II, but there is also a strong polarization in Myosin II itself. It is believed that the localization and assembly of Myosin II is regulated by phosphorylation and de-phosphorylation of Myosin Heavy Chain (MHC) by the Myosin Heavy Chain Kinase and Myosin Heavy Chain Phosphatase. How this regulation achieves the marked rearward localization of Myosin II is unclear. There is also conflicting evidence as to the role of Myosin II in chemotaxis. Cells treated with blebbistatin, an inhibitor of Myosin II ATPase activity, produced multiple sustained pseudopods in response to uniform fMLF treatment [19]. Genetic deletion of myosin in *Dictyostelium discoideum* cells produced similar results, in addition to resulting in an inability to migrate in highly confined environments [50].

Interestingly, the migration defect could be rescued by addition of myosin lacking any measurable motor function, suggesting that the actin cross-linking activity of myosin, but not the contractility, is necessary for efficient chemotaxis.

1.2.4 Communication between "frontness" and "backness" pathways

Despite much investigation into the details of the molecular signaling of both "frontness" and "backness" pathways, it is still not clearly understood how the two pathways are able to interact in order to produce the strong asymmetrical polarization observed in cells. Xu et al. [19] clearly showed that both pathways are required for proper localization of the other. Inhibiting the "frontness" pathway through PTX treatment resulted in activation of the "backness" pathway at the side of the cell exposed to a higher concentration of fMLF. Meanwhile, multiple inhibitions of the "backness" pathway elements resulted in cells that produced multiple pseudopods in a uniform concentration or cells that were unable to properly orient a pseudopod under gradient stimulation.

One potential mechanism of this observed mutual inhibition could be the interplay between PI3K and PTEN. Sequence analysis of PTEN shows an N-terminal domain that reportedly binds to PIP2 [51]. Thus, the conversion of PIP2 to PIP3 by PI3K at the leading edge could exclude PTEN, further augmenting existing PI3K feedback loops. In contrast, CDC42 has been shown to be able to recruit PTEN to the membrane of polarized cells treated with the p160-ROCK inhibitor Y27632 [46], which does not occur in untreated cells. CDC42 was also shown to be able to augment RhoA activity at the back of the cell [52]. These data suggest that the localization of RhoA activity is the predominant regulator of PTEN activity. In addition to regulating PTEN activity, RhoA

has also been shown to inhibit Rac activity via the Rac regulator ARHGAP22 [53]. Given that RhoA activity has been shown to exist primarily along the sides and posterior of polarized cells, this could explain how RhoA-ROCK signaling is able to restrict the “frontness” pathway to the leading edge.

It is noteworthy that the spatio-temporal observations of RhoA activity showed that RhoA was first activated in the cytoplasm within 30 seconds of uniform fMLF stimulation, but was not strongly localized to the sides and rear of the cell until between 1.5 and 3 minutes [45]. This suggests that RhoA activity may not play a role in the initial localization of F-actin polymerization and other “frontness” signaling, but rather acts to stabilize the polarization of the leading edge signaling.

The “frontness” pathway, in turn, plays a role in determining the localization of RhoA and other “backness” signaling. Rho-GTPase activating proteins (RhoGAPs) play a large role in regulating Rho activity by promoting the conversion of GTP to GDP, thus inactivating the small GTPase. Specifically, the RhoA GAP, ARAP3, contains a PIP3-binding, PH domain [54, 55]. In addition, PIP3 has been shown to play a role in regulating MHCK, which phosphorylates myosin heavy chain, promoting disassembly of myosin filaments. It has also been shown that polymerized F-actin can displace both RhoA and Myosin II. The mechanism underlying this interaction is unclear, but one proposal is that the cytoskeleton can play a role in the location of lipid rafts of certain compositions [56], to which several signaling proteins have been shown to preferentially localize.

The observations described above suggest that the feedback loops involving PI3K activity and F-actin polymerization might be sufficient to provide a strong initial

polarization of the leading edge signaling. This localized “frontness” is then able to exclude the “backness” signaling, producing the observed distribution of “backness” activity and further stabilizing the location of leading edge polarization. The process is likely more complicated than this, as evidenced by several observations. First, to date, it has not been identified how GPCR signaling is regulated to give rise to spatially separated $G_{\alpha i}$ and $G_{\alpha 12/13}$ activation of the “frontness” and “backness” pathways, respectively. Second, visualization of Rac activity in live cells shows significant Rac activity in the uropod of a polarized cell [57]. In addition, cells expressing Rac mutants affecting activity exhibit a defect in uropod retraction. Third, in addition to the long-range effects of CDC42 on RhoA activity, other observations suggest that additional long-range signals could couple, and perhaps even buffer, the “frontness” and “backness” pathways such microtubules [58, 59] or membrane tension [60].

1.3 Mathematical Models of Chemotactic Polarization

The studies described in the previous section demonstrate a complicated signaling pathway involving signaling molecules, with a complex regulation of both spatial and temporal localization and patterning. In parallel with the extensive body of experimental work to decipher the molecular details of eukaryotic chemotaxis, several efforts have been made to develop mathematical models of polarization and gradient sensing. A concise, yet thorough review of the various mathematical models proposed for both gradient sensing and polarization was produced by Iglesias and Devreotes [61]. In addition, at least one study has attempted to quantitatively compare several of the classes of models proposed for eukaryotic chemotaxis [62].

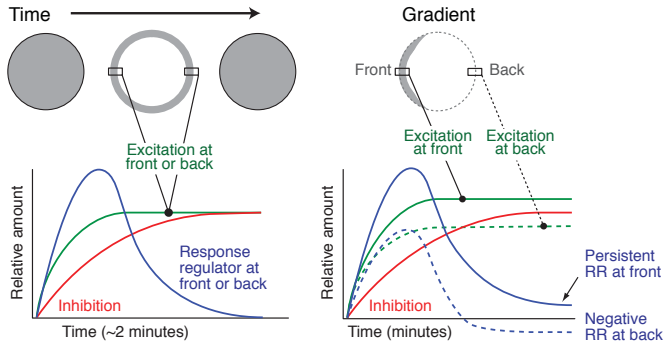

Figure 1-4 | LEGI model of chemotaxis. Left panel demonstrates the cellular response to a sudden increase in uniform concentration. Separate time scales for excitation and inhibition result in a transient global response that diminishes over time. Right panel demonstrates how same mechanism can result in sustained response to a gradient. Due to diffusion, inhibitor activity reaches uniform value throughout cell. Higher excitation at the front than back with the global inhibition results in strong internal gradient of response. Reprinted, with permission from **[66]**.

1.3.1 Local Excitation-Global Inhibition

Early models of chemotaxis focused on describing the ability of a cell to polarize in the presence of a weak gradient, as it had been shown that both neutrophils and *Dictyostelium discoideum* cells could accurately sense gradients resulting in differences as small as 1% across the cell [63]. The framework for these early models was proposed by Parent and Devreotes [20]. Here, they proposed that a system in which both an activator and inhibitor are produced by receptor stimulation could produce the observed sensitivity, provided that the activator was somehow retained locally, unable to diffuse away from the site of initial production, while the inhibitor was free to diffuse throughout the cell. Due to the differential diffusive properties of these two molecules, this model has been termed Local Excitation-Global Inhibition (LEGI). Although this model was able to properly localize proteins to the leading edge in a shallow gradient, as well as capture other aspects of chemotactic polarization, such as adaptation [64], it fails to capture several important experimental observations. First, when exposed to uniform concentration, cells respond experimentally by spontaneously polarizing. In contrast, the model predicts a global increase of activity within the cell, which then decreases to zero due to adaptation. Second, observations of the internal gradient of

PIP3 demonstrate a strong amplification of the external chemical gradient, which is not achieved by the LEGI model. Third, Xu et al. [19] demonstrated that chemoattractant gradient stimulation resulted in the activation of two separate, mutually inhibiting pathways, which cannot be accounted for in a LEGI model. Finally, the LEGI model relies on the production of a global inhibitor. To date, no molecule has been discovered to which this global inhibition can be attributed.

Modifications of the basic LEGI scheme have been proposed to address some of these issues. In one case, Ma et al. [65] propose two opposing LEGI networks. This model is able to achieve sharp gradients in internal PIP3 concentrations, similar to those observed experimentally. In addition, the model is able to recreate the response of cells to multiple stimuli as well as combinations of temporal and spatial stimuli. However, this model now requires two global inhibitors. It is conceivable that one molecule could act as an inhibitor to both pathways, but this does not resolve the issue of the lack of an identified global inhibitor. In a second case, Xiong et al. [66] propose a model in which a LEGI network drives an excitable circuit. The motivation for the addition of an excitable circuit comes from the observation of propagating waves of the actin regulator suppressor of cAMP receptor (SCAR) [67-69]. This model was able to achieve spontaneous polarization of cells and was able to qualitatively reproduce the propagating waves.

1.3.2 Mutually Antagonistic Pathways

In a different attempt to address the issues of a LEGI framework, Levine et al. [70] proposed a model similar to the LEGI models proposed previously. The main differences, however, were 1) that they required the inhibitor to first bind to the

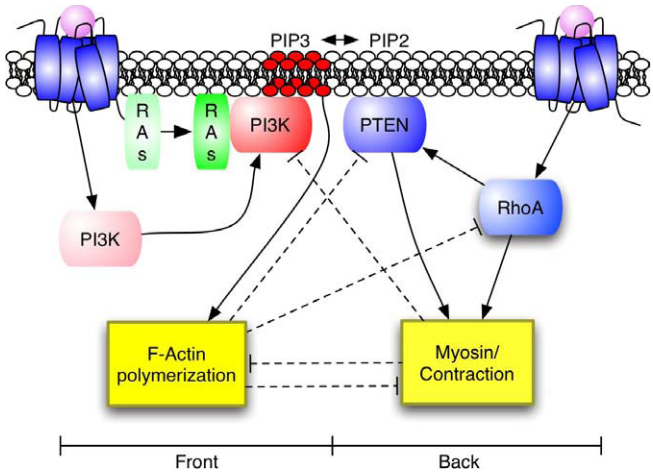

Figure 1-5 l Model of mutual antagonism. Diagram demonstrates the biochemical interactions used to model the mutual antagonism between frontness and backness pathway as was identified in the work performed by Xu et al. The key element of this model is the coincidence circuit formed by the necessity of recruiting both Ras and PI3K to the membrane following GPCR activation. Reprinted, with permission from **[73]**.

membrane before inhibiting the activator and 2) equal amounts of both inhibitor and activator were produced by receptor stimulation. This model was able to reproduce the observed strongly amplified gradient of leading edge signaling, with essentially no activity at the back of the cell. In addition, the authors propose that the roles of the two molecules could be served by the two signaling units of the heterotrimeric G-protein, G_{α} and $G_{\beta\gamma}$, thus eliminating the need for an unidentified global inhibitor. One intriguing aspect of this model, is that the profile of the inhibitor is in exact opposition to the profile of the activator. Even though the authors did not explicitly put into the model the existence of two separate, mutually inhibiting pathways, it appears that their model was able to achieve such a result. It is possible that instead of the heterotrimeric G-protein producing the two different molecules, it is possible that the Rho family of GTPases could play a similar role. The authors do state that the existence of positive feedback loops could eliminate the requirement of equal production of both inhibitor and activator. It is also possible that the addition of positive feedback loops could give rise to the possibility of spontaneous polarization.

Two independent models have been proposed based on the identification of the

divergent, mutually-inhibiting “frontness” and “backness” pathways. In the first, proposed by Narang et al. [71], it was found that the minimal number of species needed in order to achieve spontaneous polarization is three. Of these species, two were activating molecules, which were mutually antagonistic, representing the “frontness” and “backness” pathways, while the third was a global inhibitor, which could inhibit both of the other two species. This model qualitatively reproduced the effects of various small molecule inhibitors used against both the “frontness” and “backness” pathways. Interestingly, this model is also able to produce both chemoattractive and chemorepulsive responses, similar to those observed in neuronal axons [6, 72]. Finally, the author points to investigations of cytosolic inositol phosphates and reactive oxygen species as potential molecules serving the role of global inhibitor.

In the second model, Onsum et al. [73], explicitly encode the molecular interactions identified by Xu et al. [19], along with the proposed points of mutual inhibition. This model was able to achieve sharp gradients in PIP3, spontaneous polarization in response to uniform stimulation, rapid responses to changing stimuli and adaptation. It was unnecessary to include the existence of a global inhibitor to achieve these responses. Furthermore, given the direct link to biochemical interactions, the underlying assumptions of the model are significantly more straightforward to test experimentally than more general models.

1.4 Emerging Technologies for Probing Eukaryotic Chemotaxis

The extensive body of theoretical work revolving around eukaryotic chemotaxis has led to the development of sophisticated models which have been able to reproduce many of the experimental observations of chemotactic cells. To further test these

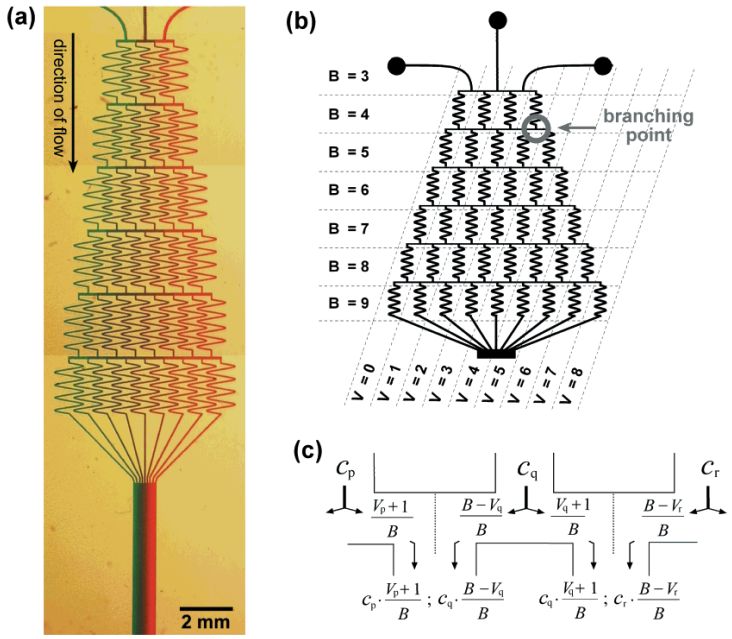

Figure 1-6 | Microfluidic gradient generator. a) Image of gradient generator with different colored dyes introduced via the separate inlets. **b**) Diagram demonstrating the multiple dilution steps of the gradient generator. **c**) Detailed diagram of the dilution occurring at a branch point. The concentrations of the two branches exiting the branching point depends on both the concentrations of the channels feeding into the branching point and the relative volumetric flow rates from each of these channels. Reprinted, with permission from **[79]**.

models for either verification or for further refinement, several new technologies have been developed to accurately probe the chemotactic response. These technologies can generally be separated into those to precisely control the external chemical environment in space and time and those to precisely perturb the internal biochemical pathways.

1.4.1 Technologies to Control the Spatio-temporal Concentration Profiles

One technology that has drawn particular interest for the study of chemotaxis is that of microfluidics. Several good reviews have been published on the different types of microfluidic technology used in the study of chemotaxis [74, 75].

The early focus of microfluidics technologies was on the generation of stable chemical gradients. Various designs were produced providing the ability to generate a wide array of gradient profiles, from simple monotonic gradients [76-78], to complex gradients consisting of non-monotonic profiles [79]. These devices function similarly, containing two or more inlets, through which solutions are introduced. These inlets then feed into a network of channels which act as serial diluters, producing multiple outlet

streams of different concentrations, which then feed into a single channel. Through cross-stream diffusion a smooth concentration profile is generated (Figure 1-6). One incredibly appealing feature of these devices is that as long as steady flow is maintained, the concentration profile will remain stable. This provides the ability to directly correlate the cellular behavior to precise chemical environment. Herzmark et al. [80] performed such a study and identified an optimal concentration at which the chemotactic response of differentiated neutrophil-like HL-60 cells. More recently, there have been several designs which have allowed for the controlled stimulation of cells by multiple directional cues. This provides the ability to study the molecular events that occur when multiple leading edges are competing, and how that competition is resolved. Additionally, there has also been a focus on using microfluidics to generate controlled three-dimensional chemotactic environments to mimic the *in vivo* environment encountered by chemotactic cells [37, 81-84].

Another keen area of interest in microfluidics is the ability to generate well-controlled temporal changes in the chemical environment. In one device [85], a cell is loaded into a small chamber. Through the use of micro-structured valves, chemokine is loaded uniformly into a region outside the chamber, without exposing the cell to the chemokine. Once the environment has stabilized, a valve can be opened, exposing the cell equally on all sides to a well-defined chemokine concentration. Such a device could help in understanding the processes involved in the spontaneous polarization of cells in uniform chemical environments. A different device utilizes two gradient generating networks, which produce gradients in opposing directions [86]. A set of valves can be manipulated to quickly switch between the two gradients, exposing cells to a rapid

gradient switch. This design provides a system to investigate the processes involved in reorienting a polarized cell.

Most recently, there has been interest in microfluidic devices in which cells migrate in confined microchannels [37, 81, 82, 87, 88]. Appealing aspects of such a system are that it simplifies both the external chemical environment as well as the cellular motion. Due to the fast diffusion of the chemokines, the cell is exposed to a steady concentration over time, and due to the confinement, only two surfaces of the cell are exposed to chemokine. In addition, the cell motion is simplified to one dimension. Studies using these devices have identified novel phenomena, such as “retrotaxis” [87] as well as the necessity of formin-mediated actin polymerization for cell motility [37]. Finally, modified versions of the microchannel, which introduce bifurcating channels provide an additional system to study the competition of two leading edges [81].

In addition to microfluidics, technology has been developed to take advantage of various properties of photoreactions to produce controlled spatio-temporal stimulation profiles. One such technology is the use of photocleavable chemokines [89, 90]. In this technology, a chemical group is added to the original molecule which prevents interaction with the receptor. When exposed to ultraviolet light, the added moiety is removed, recovering the fully functional original molecule. A similar technology uses optical tweezers to position manufactured microsources, which slowly release chemokine [91]. Finally, Karunaranthe et al. [92], replaced the formyl-peptide receptor GPCR with a blue opsin, a light-sensing GPCR. Through controlled exposure to blue light, the authors controlled both the time and location of stimulation.

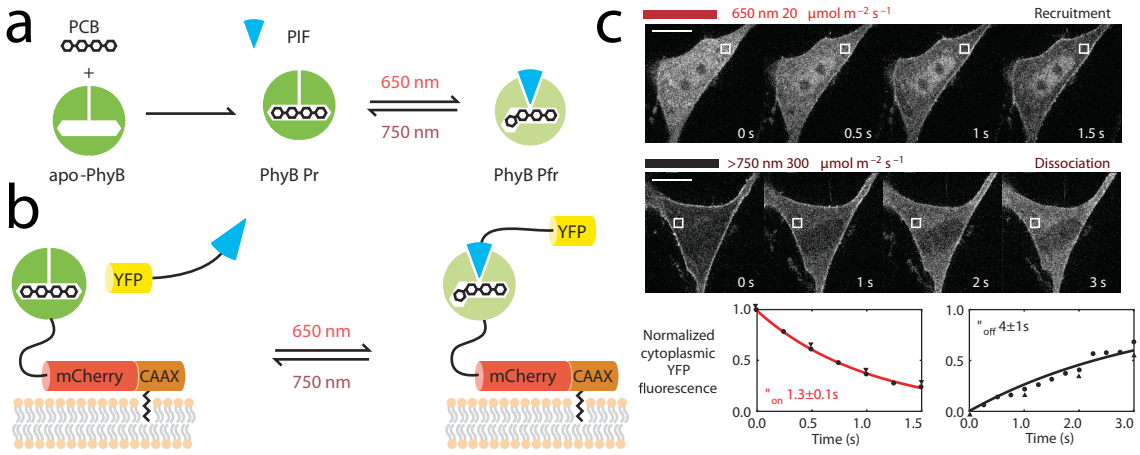

Figure 1-7 I Light induced dimerization system. a) Cartoon demonstrating the molecular interactions of the phytochrome system found in *Arabidopsis thaliana*. **b**) Cartoon demonstrating implementation of this system to target molecules to the membrane upon light exposure. The PhyB molecule was fused to an mCherry fluorophore targeted to the membrane through a CAAX domain. The PIF molecule was fused to a YFP fluorophore. **c**) Images demonstrating the response of cells expressing inducible dimerization system. Top panel demonstrates the rapid recruitment of YFP to the membrane following excitation with red light. Bottom panel shows rapid dissociation induced through infrared light excitation. Plots demonstrate measured YFP fluorescence for both situations. Reprinted, with permission from **[94]**.

1.4.2 Technologies to Controllably Perturb Internal Biochemical Pathways

An additional approach to understanding the processes of chemotactic polarization is the manipulation of various steps of the biochemical signaling pathways. Traditionally, small molecule inhibitors are used for this, but there are always concerns about the actual effects of these molecules. Many molecules used have effects on other molecules that may or may not play a role in chemotaxis. In addition, it is extremely difficult to enhance the activity of a molecule using small molecule inhibitors.

One approach to address this issue was demonstrated by Wu et al. [93], where a domain of the protein phototropin was fused to the Rac1 GTPase. Exposure to light a wavelength of either 458 or 473 nm repeatedly and reversibly activated Rac1. This technology would allow one to study the direct downstream effects of pure Rac1 activation, in the absence of the activation of other signals of the chemotactic pathway.

Another technology attempting to achieve this control relies on the inducible dimerization of molecules. This has been achieved both through photoactivation [94, 95] as well as chemical means [96]. In the former, the authors take advantage of photosensitive protein-protein interactions of the phytochrome signaling network of the plant *Arabidopsis thaliana*. Specifically, the molecule phytochrome B (PhyB) covalently binds the chromophore phycocyanobilin (PCB), rendering the complex sensitive to red and infrared light. Illumination with red light causes a conformational change in the PhyB-PCB complex, allowing it to bind to a phytochrome interacting factor (PIF). This interaction is reversed by illumination with infrared light. Using this system, induced translocation of both Rac1 and CDC42 GEFs stimulated extended membrane protrusion. In the latter, the molecule rapamycin is used, which can simultaneously bind to two naturally occurring proteins in mammalian cells, namely FKBP12 and the FRB domain of the mammalian target of rapamycin (mTOR). One potential issue with this system is that in addition to the proteins of interest, the dimerizing molecules will interact with the endogenous mTOR, which is a major regulator in numerous pathways. This issue is generally addressed by generating a chemical analogue of rapamycin as well as mutated versions of the FRB domain that are unable to interact with naturally occurring rapamycin, but can bind the analogue [97]. A system using this technology was able to demonstrate controlled activation and inhibition of Rho family GTPases on the order of seconds. Finally, a photocleavable rapamycin system was developed [98], which also provides precise spatial control of the induced dimerization and subsequent activation or inhibition.

1.5 Directional Cell Migration in Response to Physical Cues

Mammalian cells do not respond solely to chemical cues. Mechanosensation is a vital process in the sensations of touch and hearing, where mechanical deformations of cells are transformed into nerve signals to the brain. The mechanisms underlying this response involve specific mechanoreceptors, which generally convert mechanical deformation of some sort into an action potential, which is then propagated along nerve endings. Elsewhere in the body, numerous mechanical stresses exist, such as the tension in the extracellular matrix or the deformation of immune cells as they migrate through the extracellular matrix. Several studies have shown that these physical stresses are able to induce internal chemical signaling in cells. In one study, it was shown that the matrix stiffness could direct the differentiation of mesenchymal stem cells [99, 100]. Cells cultured on substrates of various stiffness generating, in order of increasing stiffness, neurons, muscle cells and bone cells. There is also evidence that mechanical deformation of primary neutrophils from being forced through small pores is able to induce structural and functional changes [101] and can even stimulate the production of polarized pseudopods.

1.5.1 Durotaxis: Matrix Stiffness Gradients Direct Cell Migration

In addition to generating global responses of cells, asymmetrical physical cues have been shown to direct cell migration. Two well studied such phenomena are those of cellular durotaxis and rheotaxis. Fibroblasts plated on a collagen coated poly-acrylamide gel, which had a sharp transition in rigidity. Fibroblasts migrating from the soft region could migrate onto the stiffer surface, while the reverse was not observed [102]. In fact, cells migrating from the stiffer surface, upon reaching the transition, turned

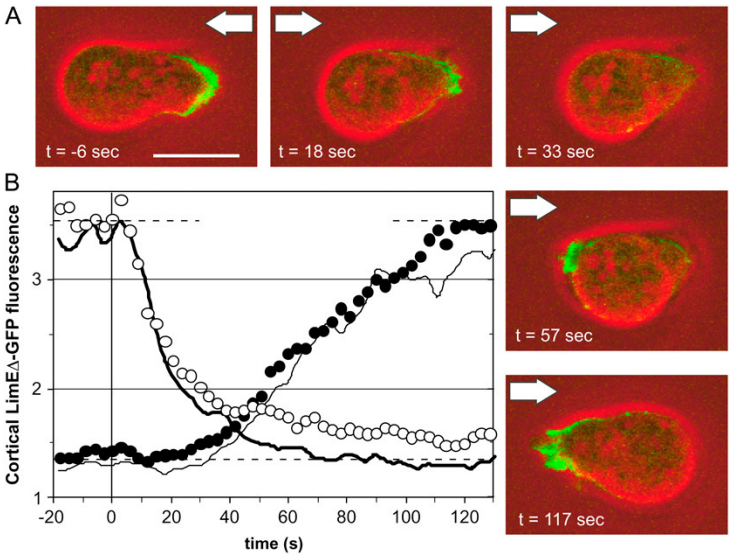

Figure 1-8 I Polarization reversal in response to switched flow. a) Cells of the slime mold *Dictyostelium discoideum* expressing LimEΔ-GFP, a marker of F-Actin, responding to a rapid flip of shear stress direction. Complete reorientation occurs within two minutes following the change. **b**) Plot of the measured cortical GFP intensity over time at both ends of the cell. Reprinted, with permission from **[107]**.

around and retracted away from the transition. Further studies using vascular smooth muscle cells demonstrated that the efficiency of durotaxis is dependent on the magnitude of the gradient in substrate stiffness [103]. Molecular studies of this process have shown that transitions in substrate stiffness are able to polarize the cytoskeleton and regulate the assembly of myosin IIb [104]. It has also been shown that rigidity sensing at the leading edge is dependent on $\alpha_V\beta_3$ integrins and the receptor protein-tyrosine phosphatase α [105]. One potential model of how integrins can serve this role suggests that on stiff substrates, the increased force results in an elongation in the linkage connecting the matrix and the cytoskeleton. This stretching could then potentially expose a phosphorylation site, somehow enhancing actin polymerization. It is further possible that the increased F-actin at the leading edge is able to produce the spatial distribution of phosphorylated myosin heavy chain observed by Raab et al. [104]. Although there is some evidence of such a stretch-dependent phosphorylation mechanism, it is still not clear to what extent it plays a role in rigidity sensing.

1.5.2 Rheotaxis: Cellular Directional Migration in Response to Fluid Flow

A further area of study in directed cell migration in response to physical cues is that of rheotaxis, where cell migration is direction by the direction of fluid flow. Using *Dictyostelium discoideum* cells, Decave et al. [106] demonstrated that a mild hydrodynamic shear stress was able to induce a migrational response, which greatly mimicked the response of cells to chemotactic factors. In a later study, Dalous et al. [107] exposed *Dictyostelium discoideum* cells to a dynamical change in the direction of the fluid flow. Under this stimulation, cells responded by rapidly relocalizing both actin and myosin, with complete reorientation occurring within approximately 90 seconds. Interestingly, the reorientation of the actin network did not require myosin II. Finally, a recent study developed a microfluidic device to mimic the environment of the interstitial tissue [108]. Here, the authors expose mammary adenocarcinoma cells embedded in the microfabricated environment to externally generated interstitial tissue-like flows. This resulted in a stress gradient along the length of the confined cell, which was mirrored by a gradient in β1-integrin activation and subsequent vinculin-paxillin-F-actin-dependent protrusions localized to the upstream edge of the cell. The authors postulate that the induced stress on the cell generates tension across the β1 integrins, which has been shown to promote the phosphorylation-independent binding of vinculin, promoting the maturation of focal adhesions, which then drives directed motion. This is a fascinating example of how a balance of forces between externally generated pressures and cellular adhesions to the matrix is able to generate directionally biased cell migration. It is possible that similar molecular mechanisms play a role in other examples of rigidity sensing and durotaxis.

1.5.3 Mechanotransduction of Directional Physical Cues

There has been much interest in understanding how directional physical cues can be transmitted to the polarization machinery of cells to produce directed cell migration. Much of this work has focused on the role of substrate adhesions and the transmission of tension generated in these adhesions. A review focusing on the molecular details of focal adhesions suggests several mechanisms of force sensing, which could be generally utilized by the various forms of mechanotaxis observed [109]. One potential mechanism is that the tension generated by the interplay between externally imposed forces and internally generated cellular forces could open certain ion channels thus regulating adhesion and migration. Another potential model suggests a role for adaptive force generation. It has been shown that cells respond to an increased resistance by the substrate, to which they are bound, by producing stronger focal adhesions and generating a larger internal force [110]. In general, it is believed that cellular mechanosensation is dependent on both external forces and the generation of internal cellular forces. In addition, several mathematical models have been proposed to explain the durotaxis phenomenon [111-113].

The environment encountered by immune cells as they move to the site of an infection is complex, likely containing multiple cues, both physical and chemical. As a result an area of increasing interest is the interplay between chemical and physical cues during directed cell migration [114]. One recent study with neutrophils showed that substrate stiffness not only regulates the force generated by cells as they migrate, but is also able to affect chemotactic efficiency, with cells on stiffer substrates exhibiting a stronger migrational bias in a chemical gradient [115]. Recent developments in

microfabrication have produced systems allowing for precise control of the physical cues experienced by cells.

In one study, Kidoaki et al. generated hydrogels with a periodic saw-tooth stiffness profile [116]. A range of stiffnesses was tested, and it was found that a peak stiffness of approximately 100 kPa and an ascending:descending elasticity gradient ratio of 1:2 supported efficient rectified cell motion. The addition of lanes of low elasticity oriented perpendicular to the saw-tooth pattern resulted in an increased rectification of the cell motion. Further study of cell motion in these environments is likely to provide valuable insight into the processes underlying cellular rigidity sensing. A similar approach by Wong et al. was used to generate polyacrylamide gels with micropatterned regions of varying rigidity. They produced primarily islands of high rigidity, but in principle, a wide array of micropatterns is achievable [117].

Le Berre et al. were able to similarly produce rectified cell motion. In this study, the authors generated an anisotropic physical environment by introducing a surface with non-adhesive tilted pillars, under which the cells were forced to crawl. Cells in these environments exhibited a strongly rectified motion along the direction, in which the pillars were tilted, and to a lesser extent perpendicular to the direction of tilt [118]. The motion of the cells in this environment was well described by a model of an active Brownian particle in a ratchet potential. The nature of this ratchet potential likely arises from the elastic interaction between the cell and the tilted pillar. Combining these technologies with existing technologies for understanding cellular chemotaxis will provide valuable insights into how physical and chemical cues interact to direct cell migration.

Chapter 2: Biased migration of confined neutrophil-like cells in asymmetric hydraulic environments

2.1 Overview

Cells integrate multiple measurement modalities to navigate their environment. Soluble and substrate-bound chemical gradients and physical cues have all been shown to influence cell orientation and migration. Here we investigate a novel form of directional sensing, the response to asymmetric hydraulic pressure. Cells confined in microchannels identified and chose a path of lower hydraulic resistance in the absence of chemical cues. In a bifurcating channel with asymmetric hydraulic resistances, this choice was preceded by the elaboration of two leading edges with a faster extension rate along the less resistant channel. Retraction of the "losing" edge appeared to precipitate a final choice of direction. The pressure differences altering leading edge protrusion rates were small, suggesting weak force generation by leading edges. The response to the physical asymmetry was able to override a dynamically generated chemical cue. Motile cells may use this bias due to hydraulic resistance, or barotaxis, in concert with chemotaxis to navigate complex environments.

2.2 Introduction

Cell migration and polarization are influenced by a complex interplay of chemical and physical cues that act locally. Chemotactic cells, such as neutrophils and Dictyostelium, integrate chemical cues over the cell surface to move up an attractant gradient [119-123]. Stiffness gradients, sensed by adhesion receptors, can also orient migration (durotaxis) [109, 113, 124, 125]. Cells must balance these, and other environmental inputs, to determine a direction of polarization and migration [126]. Given

the complex environment in tissues, it is likely that there are still unknown inputs to directional decision-making.

Microfluidics provides a programmable environment for single cells where chemical and physical cues can be precisely controlled in space and time, and polarization and migration quantified [83](Lautenschlager 2012). In particular, cellular confinement has been instrumental in observing many novel cellular behaviors such as integrin-independent motility [127] and EGF gradient sensing [128]. Additionally, cellular confinement into narrow microchannels (< 10 microns) is thought to mimic the tissue environment better than stiff 2D substrates covered with low viscosity medium.

Here we use confinement to investigate the role of cell-generated hydraulic pressure in directional decisions. We show that under strong confinement, migrating neutrophil-like cells push the column of water ahead of the cell, generating a hydraulic pressure. Cells selectively move towards a path of lower hydraulic pressure when presented with multiple paths. The morphological and signaling dynamics of this decision-making process revealed potential mechanisms that diverge from the classical PI3K-mediated chemotactic pathway. Remarkably, this physical input can out-compete conventional chemotactic signals, suggesting an important role in directing migration through tissues.

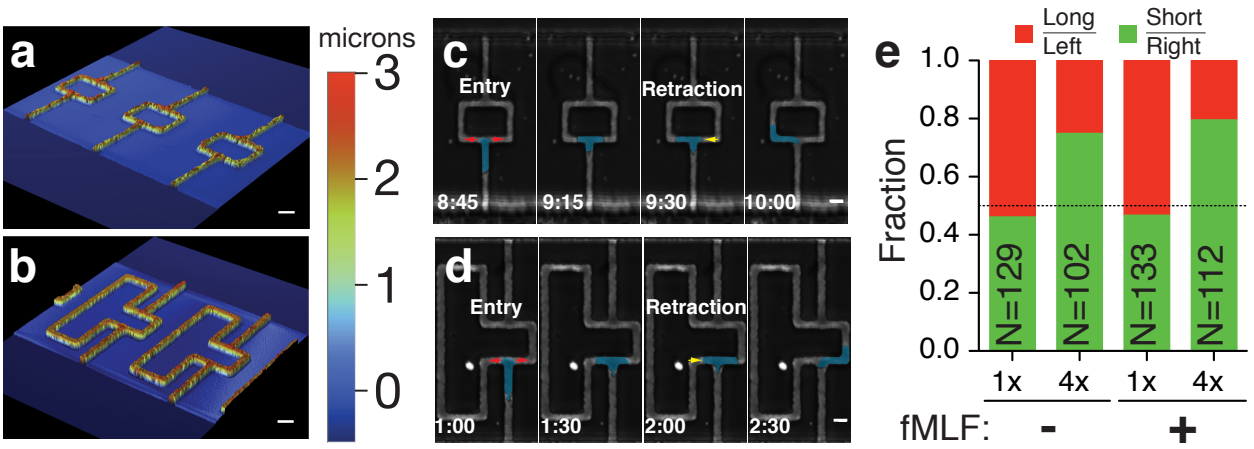

Figure 2-1 | Confined cells can identify shorter paths independent of chemical cues. a-b, Images from an optical profilometer showing 3-D geometry of bifurcating microchannel features on a silicon master for 1:1 (**a**) and 4:1 (**b**) length ratios. Scale bar, 10 microns. The color bar gives the height of the features, as measured by the profilometer. **c-d**, Time course montage of a cell migrating through a bifurcation in both 1x (**c**) and 4x (**d**) length ratio geometries. Cells are false-colored for visibility. Frames are labeled to emphasize the processes of entering the bifurcation (red arrows) and retracting one of the two leading edges extended (yellow arrow). Scale bar, 10 microns. **e**, Directional decision statistics for cells in 1:1 and 4:1 length ratio geometries and in the absence or presence of chemokine (fMLF). Green denotes cells that migrated towards the shorter length (or right) side, while red denotes cells that migrated towards the longer length (or left) side. N indicates number of cells measured.

2.3 Results

2.3.1 Asymmetric bifurcation channel length biases cell migration towards shorter path

To challenge single cells with complex hydraulic environments we used microfluidic devices that harbor bifurcating, fibronectin-coated channels, derived from designs described by Ambravaneswaran and colleagues [81]. These channels are six microns or smaller in width and three microns in height forcing differentiated HL-60 cells (a standard neutrophil model [129, 130]) to occupy the entire cross section. This generates a tight seal with respect to fluid flow across the cell length. Cells enter the channels from a lower cell reservoir either by random migration or by gentle pressure imposed during loading.

To test whether physical properties of the environment can influence cellular directional decision making, we manufactured bifurcating microfluidic channels, with

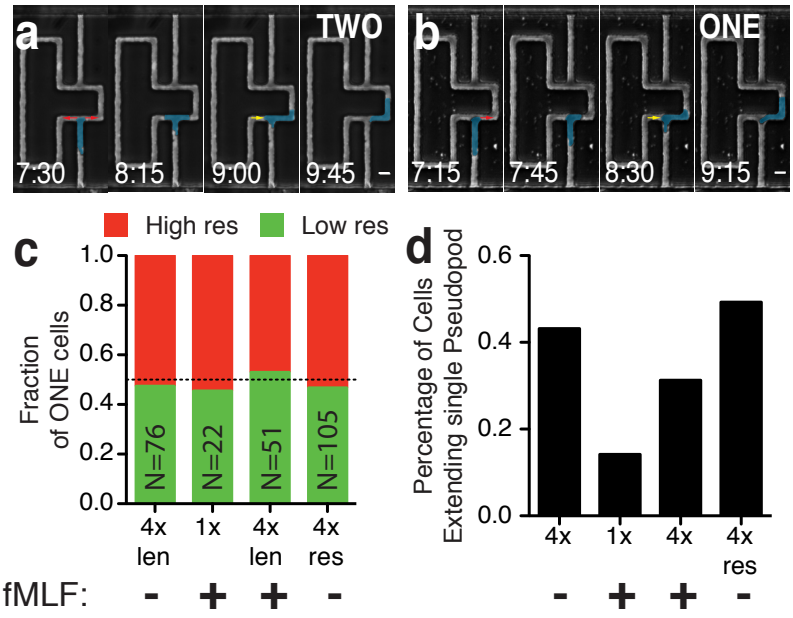

Figure 2-2 | Asymmetric directional bias requires extension of two pseudopods. a-b, Time course montages of a cell extending two pseudopods (TWO) (**a**) and only a single pseudopod (ONE) (**b**). Scale bar, 10 microns. **c**, Directional decision statistics for cells extending only a single pseudopod in the various geometries and in the presence or absence of chemokine. Statistics are shown for 1x and 4x. N represents the number of cells observed. **d**, Bar graph demonstrating the percentage of total cells which extended only a single pseudopod. Conditions not shown had fewer than 10 cells extending only a single pseudopod.

either a symmetric bifurcation (Figure 2-1a, symmetric lengths) or an asymmetric bifurcation (Figure 2-1b, 4x length asymmetry). We observed that when cells reached the bifurcation, they exhibited two different responses. In the first, the cell extended a pseudopod along each direction of the bifurcation and subsequently retracted the pseudopod from one side, while continuing to migrate along the other direction (Figures 2-1c and d). In the second, the cells, upon reaching the bifurcation, immediately began to migrate along one direction, without extending a pseudopod along the other direction (Figures 2-2a and b). Cells that extended two pseudopods showed symmetric decision-making (0.5:0.5, expressed as a fraction of total cells) in the symmetric channels but displayed a strong bias in the asymmetric bifurcations (4x) to the shorter side (0.75:0.25, p-value < 0.0001, Fisher Exact Test) (Figure 2-1e). This behavior was independent of the presence of a chemokine gradient across the channel generated by the introduction of 100 nM N-formyl-methionyl-leucyl-phenylalanine (fMLF) in the upper reservoir (Figure 2-1e, no significant difference by Fisher Exact Test). Interestingly, cells

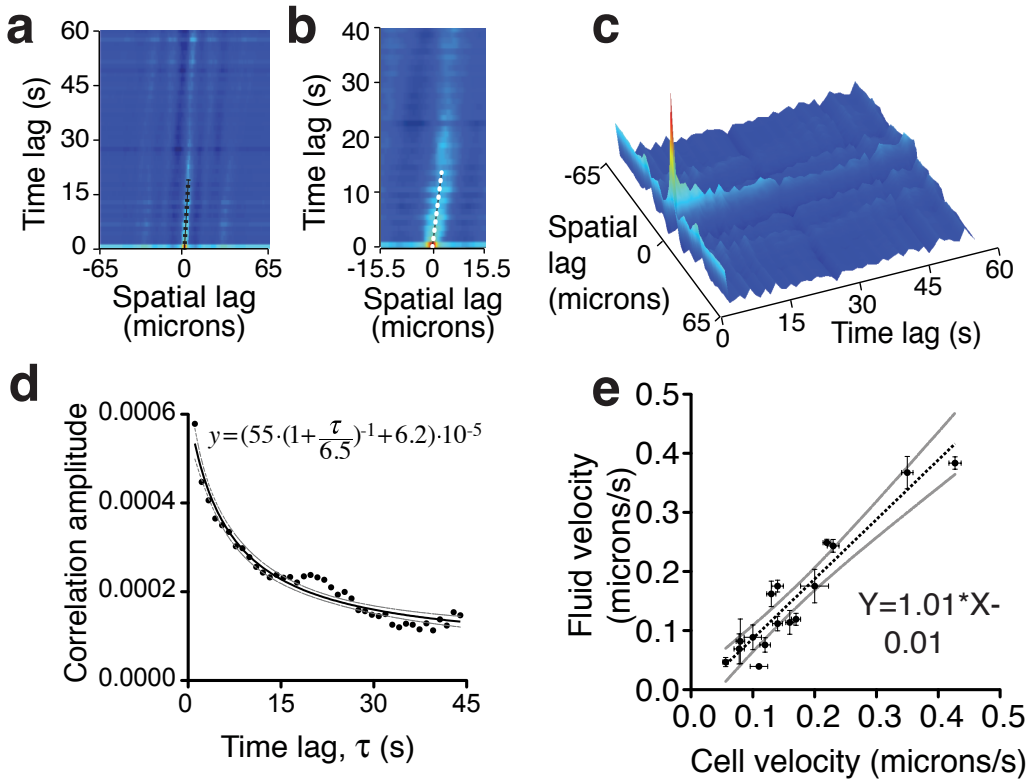

Figure 2-3 I STICS data analysis. a, Representative plot of correlation coefficient as a function of temporal and spatial lag. Dashed line shows position of center of Gaussian peak found by fit. **b**, Same plot as in **a**, but magnified to show movement of Gaussian peak. **c**, Three-dimensional plot of full spatio-temporal correlation function. **d**, Amplitude of the Gaussian fit of the correlation as a function of the time lag. Solid line is a nonlinear least squares fit of the decay according to the function described previously (17). **e**, Scatter plot of measured fluid velocity vs. cell velocity when using entire channel, rather than only the region excluded of the cell, for STICS algorithm. Nonlinear regression gave a slope of 1.01 +/- 0.09 and an intercept of -0.01 +/- 0.02.

that did not extend two pseudopods, the number of which varied greatly across the different geometries (Figure 2-2d), exhibited no significant directional bias in any of the geometries (Figure 2-2c), suggesting that the extension of two pseudopods, and competition between them, is essential for the bifurcation geometry to bias directional cellular migration.

2.3.2 Cells in confined microchannels push water

Given the tight seal formed by the cells in the microchannel [82], we speculated that the cells push water as they migrate in the channels. As a result, they would be able to detect the length difference in the asymmetric bifurcation through the different

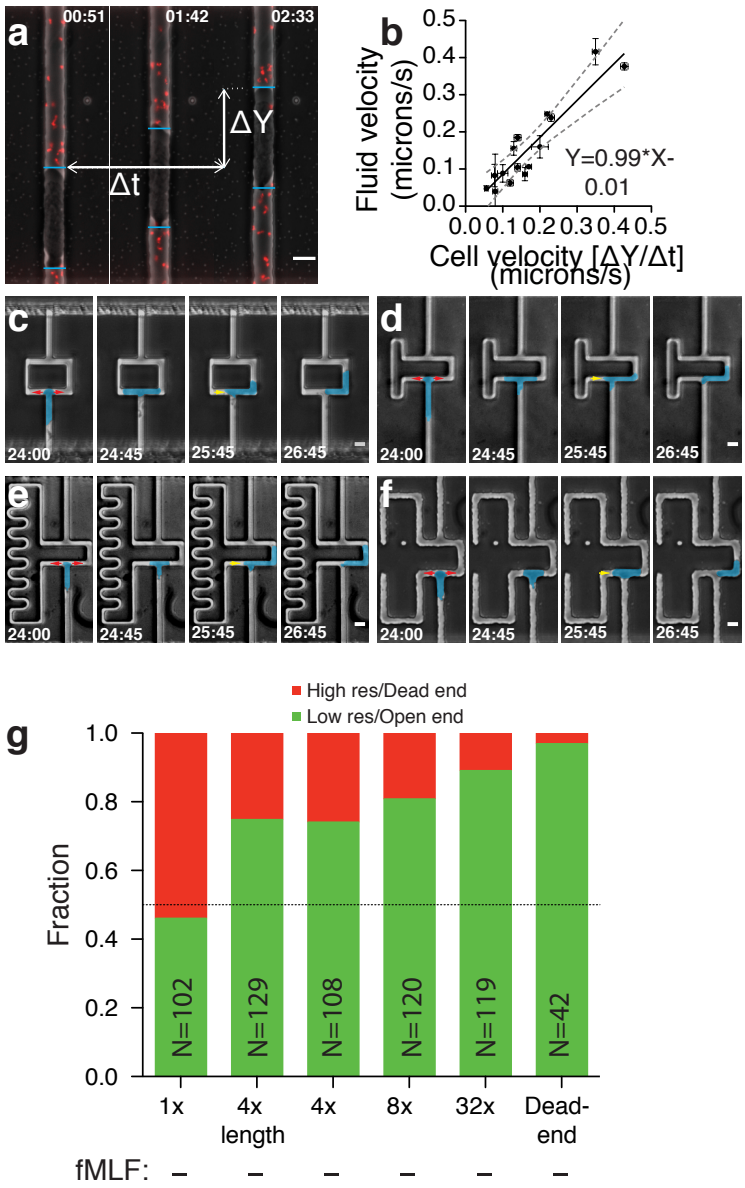

Figure 2-4 | Cells push water and can identify the path of least resistances. **a**, Time course montage of a cell in a microchannel with fluorescent beads. ΔY shows the distance travelled by the cell, while Δt shows time taken to travel ΔY. Image was acquired with a 40x oil 1.0 NA immersion objective. Correlation data was acquired with a 10x air 0.25 NA objective. Scale bar, 10 microns. **b**, Plot and fit of fluid velocity calculated by STICS (y-axis) compared to measured cell velocity (x-axis). Gray curved lines show 95% confidence interval of fit, shown by black line. A nonlinear regression gave a slope of 0.99 +/- 0.26 and an intercept of 0.01 +/- 0.05. Fit equation is shown. **c-f**, Time course montages of cell migrating in channels with resistance ratios of 4x (**c**), 8x (**d**), 32x (**e**), and dead-end (**f**). Cells are false-colored for visibility. Scale bar, 10 microns. Frames are labeled to emphasize the processes of entering the bifurcation (red arrows) and retracting one of the two leading edges extended (yellow arrow). **g**, Directional decision statistics of cells in all geometries, in the absence of chemokine (fMLF).

hydraulic loads presented to each extending pseudopod. To test if cells push water as they migrate in the microchannels, we loaded cells into straight microchannels with small fluorescent polystyrene beads in the medium (500 nm). We utilized a Spatio-Temporal Image Correlation Spectroscopy (STICS) method [131] to measure the positional fluctuations of the beads (Figure 2-3). From these measurements we were able to extract the flow velocity of the beads, and therefore the bulk fluid. Fluid velocities in the channel measured this way were identical, within our measurement error, to the

velocity of the cells themselves (Figure 2-4a) indicating that these cells do indeed push water as they move.

2.3.3 Cell migration biased by hydraulic resistance

To further test if cells responded to hydraulic resistance, and not simply channel length, we utilized the equation given by Fuerstman and colleagues [132] to fabricate devices of 3 different hydraulic resistance ratios. For the first (Figure 2-4c), the lengths of the 2 bifurcations were equal, but the hydraulic resistance of the left side was fourfold higher, accomplished by reducing the width of the downstream channel far from the bifurcation. Approximately 75% of the cells migrated along the lower resistance side (Figure 2-4g), similar to the statistics from the 4x length ratio bifurcations. For the next two geometries, a combination of increased channel length and decreased channel width was utilized to achieve resistance ratios of eight-fold and thirty-two-fold (Figure 2-4d and e), respectively. As shown in Figure 2-4g, cells in these geometries exhibited an even stronger bias, with 80% and 90% of the cells migrating toward the lower hydraulic resistance in the 8x and 32x geometries, respectively (Figure 2-4g). Finally, we fabricated microchannel devices, in which one side of the bifurcation ends in a dead-end (Figure 2-4f). When loaded into these channels, we observed that cells still extended two pseudopods, however, the pseudopod that extended along the dead-end direction did so for only a short distance, resulting in an asymmetrical extension biased towards the open-ended side of the bifurcation (Figure 2-4d). Correspondingly, nearly all cells (41 of 42 total, ~98%) migrated away from the dead-end (Figure 2-4g).

2.3.4 Pseudopod length, but not leading edge polarization predict direction of migration

To investigate a potential molecular basis of the directional decision-making we

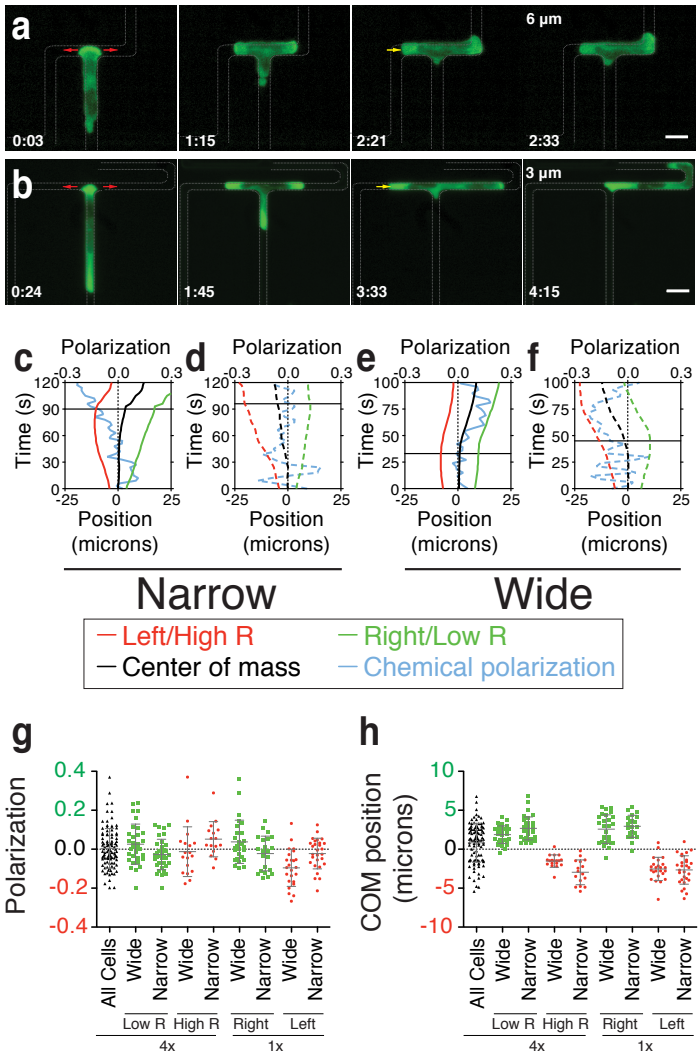

Figure 2-5 | Asymmetries in leading edge extension predict cellular directional decision. a-b, Time course montage of a cell expressing 3xPH-Akt-GFP migrating in 4x length ratio bifurcation geometry with width of 6 microns (**a**) and 3 microns (**b**). Scale bar, 10 microns. The red arrows denote the process of entering the bifurcation and the yellow arrow denotes the retraction of the non-persistent leading edge. **c-f**, Trajectories of the position of the low-resistance leading edge (green), high-resistance leading edge (red), center of mass (black) and the PH-Akt polarization (cyan) vs. time. Plots are grouped according to whether the cell migrated in narrow channels (**c,d**) or wide channels (**e,f**). Dashed trajectories represent a cell choosing high resistance channel; solid trajectories represent a cell choosing low resistance channel. Horizontal lines show the retraction time for each cell. **g-h**, Column scatter dot plots of the position of the PH-Akt polarization (**g**) and center of mass (**h**) at retraction time, for both 4x and 1x geometries. For all plots, in black is shown the distribution for cells in both narrow and wide geometries for the 4x resistance ratio. In green is shown the distribution for cells that migrate towards the low resistance/right side, grouped by the resistance ratio. In red is shown the distribution for cells that migrated towards the high resistance/left side, grouped by the resistance ratio.

imaged HL-60 cells stably expressing 3xPH-Akt-GFP (PH-Akt), a marker of phosphoinositol-3 phospho-lipids (PI3P) and an indirect readout of PI3-kinase activity. This marker is strongly enriched at the leading edge during chemotaxis in both neutrophils and the slime mold *D. discoideum* [25, 133]. Bifurcating pseudopods exhibited PH-Akt positive leading edges in microchannels of width six (wide) and three microns (narrow) (Figures 2-5a and b). In many cells, the leading edge that eventually retracted was enriched for PH-Akt right up to the time of retraction, with no obvious decrease in brightness. We quantified the maximum intensity of leading edge PH-Akt in

a three micron window at each leading edge. When observed in space-time plots, the normalized chemical polarization showed no obvious bias over the decision-making time (Figure 2-5c-f, blue line). Moreover, we observed no correlation between the initial or final asymmetry in leading edge chemical polarization and the ultimate direction chosen (Figure 2-6b and Figure 2-5g). Thus, the competition between the extended pseudopods did not appear to be mediated by differences in strength of canonical leading edge signaling.

We then turned to careful geometric analysis of the competing pseudopods. In asymmetric channels, pseudopods became asymmetrical in length over time with the low resistance branch longer, indicating that extension rates were faster on the low resistance side (Figures 2-5a and b). When plotted in space-time plots, we observed that in individual cells the center of mass position, with respect to the center of the bifurcation, rapidly biased to the final directional choice (Figures 2-5c-f, black line). This occurred even in the low percentage of cells that chose the high resistance channel. Thus, a physical asymmetry resulting from differential extension rates predicted the directional choice.

By normalizing initial pseudopod velocities we found that a bias toward the low resistance side was observable within the first five frames after entering the bifurcation, (Figure 2-6a). Comparing the initial extension bias to the final direction chosen for each individual cell, we found that the initial extension bias correlated well with the final decision of the cell (Figures 2-6a). Notably, the cells in the wide channel showed a stronger bias in the correlation of initial extension velocity with final decision when compared to the cells in the narrow channel. The bias in the center of mass, in the

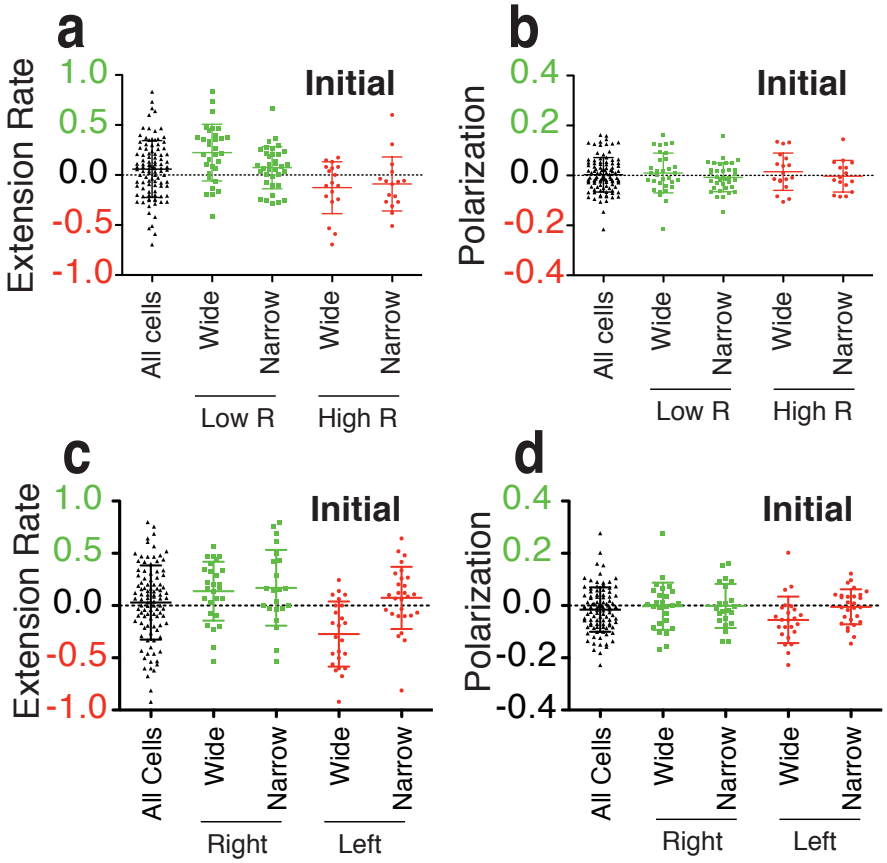

Figure 2-6 l Initial asymmetries do not correlate strongly with cellular directional decision. a-d, Scatter dot plots of the normalized extension rate (**a,c**) and PH-Akt-GFP polarization (**b,d**) as the cell entered the bifurcation for both 4x (**a,b**) and 1x (**c,d**) resistance ratios. For all plots, in black is shown the distribution for cells in both channel width geometries. In green is shown the distribution for cells that migrate towards the low resistance/right side, grouped by the bifurcation channel width. In red is shown the distribution for cells that migrated towards the high resistance/left side, grouped by the bifurcation channel width.

frame directly prior to retraction, exhibited an even stronger correlation with the direction chosen by the cell (Figure 2-5h). In this case the cells in narrow channels exhibited a modestly stronger correlation.

To verify that the observed correlation between extension asymmetry and direction chosen was not a result of the physical asymmetry of the bifurcating channels, we imaged HL-60 cells in both wide and narrow symmetrical bifurcating channels. As shown in Figure 2-5h, cells in symmetrical bifurcations exhibit a very similar correlation, with only a small number of cells migrating in a direction opposite that of the center of

mass, and in those cases the center of mass is quite close to the bifurcation. Similarly, cells in symmetrical bifurcations exhibited no obvious correlation between polarization of PIP3 and the direction chosen (Figure 2-5g).

2.3.5 Distance of uropod from bifurcation determines timing of pseudopod retraction

We observed that the length of time over which the cell was extending two pseudopods before retraction increased with increasing cell length (Figure 2-7a). We eliminated the notion that these cells moved slower by measuring velocities in wider and narrower channels and seeing no difference in cell motility rates (Figure 2-7c). As shown in Figure 2-7b, longer cells extended longer pseudopods, but since there is no obvious difference in velocities between long and short cells, the longer cells must have taken a longer time to decide. Two appealing models could explain this observed relationship. First, every cell might extend a specific fraction of its length into the bifurcations prior to retracting one leading edge. Thus, the cell will not retract one leading edge until the distance between the bifurcation and the back of the cell is a certain fraction of the cell length. Second, the absolute distance of the back of the cell from the bifurcation determines when the cell retracts one leading edge. In Figure 2-7d is shown the fractional back distance vs. the cell length. A linear regression to this data (not shown) gives a negative slope, which is significantly different than 0. This suggests that the fractional back distance is not an invariant with respect to cell length. If, on the other hand, the absolute distance of the back from the bifurcation is invariant with respect to cell length, the data would fit a hyperbolic curve. Calculating such a fit using the function Y=A/X, gives a value for A of 7.642 (r2 = 0.991). The result of this fit, with 95% confidence intervals is shown in Figure 2-7d. This would imply that the cell does

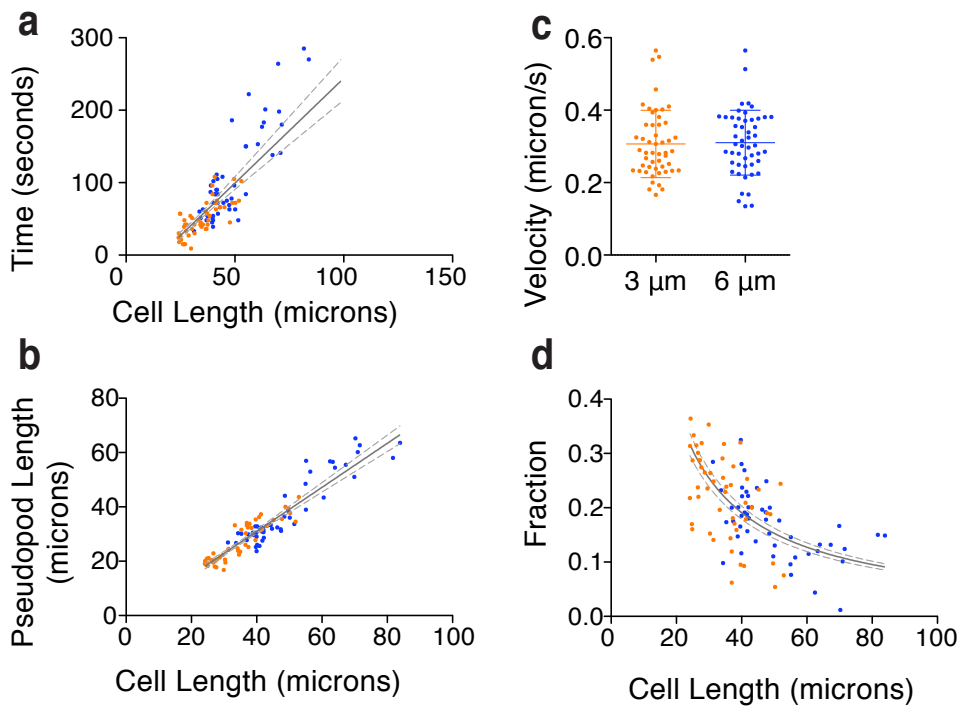

Figure 2-7 | Timing of the cell decision is influenced by cell back-bifurcation distance. a, Scatter plot of time between the bifurcation entry and retraction times vs. the cell length. Solid line is a linear regression of the data, and the dashed lines are the 95% confidence bands for the fitting. Orange points indicate cells in wide channels, blue points indicate cells in narrow channels. **b**, Scatter plot of the total length of both pseudopods extended vs. cell length. Lines show a linear regression (solid line) and the 95% confidence bands (dashed line). Orange points indicate cells in wide channels, blue points indicate cells in narrow channels. **c**, Velocities of back domain from cells migrating in wide and narrow channels **d**, Scatter plot of the fractional back distance (relative to cell length) vs. cell length. Orange points indicate cells in wide channels, blue points indicate cells in narrow channels. Hyperbolic fit to data is shown.

not decide which direction to migrate until the back of the cell is approximately 7.5 microns from the center of the bifurcation.

One potential mechanism by which the absolute back distance could regulate the timing of the directional decision is through cytoskeletal tension. Cortical acto-myosin as well as activated myosin are both polarized to the back of the cell during migration. This would suggest that the uropod of the cell is quite stiff. As this stiff structure approaches the bifurcation, it could experience increased tension due to being pulled around the corners of the bifurcation. This increase in tension may elicit a signaling event from the back of the cell to the front—either a diffusible signal or via membrane tension—to

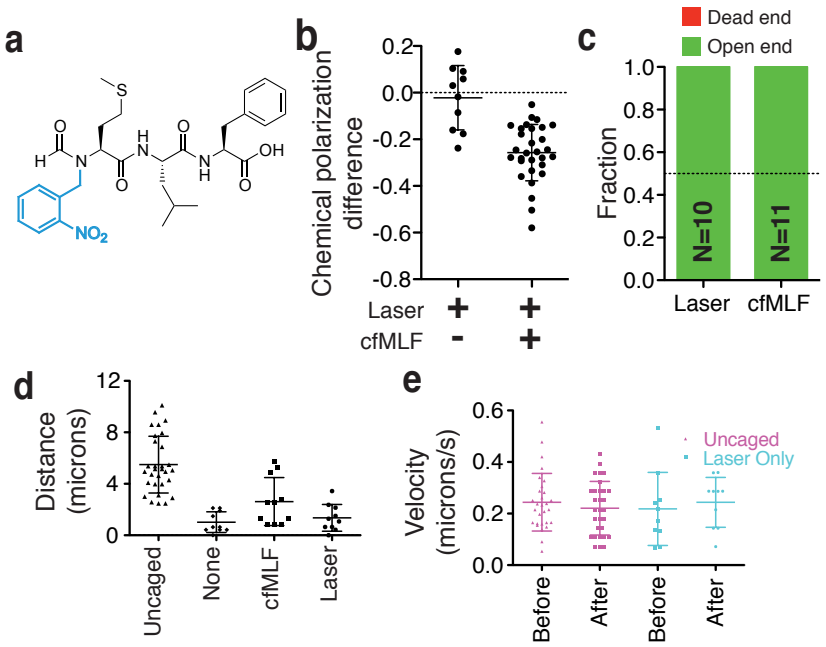

Figure 2-8 | Characterization of caged fMLF. a, Chemical structure of caged compound. Nitryl-benzyl group highlighted in cyan. **b**, Scatter dot plot showing the maximum change in polarization of cells directly prior to and within 21 seconds following laser activation, both in the absence and presence of caged fMLF. A negative value for polarization results when more PH-Akt localizes to the dead end leading edge than to the open end leading edge. **c**, Fraction of cells deciding after laser activation alone (Laser) or laser activation in the presence of caged fMLF (cfMLF). **d,** Column scatter dot plot of the maximum distance the dead-end side leading edge extended towards the dead-end. Data is shown (left to right) for cells in the presence of caged fMLF and laser excitation, the absence of both caged fMLF and laser excitation, the presence of only caged fMLF and the presence of only laser excitation. **e**, Column scatter dot plot of extension velocity of open end leading edge for cells that were exposed to both caged fMLF and laser excitation (purple) and laser excitation only (cyan), both directly prior to laser excitation and ~18 seconds following laser excitation.

signal the retraction of the shorter pseudopod. Further studies would be required to identify the activating step for pseudopod retraction, but the analysis here favors a back-generated signal.

2.3.6 Chemokine stimulation can overcome hydraulic resistance to direct migration

Having observed no apparent correlation between PIP3 chemotactic signaling and directional choice in asymmetric channels, we investigated competition between physical and chemical inputs. A “caged”, or photocleavable, version of fMLF (cfMLF) was synthesized (Figure 2-8a) by appending a nitrylbenzyl moiety to the formyl group. This derivative appeared to lack any chemotactic activity. When exposed to UV light, the

Figure 2-9 | Western blot analysis of photocleavable fMLF. Samples were prepared as described in Materials and Methods. Blotting for pAkt and Akt was performed on separate membranes produced from the same set of samples. As a loading control, the samples were probed for α-Tubulin. From here, it can be seen that a high concentration of caged fMLF in the absence of UV photocleavage is able to activate cells above the baseline level of activation. Furthermore, UV exposure is able to increase the ability of the compound to activate the cells, but does not reach the full activity of unmodified fMLF.

bond to the nitrylbenzyl is cleaved, liberating active fMLF. We tested cfMLF by uncaging it in a dead-end channel that cells rarely enter, and observed the effect on cells expressing PH-Akt-GFP. Measurements of fluorescence intensity made at each leading edge immediately prior to as well as 18 seconds following uncaging showed a dramatic increase in chemical polarization toward the dead-end (Figure 2-8b) indicating that photo-liberated fMLF activates canonical signaling pathways.

It can also be seen in Figure 2-8b, that cfMLF alone appears to promote farther pseudopod extension into the dead-end compared to no cfMLF, with or without laser exposure. This suggests that the cfMLF compound alone might be able to activate the cells to some extent. To test this, a Western Blot analysis was performed to test the ability of cfMLF to chemically activate cells as compared to unmodified fMLF and photo-liberated cfMLF. As can be seen in Figure 2-9, a high concentration (100 nM) of cfMLF is able to chemically activate cells, but to a much lower extent than the same concentration of unmodified fMLF or photo-liberated cfMLF.

To probe the competition between chemical and hydraulic stimuli, cfMLF was uncaged in the dead-end side of a dead-end bifurcation soon after cells started to

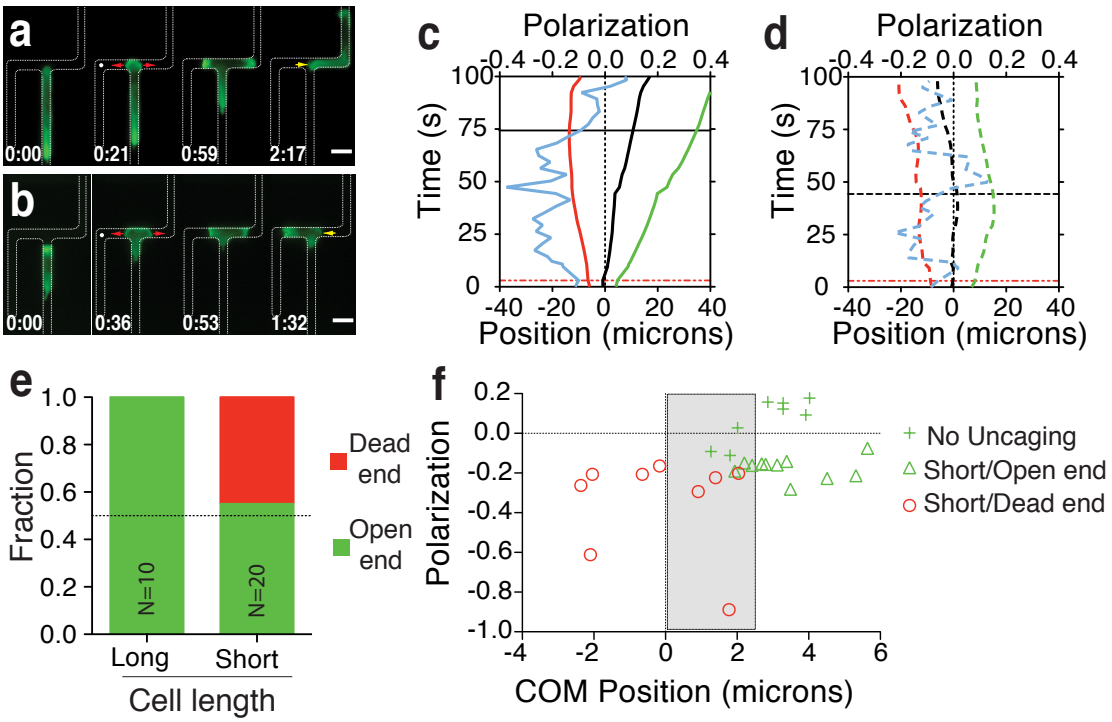

Figure 2-10 | Physical asymmetry can override chemical activation. a-b, Time course montages of cells in the presence of caged fMLF exposed to laser excitation. Location of uncaging (white dot) and uncaging time are shown in the second image of the panel. Cells migrated towards the open end (**a**) or towards the dead end (**b**), albeit with different statistics. Scale bar, 10 microns. The red arrows denote the process of entering the bifurcation and the yellow arrow denotes the retraction of the non-persistent leading edge. **c-d**, Leading edge trajectories as shown previously for cells exposed to uncaging of caged fMLF and migrating either away from the dead-end (**c**) or toward the dead end (**d**). Note the increase in polarization magnitude after cfMLF uncaging. Red line represents the uncaging time. **e**, Directional decision statistics for cells that were exposed to laser excitation in the presence of caged fMLF. Cells were grouped according to whether they were longer (Long) or shorter (Short) than 40 microns. **f**, Scatter plot of the maximum polarization (negative is towards the dead-end) following uncaging and the COM bias directly prior to retraction. Shown are all short cells exposed to uncaging and cells in dead-end bifurcations not exposed to uncaging. Gray box marks the region in which some cells with a physical bias away from the dead-end migrate toward the dead-end.

extend two pseudopods into the channels. We found that many cells (70%) migrated down the open channel despite exhibiting strong PIP3 polarization towards the dead-end side (Figure 2-10a). Thus the chemical signal polarized the signaling machinery towards the high chemoattractant side, but the response to hydraulic resistance overrode this signal to direct cell migration. Dynamics of the response of the cells that entered the less resistive channel were similar to those in the absence of uncaging, with the notable exceptions of chemical polarization towards the dead end after uncaging

(Figures 2-10c-d) and farther extension of the pseudopod down the dead-end following uncaging (Figure 2-8d). A subset of cells (30%) did enter the dead end channel when cfMLF was uncaged (Figure 2-10b). These cells retracted the leading edge that had extended toward the open end and migrated a short distance into the dead-end, at which point, they ceased to continue migrating, but did not retreat from the dead-end. This effect was dependent on both the presence of cfMLF and laser activation, since either one alone did not cause cells to enter the dead end channels (Figures 2-8c). When the directional choice statistics were analyzed we found that the cells that entered the dead-end channel were all short (< 40 microns) (Figure 2-10e). Interestingly, the cells that entered the dead end channel exhibited center of mass biases both into and away from the final directional choice implicating a competition between chemical and physical inputs at small physical asymmetries (Figure 2-10f).

2.4 Discussion

Here we have identified a novel physical input to cellular directionality, hydraulic pressure generated by cell migration. The influence of this input was revealed by observing confined, chemotactic cells presented with asymmetric hydraulic environments and demonstrating that they were able to determine the path of lesser hydraulic resistance, a phenomenon consistent with the term “barotaxis”. Notably, this choice did not require chemical cues, unlike previous work using similar bifurcated channels [81]. The decision-making dynamics involved two phases: 1) generation of an initial physical asymmetry manifest as differential extension of two leading edges and 2) retraction of the leading edge closest to the bifurcation. Together these activities resulted in biased migration toward the lower resistance channel.

Analysis of the dynamics of leading edge extension revealed that the physical asymmetry in pseudopod extension was a strong predictor of the direction of cell migration. However, measurements of canonical leading edge polarization signaling did not appear to correlate with this physical asymmetry. Thus, the mechanisms underlying the generation of extension asymmetries, whether active or passive, are different from those underlying the response to a chemotactic stimulus. This is further supported by our results using a photocleavable fMLF analog, which showed that the hydraulic input can overcome a strong chemical stimulus, and does so downstream of leading edge PIP3 synthesis, a canonical chemotactic polarization marker.

Further, our analysis of the timing of retraction favors a model in which a signal is generated by the back of the cell once it has come close enough to the bifurcation. This signal then initiates the retraction of the pseudopod closest to the bifurcation, which suggests an important role for the uropod of a polarized cell in resolving the competition between multiple stimuli.

2.5 Materials and Methods

2.5.1 Cell Culture and Stable Line Production:

HL-60 cultures were maintained in RPMI 1640 (Invitrogen, 11875119) media supplemented with 20% FBS (Invitrogen, 26104), 1% Penstrep (Cellgro, 30-002-CI), and 25 mM sterile filtered HEPES (Fisher Scientific, BP310), and were passaged every 2-3 days. Cells were differentiated in complete media supplemented with DMSO to a final concentration of 1.3%. Cells differentiated for at least 5 days and not more than 7 days were used for experiments.

Cell lines stably expressing PH-Akt-GFP were generated via retroviral infection,

as described previously [126]. Briefly, Plat-GP cells (Cell Biolabs, San Diego, CA) were used to produce retrovirus by co-transfection with a pBABE packaging vector (pBABEblast, pJag98, [134]) containing the cDNA for 3xPH-Akt-GFP (cDNA obtained from Dr. Lew Cantley, Harvard Medical School) and VSV-G, using Fugene 6 (Roche, Germany). The viral supernatant was collected after 48-72 hours and filtered using a 0.45 micron syringe filter. Polybrene was added to the supernatant at a final concentration of 16 micrograms/mL. Cells were suspended in one well of a 6-well plate at a concentration of 10^6/mL in a volume of 2 mL. To this suspension was added 5 mL of viral supernatant and the cells were spun at 1000xg for 90 minutes in a swinging bucket rotor. Cells were then incubated for 5 hours at 37 C. Following this incubation, cells were pelleted and resuspended into 2 mL fresh media. The next day, 2 mL of fresh media was added to the cells. The next day, cells were placed under selection in 1 micrograms/mL blasticidin. Once a stable pool of blasticidin resistant cells was obtained, cells were sorted for GFP expression (HMS/Systems Biology Flow Cytometry Facility).

2.5.2 Microfluidic Device Fabrication

Microfluidic devices were generated as described previously [81]. High-resolution film (Fineline Imaging, Colorado Springs, CO) or chrome (Advanced Reproductions Corp, Andover, MA; Front-Range Photomasks, Colorado Springs, CO) masks were used to generate photoresist masters. SU-8 (Microchem, Newton, MA) was spun onto silicon wafers at a rate according to the feature height desired. The photoresist was then exposed to UV light using a mask aligner (Neutronix Quintel, Morgan Hill, CA). Unexposed SU-8 was developed away. PDMS was then either spun (for membranes) or poured onto the wafers, cured overnight at 70 C. The top layer of the devices was then

cut out, access holes were punched for pneumatic valve control using a 0.75 mm diameter punch, and the devices were then bonded to the spun membrane using oxygen plasma. These devices were again cut out and additional fluid access holes were punched and the devices were then bonded to either 1x3 glass slides (Fisher Scientific, Pittsburgh, PA), or 45x50 mm No. 1.5 coverslips (Fisher Scientific, Pittsburgh, PA).

2.5.3 Microfluidic Device Operation

Tygon tubing (Greene Rubber Company, 2007900S-54HL) and 30 gauge blunt syringe needles (Brico Medical Supplies, BN2505) were used to connect syringes to the microfluidic devices. The outer diameter of the tygon tubing (0.03 in) is slightly larger than the diameter of the hole punched, so when the tubing was inserted into the hole, a seal was created. Each of the pneumatic valve control chambers was connected to a 1 mL syringe. To close the valves, the syringe was compressed from a volume of 0.2 mL to approximately 0.05 mL. To open the valves, the syringes were pulled open from a volume of 0.2 mL to the maximum volume of the syringe.

Fibronectin was adsorbed onto the channel walls by filling the device with a solution containing 50 micrograms/mL fibronectin (Sigma-Aldrich, F0895) in 50 mM Tris-HCl. Any air bubbles present were removed by pressurizing the device. The solution was incubated in the device for 1 hour at room temperature and then rinsed out with HBSS supplemented with 25 mM HEPES and 0.2% human serum albumin.

Each inlet was connected to a syringe, with the plunger removed. One syringe contained a solution of HBSS, while the other contained a solution of HBSS with fMLF. Fluorescein was added to the syringe containing fMLF to visualize the interface of the

two inlet streams for balancing the stream pressures. For experiments in which no chemokine was introduced, the inlet tubing was clamped off to eliminate any flow through the device. To reduce the introduction of air bubbles while loading cells, a drop of HBSS was placed onto the cell inlet hole prior to removing the priming tubing.

To load cells into the device, 2-3 mL of differentiated cells were pelleted and 30 μL of the cell pellet was taken and placed into a blunt needle with a short section of tubing. The cells were then pushed through the tubing by applying pressure to the top of the needle with a finger, until a small drop appeared at the end of the tubing in order to provide a liquid-liquid interface while inserting the tubing to prevent the introduction of air bubbles. The cells were then pushed into the device by applying pressure with a finger and the on-chip valves were manipulated to ensure that the cells were loaded on only 1 side of the microchannels, and were forced into the entrance of the microchannel.

2.5.4 STICS Image Acquisition and Analysis

Devices were prepared and cells were loaded as described above, with the addition of 500 nm diameter red fluorescent polystyrene beads (Invitrogen, F8812). Images were acquired with a 10x Ph1 ADL objective at a frame rate of 1 frame every 1.1 seconds, in both RFP and bright-field channels. Each microchannel was then extracted from the image and averaged across the width of the microchannel, to generate a 1-D array at each time point. The resulting 2-D array (1 spatial and 1 temporal) was analyzed and a spatio-temporal correlation function was calculated using a modified version of the STICS algorithm [131]. A Gaussian curve was then fit to the spatial correlation function for each time-lag. The center of each Gaussian fit was extracted,

and a line was fit to the center position vs. time lag data to determine the fluid velocity. The range of time lags for fitting the line was selected so that the diffusion constant output by the algorithm was no larger than 1.1 μm2/s (near the expected diffusion constant of the beads). To estimate the measurement error in the fluid velocity, the inverse of the variance for each Gaussian fit was used in a weighted nonlinear least-squares fit of the Gaussian position vs. time lag. The velocity of the cell was determined by measuring the distance the front of the cell had traveled over the time period that was analyzed and dividing by the duration of the time period. Only cells that persistently migrated were analyzed. All analysis was performed in Matlab (Mathworks Inc.). Images were analyzed using only a portion of the channel in which the cell is not present (Figure 2a), as well as using the entire region for certain channels (Figure S2f). Both methods gave similar results.

2.5.5 Polystyrene Bead Functionalization

The polystyrene beads were covalently modified with human serum albumin (HSA) by EDC mediated cross-linking. Briefly, 500 μL of the beads were incubated for 15 minutes with 500 μl of HSA in MES buffer at 5mg/ml. Next, 200 μl of 1-ethyl-3-(3-dimethylaminopropyl)carbodiimide (EDC) in water at 10mg/ml was added to the solution, covered with aluminum foil, and incubated for two hours at room temperature. Following this incubation, 300 μl of Glycine in MES buffer at 500mM was added to the solution and incubated for 30 minutes at room temperature to quench the reaction. The suspension was pelleted and washed with water three times, and finally re-suspended in 500 μl of Hank's Balanced Salt solution supplemented with 0.2% HSA.

2.5.6 Caged fMLF Assay

For the caged-fMLF (cfMLF, synthesized by New England Peptide) experiments, cells were loaded into the device as described above, with the exception that before loading the cells, the device was flushed with an HBSS solution containing 100 nM cfMLF. In addition, cfMLF was added to the needle with the cells to a final concentration of 100 nM. To uncage the fMLF, a two-photon IR laser (Mai Tai, Spectra Physics) was used at a wavelength of 780 nm and a power of 100 mW. The laser excitation was performed for a duration of 3s at various times after the cell had blocked off the bifurcation to ensure stimulation of only one side of the cell.

2.5.7 Image Acquisition and Analysis

Cells were imaged on a Nikon TE2000 microscope (Nikon) with either a 20x Ph1 ADL (Nikon) or 60x Ph3 Plan Apo (Nikon) objective. The microscope was controlled with the Volocity software package (Perkin Elmer, Waltham, MA). For images taken with the 20x objective, ten xy-positions (LUDL BioPrecision XY controlled stage) were taken at a frame rate of 1 frame every 15 seconds, acquiring only bright-field. For images taken with the 60x objective, images were acquired at a frame rate of 1 frame every 3s, in both the GFP and bright-field channels.

For each cell, the central 30% of the channel was extracted, and the image was averaged over the width of the channel for each time point, generating a one-dimensional intensity profile. The edge of the cell was then determined, at each time point, by applying a non-linear filter [135] and thresholding based on maximum and minimum intensities of this intensity profile. All images were analyzed with in-house Matlab (MathWorks Inc.) algorithms.

Fluorescence measurements of Ph-Akt-GFP were taken by measuring the integrated intensity of the first three microns of the extended pseudopod and then normalized by subtracting the value for the high resistance side from the low resistance side and then dividing by the sum of the values. The result is a value that can vary from -1, polarized to the high resistance side, to +1, polarized to the low resistance side. Pseudopod velocities were also normalized using the same approach.

2.5.8 Western Blot Analysis of caged fMLF:

Three different concentrations were tested for each of unmodified fMLF, caged fMLF and uncaged fMLF. A UV DNA gel viewing box with a peak intensity at 312 nm, was used to uncage the caged fMLF. For each condition tested, 8 x 10^6 cells were pelleted at 1500 rpm in a micro-centrifuge for 5 minutes. The cells were then resuspended in PBS and pelleted again. Following this rinse, cells were resuspended in 90 µL PBS and 10 µL of the respective concentration and compound was added to the solution. The sample was then placed at 37 C for 1 minute. The sample was then centrifuged in a micro-centrifuge at max speed for 10-15 seconds. The supernatant was aspirated and the pellet was resuspended in Lysis Buffer (HBS buffer, 1mM DTT, 1mM PMSF, protease inhibitor) and incubated on ice for 30 minutes. The sample was then centrifuged at max speed at 4 C for 15 minutes. The supernatant was then removed and 30 µL was added to 10 µL 4x sample buffer (40% glycerol, 8% SDS, 0.125 M Tric-HCl, 0.02% bromophenol blue, 10% beta-mercaptoethanol). The sample was then run on a 10% polyacrylamide electrophoresis gel and transferred to a nitrocellulose membrane and blotted for phosphorylated Akt (Cell Signaling Technologies, 4060), Akt (Cell Signaling Technologies, 9272) and α-tubulin (Sigma Aldrich, T7451).

Chapter 3: Chemotaxis in Confined Microchannels Reveals Structural Memory

3.1 Overview

The directional response of cells to asymmetric chemical environments involves a complex process, which includes sensing the direction of the gradient, generating an internal biochemical asymmetry and generating migratory motion. To understand how these modules are coordinated to generate directed cell motion requires quantitative measurements of both the cellular response and the external chemical environment experienced by the cells. Here, I investigate the response of cells in confined microchannels to various static and dynamic chemotactic environments. Cells are able to regulate their chemotactic response by altering the persistence, or the time over which they remain polarized. In addition, both uniform concentration and dynamic environments revealed an unexpected directional bias of polarization, which I showed to be the result of a structural memory element, dependent on both microtubules and moesin.

3.2 Introduction

Our understanding of the mechanisms underlying chemotactic polarization has increased tremendously since the initial studies of neutrophils performed by Sally Zigmond roughly 40 years ago [63, 136-138]. In these initial studies, it was identified that cells could respond to even small gradients of certain chemicals by orienting their migration towards higher concentrations of the chemical. Since then, the ever-increasing availability of biologic probes, genetic tools and image processing techniques has led to the identification of two primary signaling modules responsible for

establishing and maintaining chemotactic polarization. These modules were given the names “frontness” and “backness” by Henry Bourne [19], related to the prevalence in determining the leading or trailing edges of a polarized cell, respectively. The “frontness” pathway is dependent on signaling through the G_{ai} class of G-proteins in G-protein coupled receptor (GPCRs) signal transduction [16, 17]. The small Rho-family GTPases, Rac1 and CDC42 are subsequently activated at the leading edge [33, 139], resulting in polarized actin polymerization, directed towards the leading edge of the cell. In contrast, the “backness” pathway is activated via the $G_{12/13}$ class of G-proteins [19], resulting in the activation of the small GTPase RhoA [45] and ultimately leading to polarized myosin contraction directed towards the leading edge.

As demonstrated in the first chapter of this dissertation, the biochemical pathways both within and connecting these modules are quite complex and more connections are continually being discovered. In an attempt to better understand how these complex modules can work, several mathematical models have been developed [64-66, 73] to describe the observed features of the phenomena of gradient sensing and polarization. However, connecting the result from these models to the experimental data has been difficult. The primary difficult lies both in the complexity of the external environment in the assays used and the complicated motion of the cells through this environment. Assays, such as a Zigmond chamber or micropipette stimulation [75, 138, 140], rely on diffusion to generate a gradient, to which the cell responds. Although these assays are quite useful measuring a cells ability to orient in the direction of a gradient, it is difficult to relate the cellular response directly to the external environment experienced by the cell, due to the time evolution of the concentration field over time

through diffusion. Microfluidic technology has produced the ability to generate gradients, which remain stable over time periods as long as several hours [77-79, 141]. However, due to the complex, biased-random walk trajectories taken by the cells in such an environment, it is still extremely challenging to describe the chemical environment experienced by the cell over time.

Several recent publications have made use of microfabrication techniques to generate confining microchannels [82, 142], in which the cellular motion is greatly simplified, reduced to motion along a single dimension. In addition, the strong confinement insides the microchannels allows for the generation of a temporally stable chemical environment. In the following work, I utilize this system to systematically expose cells to various chemotactic environments, characterized by both a baseline concentration and concentration difference. I show that cells respond to weak chemotactic environments with varied levels of persistence, which is measured by the length of time over which a cell remains polarized. In addition, exposing cells to uniform concentrations of chemokine reveals an unexpected propensity to re-polarize in the previous direction of polarization. Through dynamically changing the chemical environment, I show that this directional bias is due to a structural memory element, which is dependent on both microtubule polymerization and moesin activation.

3.3 Results

3.3.1 Cellular Persistence in Static Chemical Difference

I used microfabrication to generate microchannels similar to those published by Irimia et al. [82]. The cross-section of these microchannels (5 microns wide, 3 microns high) are small enough to completely confine cells and allow motion along only one

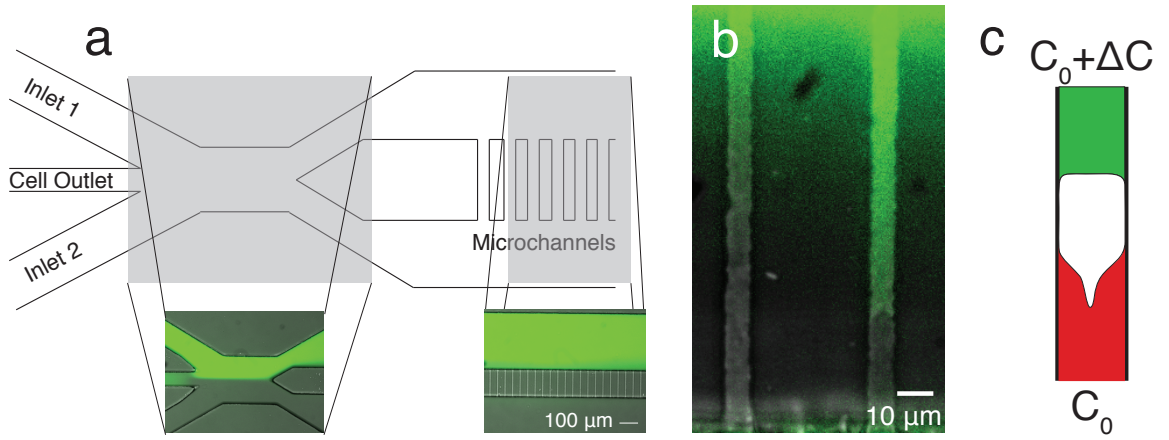

Figure 3-1 l Diagram of operating principles of microfluidic device. a) Cartoon of device geometry. Two inlet channels are used to introduce chemokine solutions into the device. The cell outlet channel is used when cells are introduced into the device from the outlet, downstream of the microchannel region. Insets demonstrate the positioning of the interface between the two inlet flows to balance pressure and maintain concentration difference across the microchannels. Fluorescein dye was used to visualize the separate streams. **b**) Image of microchannels at 40x magnification. Microchannel on right contains a cell. **c**) Cartoon of cell in microchannel with a concentration difference across parameterized by a baseline concentration and a concentration difference.

dimension. As shown in Figure 3.1, the two ends of the microchannel connect to separate reservoirs, which can be kept at different concentrations. Once a cell enters the microchannel it occludes the cross-section, providing the ability to independently expose each end of the cell to different concentrations. Furthermore, due to the fast diffusion (D~500 micron^2/s) of the chemokine used, N-formyl-methionyl-phenylalanine (fMLF), the chemical concentration at both ends of the cell equilibrates extremely quickly, producing an essentially constant chemical environment during the entire time the cell is in the microchannel. This chemical environment can be described by the lower of the two concentrations introduced (i.e. a baseline concentration, C_0) and the magnitude of the difference between the two concentrations (ΔC).

To understand how both the concentration difference and the baseline concentration affect the chemotactic response of a cell, I exposed cells expressing the leading edge marker PH-Akt-GFP, which acts as a readout for production of the

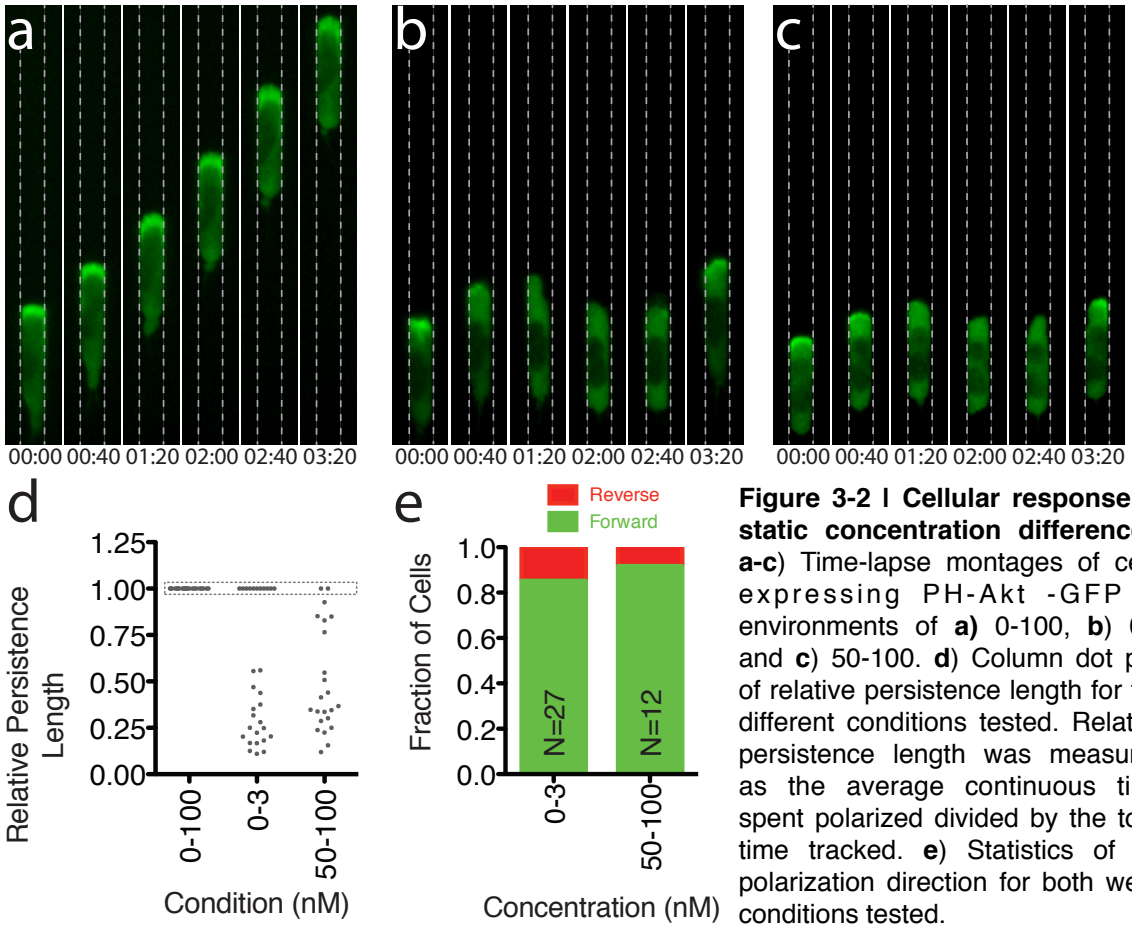

Figure 3-2 I Cellular response to static concentration differences. **a-c**) Time-lapse montages of cells expressing PH-Akt -GFP in environments of **a)** 0-100, **b**) 0-3 and **c**) 50-100. **d**) Column dot plot of relative persistence length for the different conditions tested. Relative persistence length was measured as the average continuous time spent polarized divided by the total time tracked. **e**) Statistics of re-polarization direction for both weak conditions tested.

membrane lipid, phosphoinositol(3,4,5)-trisphosphate (PIP3), to three different chemical conditions. These can be described as the following: 1) a large concentration difference (ΔC=100 nM) across the cell with no background concentration (C_0=0 nM), 2) a small concentration difference (ΔC=3 nM) across the cell with no background concentration (C_0=0 nM), and 3) a large concentration difference (ΔC=50 nM) across the cell with a large background concentration (C_0=50 nM). The concentrations chosen were selected based on an equilibrium binding coefficient of 10-15 nM, similar to what has been reported in the literature [63, 80]. Through the manipulation of on-chip micro-structured valves, cells were introduced into the device such that they would only enter the microchannels from the reservoir with the lower of the two concentrations. Interestingly,

I observed for all conditions that at least a subset of cells remained persistently polarized and migrated the entire length of the channel, suggesting that a static concentration difference is sufficient to drive a chemotactic response.

For each condition, I measured the percentage of the trajectory over which the cell remained polarized. As Figure 3.2d demonstrates, all cells exposed to a large difference and zero baseline concentration responded by maintaining a persistent polarization during their entire trajectory. In contrast, for the other two conditions, which are expected to have small differences in the bound receptor numbers from front to back, a likely determinant of directional sensing, the majority of cells do not maintain persistent polarization. Instead, these cells will fluctuate between polarized and unpolarized. When cells re-polarize, it was observed that the direction of re-polarization was predominantly in the direction towards the higher of the two concentrations. This is consistent with a model that cells are able to detect and orient in response to a small percentage difference in bound receptors across the cell.

3.3.2 Cellular Persistence in Uniform Concentrations Under Confinement

In comparison to the response of HL-60 cells to a stable gradient in an unconfined setting, cells in confined microchannels exhibit a surprisingly strong directional bias to a weak chemotactic stimulus. To test the effect of confinement on the persistence of polarization and the directional bias of re-polarization, cells were allowed to enter microchannels in a uniform concentration of chemokine. To assess any potential effect of the magnitude of the concentration, four different concentrations were chosen, namely 0 nM, 3 nM, 10 nM and 100 nM. To control for any potential bias due to the geometry of the microchannels, cells were introduced into the device such that they

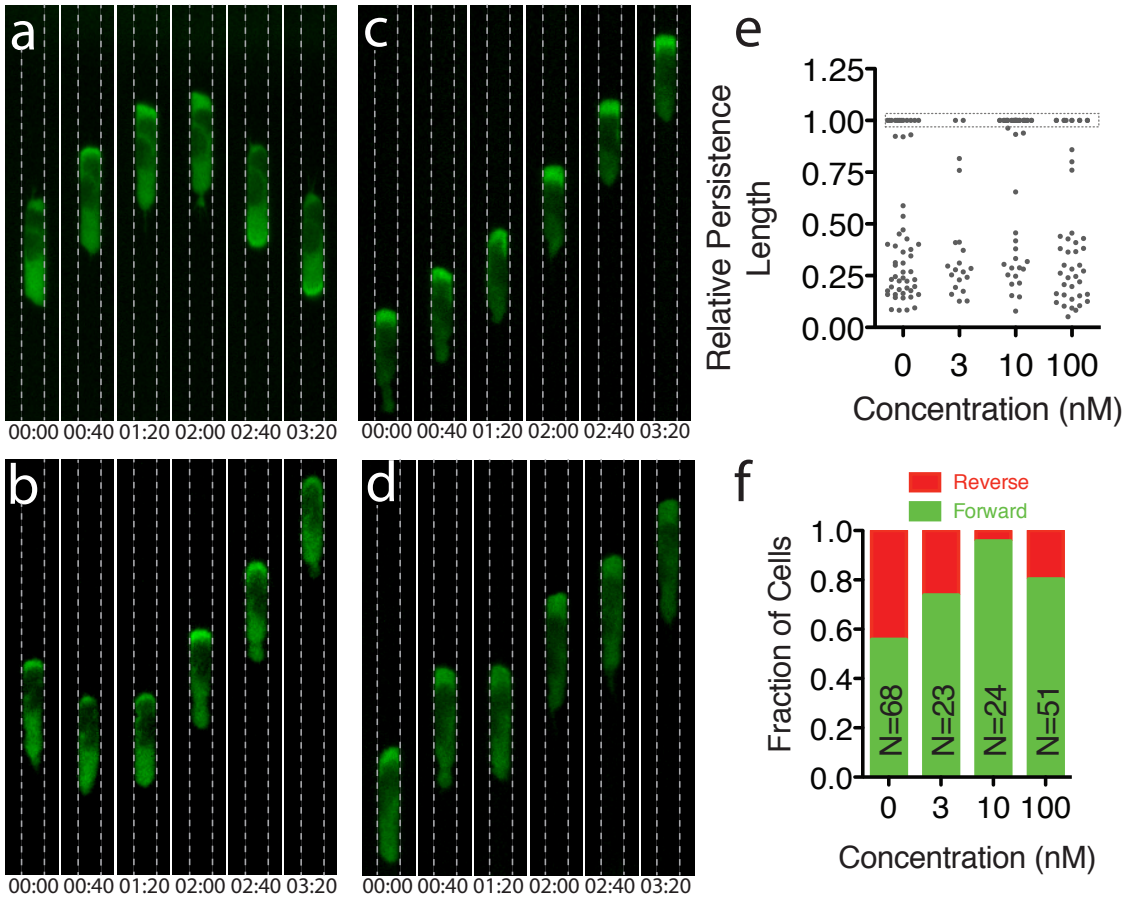

Figure 3-3 I Cellular responses static uniform conditions. a-d) Time-lapse montages of cells in static uniform concentrations of **a**) 0 nM **b**) 3 nM **c**) 10 nM and **d**) 100 nM. **e**) Column dot plot of relative persistence length for the different static uniform conditions tested. **f**) Statistics of re-polarization direction for the static uniform concentrations tested. Green represents cells that re-polarized in the same direction, while red represents cells that switched direction.

could enter the microchannels from either end.

As shown in Figure 3.3e, cells in 0 nM do exhibit a polarization persistence. Approximately 22% of the cells in this condition remained polarized during the entire time they were imaged. Interestingly, cells in both 100 nM and 3 nM uniform concentrations exhibited a similar level of persistence compared to cells at 0 nM, as measured by the percentage of the time course, during which the cells were polarized (Figure 3.3). For all three conditions, fewer than 25% of the cells maintained persistent polarization, with 22%, 10% and 24% exhibiting such behavior for 0 nM, 3 nM and 100

nM, respectively. A statistical comparison of this data, using a Fisher Exact Test, gives that none of these conditions are statistically significantly different from each other. In contrast, however, nearly 60% of cells at a concentration of 10 nM maintained persistent polarization during the entire time tracked. A Fisher Exact Test of this condition with the other three shows that 10 nM is statistically significantly different from the other three conditions, with left-tailed p-values less than 0.025. It is interesting that both low and high concentrations induce markedly lower persistence than a concentration close to that of the equilibrium binding coefficient for the formyl-peptide receptor.

In all conditions, of the cells that did not persistently maintain polarization, many of the cells depolarize and subsequently re-polarize. When the direction in which the cells re-polarized was compared to the previous direction of polarization, it was found that cells in 0 nM fMLF would re-polarize in the same direction as previously polarized 55% of time (N=68), essentially flipping an unbiased coin. Meanwhile, cells in 3 nM, 10 nM and 100 nM exhibited a much stronger directional bias, with 73% (N=23), 96% (N=24) and 80% (N=51) of cells re-polarizing in the same direction as previously polarized, respectively (Figure 3-3f). Both the 10 nM and 100 nM conditions were statistically different than 0 nM, with left-tailed p-values less than 0.005. In contrast, a Fisher Exact Test comparing 3 nM to 0 nM results in a p-value of approximately 0.1. Consistent with the observations of persistent polarization at 10 nM, a comparison the re-polarization statistics at 10 nM to both 3 nM and 100 nM produces a p-value less than 0.05 for both comparisons.

The unexpected observation of both strong persistent polarization and a strong directional bias for cells that re-polarize suggests chemokine stimulation of cells in

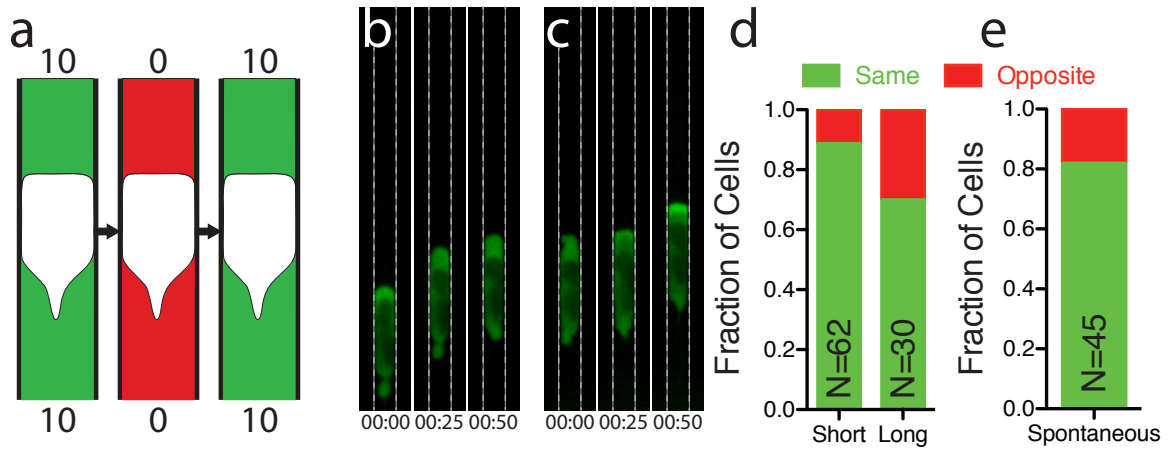

Figure 3-4 I Cellular responses to dynamic changes of uniform concentration. **a**) Cartoon demonstrating dynamic forced depolarization-polarization cycle, to which cells were exposed. **b-c**) Time-lapse montages of cell expressing PH-Akt-GFP responding to **b**) removal and **c**) reintroduction of 10 nM uniform concentration of fMLF. **d**) Statistics of re-polarization direction upon reintroduction of chemokine when cells were exposed to no chemokine for 90 seconds (short) or 10 minutes (long). **e**) Statistics of cells that spontaneously re-polarized after chemokine was removed and prior to reintroduction of chemokine. Green represents cells that re-polarized in the same direction, while red represents cells that switched direction.

confined microchannels might induce a type of long-lived directional memory in the cell, which is able to both stabilize polarization and bias the direction of re-polarization.

3.3.3 Cellular Directional Bias During Forced Depolarization and Re-polarization

To better understand the observed phenomenon of directional bias, cells were exposed to a forced depolarization-polarization cycle (Figure 3-4a). To achieve this, cells expressing PH-Akt-GFP were allowed to enter the microchannels in a uniform concentration of 10 nM fMLF. Once inside the microchannels, the chemokine was washed away, exposing the cells to a uniform concentration of 0 nM. In response to the removal of chemokine nearly all cells depolarized within approximately 45 seconds (Figure 3-4b). The cells were held in this chemical environment for a period of time and the uniform 10 nM concentration was reintroduced. Figure 3.4a provides a diagram of the dynamic environment experienced by the cells. In response to this dynamic stimulus, the cells re-polarized and the direction of polarization was measured. As

shown in Figure 3.4d, greater than 90% of the cells re-polarized in the direction of previous polarization, when cells remained in the 0 nM condition for only 1.5 minutes. These results were independent of both the direction, from which the cell entered the microchannel.

A natural question arising from this observation is over what length of time the directional bias persists. To address this question, cells were exposed to a similar forced depolarization-polarization cycle, increasing the amount of time the cells remained at 0 nM fMLF to 10 minutes. As shown in Figure 3.4d, this resulted in only 70% re-polarizing in the same direction as previously polarized. Comparing the two different lengths of time using a Fisher Exact Test gives a p-value of 0.0295.

Interestingly, it was also observed that following the forced depolarization, a fraction of the cells would spontaneously re-polarize prior to reintroduction of the chemokine. This rarely occurred when the chemokine was removed for only 1.5 minutes, but occurred with a much greater frequency when the chemokine was removed for 10 minutes. Similarly to when cells re-polarized in response to the re-addition of chemokine, it was found that 80% (Figure 3.4e) of cells that spontaneously polarized did so in the direction, in which they had been previously polarized. These results strongly suggest an internal directional memory that persists following a depolarization of the cell, and which is able to bias the direction in which a cell re-polarizes.

Finally, I tested whether the external chemical environment might be able to somehow overcome this directional memory. To address this, cells were again exposed to a similar dynamic environment as described above. However, instead of reintroducing

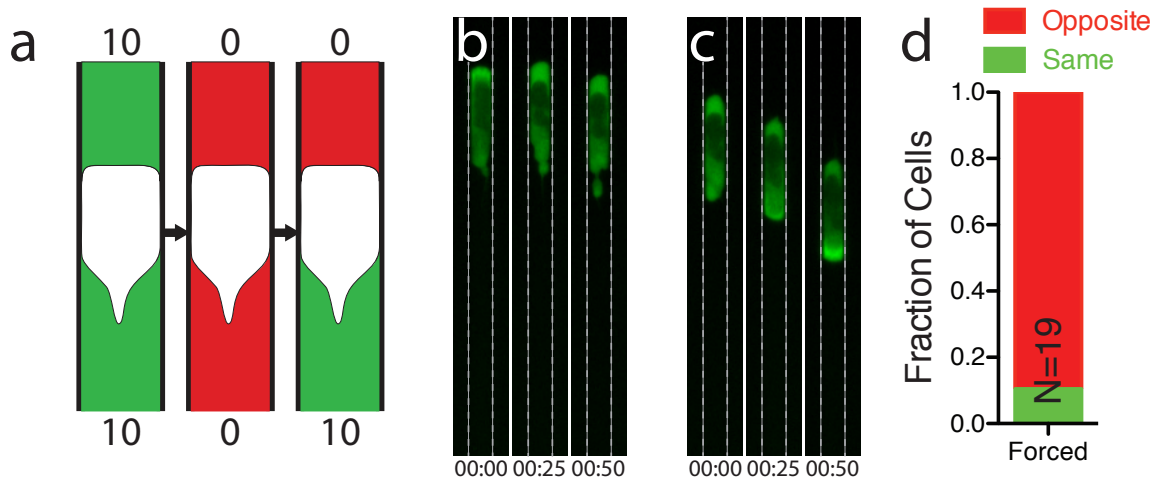

Figure 3-5 l Cellular responses to a forced flipping depolarization-polarization cycle. a) Cartoon demonstrating dynamic forced flipping cycle, to which cells were exposed. **b-c**) Time-lapse montages of cell expressing PH-Akt-GFP responding to **b**) removal of chemokine and **c**) introduction of opposing 10 nM concentration difference of fMLF. **d**) Statistics of re-polarization direction upon reintroduction of chemokine. Green represents cells that re-polarized in the same direction, while red represents cells that switched direction.

chemokine on both ends of the channel to generate a uniform concentration, fMLF was reintroduced on only one end of the channel, generating a concentration difference across the cell. Figure 3.5a demonstrates the dynamic environment experienced by these cells. Cells were separated into two populations based on their orientation relative to the imposed concentration difference prior to the removal of chemokine. The first population included all cells, which were initially polarized so that when the concentration difference was introduced, the previous leading edge of the cell was exposed to chemokine and the trailing edge was unstimulated. It was observed that all cells in this population re-polarized in the same direction, in which they had previously been polarized. Meanwhile the second population included all cells, which were initially polarized so that the previous trailing edge was exposed to chemokine and the leading edge was unstimulated. As shown in Figure 3.5d, nearly 90% of these cells flipped direction of polarization upon reintroduction of the concentration difference, to orient in

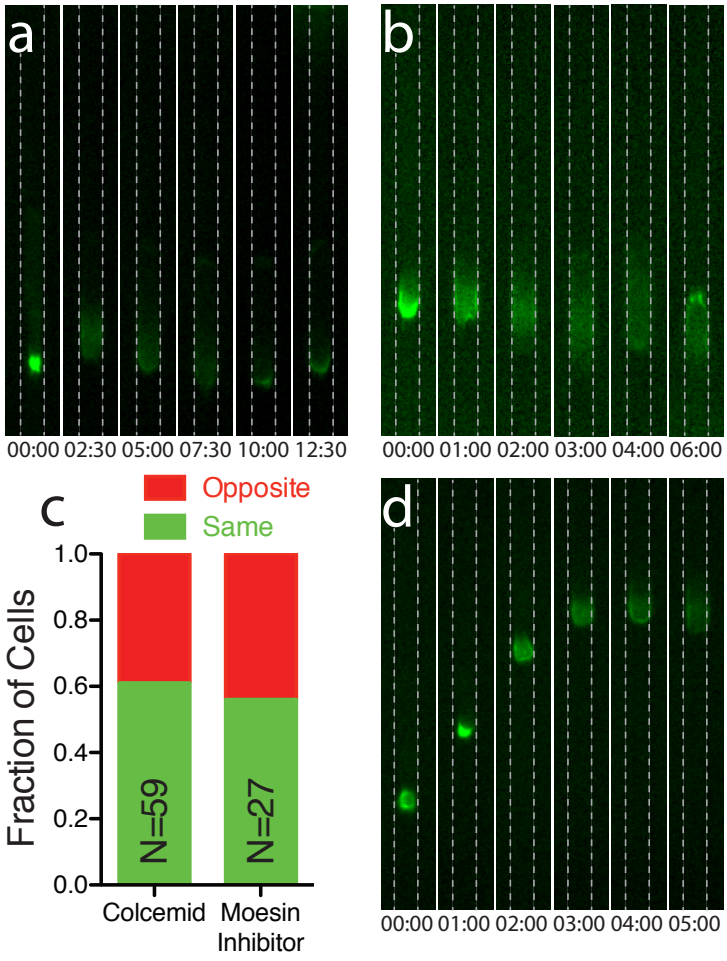

Figure 3-6 I Molecular nature structural memory. a) Time-lapse montage of cell expressing moesin-GFP responding to removal of chemokine. Localization of moesin to the rear of the cell persists for greater than 12.5 minutes. **b**) Time-lapse montage of a cell expressing moesin-GFP following removal of chemokine and simultaneous introduction of moesin inhibitor. An increased time step was chosen for the last panel to demonstrate ability of cell to re-polarize. Chemokine was reintroduced at 05:00. **c**) Statistics of re-polarization direction of cells expressing PH-Akt-GFP in response to forced depolarization-polarization cycle in the presence of a microtubule or moesin inhibitor. **d**) Time-lapse montage of cell expressing moesin-GFP following removal of chemokine. The strong polarization of moesin to the rear of the cell persists for nearly 3 minutes following chemokine removal. During this time, the cell continues to migrate forward at nearly a constant speed.

the direction of the concentration difference. This shows that the strong directional memory evident in uniform concentrations of chemokine can be overcome by an imposed competing directional chemotactic stimulus.

3.3.4 Molecular Nature of Directional Memory

Given the relatively long-lived nature of the directional memory observed, it is likely to be the result of some asymmetrical structure inside the cell. One such potential structure would be the microtubule network inside the cell. Previous observations in neutrophils demonstrated that microtubules redistribute to the sides and rear of a cell upon polarization [143]. In addition, it is reasonable to expect that microtubules persist over the duration of the experiment. To test the role of microtubules in cellular

directional memory, cells were again exposed to a forced depolarization-polarization cycle. In this case however, the microtubule depolymerizing drug colcemid was added to the buffer solution used to wash out the chemokine. Thus, microtubules were inhibited until the cells were not stimulated, and the effect of the drug on the ability of the cell to polarize and the direction of polarization could be assessed. As shown in Figure 3.6, cells treated with this dynamic environment exhibited a greatly decreased directional memory, with only 60% of the cells re-polarizing in the same direction as previously polarized.

Another potential molecule, which could provide a long-lived structure inside a cell is the ERM family protein, moesin. Members of the ERM protein family have been shown to bind to both cortical actin and the cell membrane, forming a direct link between the cytoskeletal cortex and the membrane. Measurements of moesin turnover at the cell cortex have shown that it is a relatively stable structure [144]. Figure 3.6 shows a cell expressing a GFP-tagged moesin. This cell was exposed to a forced depolarization as previously described. This clearly demonstrates that moesin strongly localizes to the rear of a polarized cell. Furthermore, the distribution of moesin within the cell exhibits a rearward asymmetry even after more than 10 minutes (Figure 3-6a).

To test whether moesin plays a role in the directional memory, cells were treated with a moesin inhibitor (7-(3,5-dibromo-4-hydroxyphenethylamino) quinoline-5,8-dione). This inhibitor binds to moesin and blocks the phosphorylation that is necessary for proper actin binding. Cells expressing moesin-GFP treated with this inhibitor exhibited a nearly symmetrical distribution of moesin within 4 minutes after introducing the drug (Figure 3-6b). Cells expressing PH-Akt-GFP were then treated similarly as with

microtubule inhibition, with the exception that the drug was not washed out and chemokine reintroduced until 4 minutes following the forced depolarization. As shown in Figure 3.6c, cells treated with the moesin inhibitor exhibited a nearly unbiased response, with only 55% of the cells re-polarizing in the same direction as previously polarized. The near complete disruption of directional memory resulting from moesin inhibition strongly suggests that moesin plays an important in this phenomenon.

Finally, as shown in Figure 3.6d, many cells expressing moesin-GFP maintained a strongly polarization distribution of moesin for a significant time following removal of the chemokine. Although a similar response was extremely infrequently observed in cells expressing PH-Akt-GFP, the frequency of such a response in cells expressing moesin-GFP was significantly higher.

3.4 Conclusions

Here I described the response of cells to various chemotactic environments in confined microchannels. Due to the confinement of the microchannels, I was able to expose cells to a static chemotactic environment in which both the baseline concentration and concentration difference across the cell remained constant over time. It is important to note that this static difference was sufficient to drive chemotactic behavior. This suggests that cells are able to employ a spatial sensing mechanism, in which the magnitudes of the concentration along the cell membrane are compared. However, this does not rule out a role for a temporal sensing mechanism.

Cells were exposed to weak chemotactic environments, by generating either a small difference across the cell, or a high baseline concentration. The response of the cells to these environments revealed that a decreased chemotactic response in such

environments is the result of a decreased persistence, as measured by the percentage of the time tracked, over which the cell remained polarized. The ability of both a small concentration difference and a high baseline concentration to decrease cellular persistence is consistent with a model that the chemotactic response is driven by the difference in bound receptors between the leading and trailing edge of the cell. A similar model was proposed by Herzmark et al. [145] based on the response of HL-60 cells exposed to a stable gradient of chemokine. However, this study generated exponential gradients to maintain a constant value for the ratio of the concentration difference and average concentration across the cell. As a result, the cells experience a changing concentration difference and average concentration as they migrate through the gradient. In comparison, microchannels provide the ability to measure the response to a single concentration difference and average concentration.

It was also observed that in both weak chemotactic conditions cells that depolarized and subsequently re-polarized almost exclusively did so in the same direction, in which they had been previously polarized. Similarly, cells exposed to uniform concentrations of chemokine in confined microchannels exhibit a strong directional bias. Merely being confined in microchannels is not sufficient to induce this directional bias, as cells that spontaneously polarize without any chemokine do not exhibit a directional bias. This is in sharp contrast to the results shown by Herzmark et al. [145], in which a subset of HL-60 cells in a stable gradient migrated a significant distance against the gradient.

It is intriguing that the cellular directional bias is dependent on chemokine activation. As measured by the ability to localize the PH-Akt-GFP leading edge marker,

cells that polarize without chemokine do not appear different from those that polarize under chemokine stimulation. However, cells in these conditions do differ greatly in the directional bias they exhibit. One possible explanation of this discrepancy is that the activation of directional memory is independent of leading edge PIP3 production. Instead, chemokine stimulation is able to activate multiple pathways, one of which results in the directional bias. It is also feasible that although spontaneous polarization activates leading edge PIP3 production, the pathway responsible for the directional bias might only be activated by chemokine stimulation. It would be interesting to see how moesin over-expression could affect persistence in both the absence of chemokine and the presence of a uniform, low concentration of fMLF.

One interpretation of the observed directional bias is that a polarized cell develops a structural memory, which can then bias the direction of (re-)polarization. This interpretation is further supported by the observation that cells exposed to a depolarization-polarization cycle, in which the chemokine is removed and then reintroduced after some time, are extremely biased to polarize in the same direction as they had previously been polarized. Inhibition of either microtubule polymerization and moesin activation is able greatly diminish, if not completely abolish this directional memory. How these elements are able to interact with the polarization signaling pathway is unclear. However, moesin has been shown to bind microtubules [146] and both moesin and microtubules have been shown to interact with guanidine nucleotide exchange factors (GEFs) for the GTPase RhoA [147-149], which has been shown to be most active at the sides and rear of a polarized cell [45]. It is intriguing to think that moesin and microtubules might interact to help localize the other. The slow turnover of

both of these molecules might act synergistically to maintain an asymmetrical distribution of activating GEFs for RhoA and thus bias the direction of polarization when chemokine is reintroduced. Such a mechanism could also explain how the activation of the memory would be dependent on chemokine stimulation. It has been shown that RhoA is activated through an independent pathway from that of the leading edge PIP3 production. Thus it is feasible that RhoA may not become active in the absence of chemokine stimulation.

In retrospect, the observation of a directional bias in a chemotactic cell is perhaps not as surprising as one might think. Cells exposed to a uniform concentration of chemokine while on a flat surface, in an unconfined setting, respond by polarizing in a random direction and subsequently migrating in trajectories often considered to be random walks. However, as they migrate, cells change direction by turning, as opposed to completely depolarizing and subsequently re-polarizing in a new direction. This is also suggestive of a structural memory inside the cell acting to maintain a specific front and back. The confinement of cells in microchannels has served merely to elucidate the phenomenon, as a change of direction would require the cell to depolarize and then re-polarize in the opposite direction.

Finally, it was observed that many cells expressing moesin-GFP, when exposed to a forced depolarization by removal of the chemokine, continued to migrate, unaffected. It is likely that expression of this construct results in an over-expression of moesin and possibly an over-activation of the structural memory, which is then able to maintain persistent polarization. The potential interplay of directional memory and persistence is intriguing, with possible implications for how cells might be able to

navigate the complex environments found in tissues and reach the site of an infection. As cells migrate through tissue from the blood to the site of an infection, they likely experience chemical gradients emanating from multiple sources. To properly fight an infection, it is important that neutrophils are able to traverse the entire extent of the affected tissue. The ability of a structural memory to enhance the directional persistence of a polarized cell could allow the cell to avoid getting trapped at a single source.

3.5 Materials and Methods

3.5.1 Cell Culture and Stable Line Production:

HL-60 cultures were maintained in RPMI 1640 (Invitrogen, 11875119) media supplemented with 20% FBS (Invitrogen, 26104), 1% Penstrep (Cellgro, 30-002-CI), and 25 mM sterile filtered HEPES (Fisher Scientific, BP310), and were passaged every 2-3 days. Cells were differentiated in complete media supplemented with DMSO to a final concentration of 1.3%. Cells differentiated for at least 5 days and not more than 7 days were used for experiments.

Cells stably expressing moesin-GFP were a kind gift of Dr. Guillaume Charras.

Cell lines stably expressing PH-Akt-GFP were generated via retroviral infection, as described previously [126]. Briefly, Plat-GP cells (Cell Biolabs, San Diego, CA) were used to produce retrovirus by co-transfection with a pBABE packaging vector (pBABEblast, pJag98, [134]) containing the cDNA for 3xPH-Akt-GFP (cDNA obtained from Dr. Lew Cantley, Harvard Medical School) and VSV-G, using Fugene 6 (Roche, Germany). The viral supernatant was collected after 48-72 hours and filtered using a 0.45 micron syringe filter. Polybrene was added to the supernatant at a final concentration of 16 micrograms/mL. Cells were suspended in one well of a 6-well plate

at a concentration of 106/mL in a volume of 2 mL. To this suspension was added 5 mL of viral supernatant and the cells were spun at 1000xg for 90 minutes in a swinging bucket rotor. Cells were then incubated for 5 hours at 37 C. Following this incubation, cells were pelleted and resuspended into 2 mL fresh media. The next day, 2 mL of fresh media was added to the cells. The next day, cells were placed under selection in 1 micrograms/mL blasticidin. Once a stable pool of blasticidin resistant cells was obtained, the cells were then sorted for GFP expression (HMS/Systems Biology Flow Cytometry Facility).

3.5.2 Microfluidic Device Fabrication

Microfluidic devices were generated as described previously [81]. High-resolution film (Fineline Imaging, Colorado Springs, CO) or chrome (Advanced Reproductions Corp, Andover, MA; Front-Range Photomasks, Colorado Springs, CO) masks were used to generate photoresist masters. SU-8 (Microchem, Newton, MA) was spun onto silicon wafers at a rate according to the feature height desired. The photoresist was then exposed to UV light using a mask aligner (Neutronix Quintel, Morgan Hill, CA). Unexposed SU-8 was developed away. PDMS was then either spun (for membranes) or poured onto the wafers, cured overnight at 70 C. The top layer of the devices was then cut out, access holes were punched for pneumatic valve control using a 0.75 mm diameter punch, and the devices were then bonded to the spun membrane using oxygen plasma. These devices were again cut out and additional fluid access holes were punched and the devices were then bonded to either 1x3 glass slides (Fisher Scientific, Pittsburgh, PA), or 45x50 mm No. 1.5 coverslips (Fisher Scientific, Pittsburgh, PA).

3.5.3 Microfluidic Device Operation

Tygon tubing (Greene Rubber Company, part no., 2007900S-54HL) and 30 gauge blunt syringe needles (Brico Medical Supplies, BN2505) were used to connect syringes to the microfluidic devices. The outer diameter of the tygon tubing (0.03 in) is slightly larger than the diameter of the hole punched, so when the tubing was inserted into the hole, a seal was created. Each of the pneumatic valve control chambers was connected to a 1 mL syringe. To close the valves, the syringe was compressed from a volume of 0.2 mL to approximately 0.05 mL. To open the valves, the syringes were pulled open from a volume of 0.2 mL to the maximum volume of the syringe.

Fibronectin was adsorbed onto the channel walls by filling the device with a solution containing 50 micrograms/mL fibronectin (Sigma-Aldrich, F0895) in 50 mM Tris-HCl. Any air bubbles present were removed by pressurizing the device. The solution was incubated in the device for 1 hour at room temperature and then rinsed out with HBSS supplemented with 25 mM HEPES and 0.2% human serum albumin.

Each inlet was connected to a syringe, with the plunger removed. One syringe contained a solution of HBSS, while the other contained a solution of HBSS with fMLF. Fluorescein was added to the syringe containing fMLF to visualize the interface of the two inlet streams for balancing the stream pressures. To reduce the introduction of air bubbles while loading cells, a drop of HBSS was placed onto the cell inlet hole prior to removing the priming tubing.

To load cells into the device, 2-3 mL of differentiated cells were pelleted and 30 µL of the cell pellet was taken and placed into a blunt needle with a short section of tubing. The cells were then pushed through the tubing by applying pressure to the top of

the needle with a finger, until a small drop appeared at the end of the tubing in order to provide a liquid-liquid interface while inserting the tubing to prevent the introduction of air bubbles. The cells were then pushed into the device by applying pressure with a finger and the on-chip valves were manipulated to control whether cells were loaded on only side of the microchannels or on both sides.

To expose cells to dynamic changes in the chemical environment, cells were loaded into a device as described above and allowed to enter the microchannels in a uniform concentration of 10 nM fMLF, by clamping off the tubing from the 0 nM reservoir. The chemokine was then washed away by clamping off the 10 nM inlet tubing and releasing the 0 nM tubing. Chemokine was reintroduced by again clamping the 0 nM inlet tubing and releasing the 10 nM inlet tubing. For the experiments in which either microtubule or moesin inhibition was tested, either 10 μm colcemid (EMD Millipore) or 10 μm NSC688394 (EMD Millipore) was added to the 0 nM reservoir.

3.5.4 Image Acquisition and Analysis

Cells were imaged on either a Nikon TE2000 microscope (Nikon) or a Nikon Eclipse Ti (Nikon) with a 40x Ph3 Plan Apo (Nikon) objective. The microscopes were controlled with the Volocity software package (Perkin Elmer, Waltham, MA) or Nikon Elements (Nikon), respectively. Images were acquired at a frame rate of 1 frame every 5s, in both the GFP and bright-field channels.

For each cell, the central 30% of the channel was extracted, and the image was averaged over the width of the channel for each time point, generating a one-dimensional intensity profile. The edge of the cell was then determined, at each time point, by applying a nonlinear filter (Chung 1991) and an adaptive threshold was

implemented with a constraint on cell length determined from the previous frame to find the edges of the cell. All images were analyzed with in-house Matlab (MathWorks Inc.) algorithms.

For each time point, the integrated intensity of a 5 micron deep region at each end of the cell was measured. The polarization was then determined by subtracting the value for one side of the cell from that for the other side and then normalized by dividing by the sum of the values. In the case when a concentration difference was introduced, the end of the cell at the lower concentration was subtracted from the end at the higher concentration. In the case when a uniform concentration was used, the subtraction order was determined based on the direction of the initial polarization when the cell first entered the microchannel. The result is a value that can vary from -1, polarized to the low concentration (or opposite the initial direction), to +1, polarized to the high concentration (or along the initial direction).

Chapter 4: Discussion and Future Directions

4.1 Cellular Responses in Bifurcation Microchannels

Our observations of cells in bifurcating microchannels elucidated a fascinating phenomenon in which the direction of migration for cells is biased by the relative hydraulic resistances of the two channels. A deeper understanding of this phenomenon and the underlying mechanisms requires further study into three sub-processes. First, it is necessary to better characterize the sensitivity of the cells to various baseline resistances and resistance differences. This may also elucidate the nature of the forces that bias pseudopod extension. Second, the experimental system provides an excellent opportunity to observe the processes involved in the competition between two extending pseudopods. Understanding how cells are able to determine which of the pseudopods is longer is vital to understanding directional migration, and has implications for situations where cell may need to resolve other competing stimuli such as those seen during chemotaxis in tissue. Finally, understanding what determines the timing of when one of the pseudopods is retracted could provide insight into the mechanisms underlying the maintenance of a single direction of polarization.

4.1.1 Mechanisms of Force Sensitivity

One particularly interesting question that arises from our observations of cells in bifurcating microchannels is how the small differences in forces resulting from the fluidic resistance are able to bias the direction of cell migration. Numerous studies of cells migrating on flat surfaces have shown that cells are capable of generating forces of up to 10's of nanonewtons as they migrate [150-152]. In addition, Usami et al. demonstrated that neutrophils in a confined micropipette were able to migrate against

an externally imposed pressure difference resulting in forces up to 30 nanonewtons in magnitude [153]. The force necessary to push a column of water through a microchannel is given by the following equation:

$$F = v * R * A^2$$

where v is the cell velocity, R is the hydraulic resistance of the channel and A is the channel cross-section. Substituting the approximation for the hydraulic resistance of a rectangular channel, given by Fuerstman et al. [132] gives the following equation:

$$F = \frac{12\mu L w v}{h\left(1 - 0.63\frac{h}{w}\right)}$$

Using a length of 50 μm, a width of 6 μm, a height of 3 μm, the viscosity of water and a cell velocity of 0.5 μm/s, gives a force of approximately 1 piconewton. Thus, the difference in force between the two branches of the bifurcation is only 100s of femtonewtons. This leads to the question of how cells capable of generating forces as high as 10's of nanonewtons can be sensitive to force differences that are five orders of magnitude smaller.

One potential explanation is that the force sensitivity of cells is dependent on the magnitude of the force being generated by the cells. This model would suggest that the same difference in fluidic resistance will generate a smaller directional bias at a higher baseline resistance. Through manipulating both the length and cross-section of the

bifurcating microchannels, it is possible to generate resistances up to 100-fold higher than those used in this study. Measuring the directional bias in these channels, in which either the absolute resistance difference or the relative resistance difference is left unchanged, can provide valuable insight into whether the force sensitivity of cells is dependent on the baseline force generated by the cells as they migrate.

The force generating capability of both actin and myosin are areas of high interest in the field of cell biophysics. *In vitro* studies of both actin and myosin have shown that a single polymerizing actin filament can generate up to 1.5 pN of force [154], while the myosin power stroke is capable of generating a peak force of approximately 5 pN [155]. In contrast, a meshed actin network has been shown to be capable of generating forces of several hundred nanonewtons in magnitude [156]. In addition, fast-moving fish keratocytes have been measured to generate adhesion forces of up to 20 nanonewtons [152], while fibroblasts can produce forces as high as 1200 nanonewtons [157]. It is generally thought that these forces are generated by myosin contractility, which is supported by the fact that actomyosin networks reconstituted *in vitro* have been shown capable of generating these large forces [158].

Despite this evidence of the large force generating capacity of the cytoskeletal network, relatively small forces have been shown to disrupt leading edge protrusion of keratocytes. A micropipette was used to generate small-scale flows in opposition to the migration of keratocytes. The forces generated by these flow were calculated to be approximately 13 pN. One model that would explain this is that the large contractile forces generated at the back of the cell are dissipated by the viscoelastic cytoplasm as well as the friction of adhesions [159]. This model would predict that disrupting this

dissipation would result in a decreased sensitivity of the cells to piconewton-scale forces. It is unclear what provides the viscoelastic properties of the cytoplasm, but one possibility is the intermediate filament network. Many types of intermediate filaments are found inside the cell, and can generate an extensive network of filaments. In addition, these filaments can interact with both focal adhesion complexes as well as other components of the cytoskeleton. Thus, it is possible that intermediate filaments could instill the cytoplasm with properties of a porous gel, capable of dissipating forces generated by both adhesions and intracellular fluid flow. Moreover, it has recently been shown that formin-mediated F-actin polymerization is necessary for the migration of cells in confinement, which could contribute to the viscoelastic properties of the cytoplasm [37]. The authors propose that role of the formin-mediated F-actin is to generate a physical barrier in the cell, which prevents the retrograde motion of the branched network generated at the leading edge, instead enabling new polymerization to exert forces to propel the leading edge forward. It is appealing to think that such a structure could imbue the cytoplasm with significant visco-elastic properties.

Even if the separation of leading edge and trailing edge forces can be explained, it is unclear how the leading edge is even able to detect the magnitude of the resistant force. One appealing model is that the rate of actin polymerization is dependent on the load, and thus the cells are biased toward the lower resistance bifurcation due to an increased actin-mediated protrusion rate. However, given that *in vitro* actin networks can generate hundreds of nanonewtons of force and exhibit a load-independent extension rate within this range, this model is unlikely. Nevertheless, such a model could be tested by direct measurement of the actin polymerization rates at the leading

edges, through methods such as Fluorescence Recovery After Photobleaching or Fluorescent Speckle Microscopy.

Another potential mechanism lies in the function of the actin regulator WAVE. This molecule has been shown to exhibit propagating waves within the cell [69] and is reportedly extremely sensitive to physical perturbations [68]. It is feasible that the leading edge forces could regulate the intensity and dynamics of these waves, thus affecting actin polymerization and protrusion. Measurements of WAVE activity in both pseudopods during extension into a bifurcating microchannel could provide insight into the effect of hydraulic resistance on actin polymerization.

Substrate adhesions are another potential point of force sensing. The difference in force required at each leading edge could result in differential rates of adhesion formation, which in turn could regulate downstream signaling to the actin polymerization network, and thus leading edge protrusion. Visualizing adhesion formation on the timescales of fast cell migration would be extremely difficult. However, disrupting the ability of the cell to adhere to the surface would provide insight into the role of adhesions in this process. This could be achieved by coating the channels with (poly)-ethylene glycol (PEG) [160, 161]. The surface chemistry of this coating provides a surface which the adhesion molecules involved in neutrophil migration, including integrins and selectins [162, 163], cannot stick.

Finally, it is also possible that the physical properties of the membrane itself are sensitive to the forces generated. It is feasible that the differences in forces could generate differential, micro-scale curvature of the membrane. Several studies have identified regulators of Rho family GTPases, containing a BAR domain, which is a lipid

binding region believed to be sensitive to local membrane curvature and tension [164].

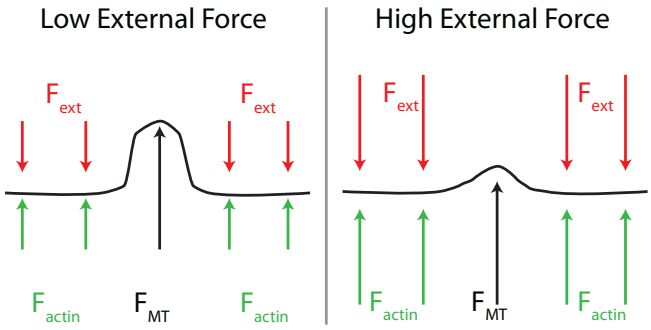

Figure 4-1 I Model of microtubule induced curvature. Under low external force, the actin network also generates a low force. Thus, the local forces applied by microtubules can cause a large local deformation of the membrane. Under high external force, the actin network is able to adapt, while the microtubule force remains unchanged. As a result, the local microtubule-generated forces produce significantly less membrane deformation.

Visualizing the activation dynamics of the GTPases CDC42 and Rac at both leading edges would provide insight into whether such a signal transduction mechanism is involved.

A set of follow-up experiments performed by Chi-Han Chang, another graduate student in our lab, using the microtubule inhibitor maytansine have demonstrated that disruption of microtubules significantly diminishes the ability of the cell to determine the direction of lower resistance. However, microtubule inhibition does not appear to alter the correlation between the pseudopod extension asymmetry and the ultimate direction of migration. It is noteworthy that several studies suggest that microtubules can play a role in Rho family GTPase signaling [165-167], presumably by either sequestering signaling molecules, or by allowing for trafficking of signaling molecules to the GTPases. Additionally, microtubules themselves are able to exert forces on the membrane. In contrast to the meshed actin network found at the leading edge, microtubules are likely to be sparsely distributed around the membrane. Thus, when forces are generated by microtubules, they would be highly localized, generating localized regions of high membrane curvature at the point of contact (Figure 4-1). If at the same time, the cell is generating additional forces on the membrane, as might be

expected while pushing a column of water, this could result in diminished curvature generated by the localized microtubule forces. A potential experiment to test this model would employ biosensors of membrane curvature [168]. In addition, microtubules could be imaged to determine if regions of high curvature coincide with microtubules. Alternatively, the extent of membrane curvature could also be measured following treatment with microtubule inhibitors.

4.1.2 Molecular Mechanisms of Directional Decision

Whatever the mechanism of force sensing, active or passive, our data demonstrates that the direction of migration in bifurcating microchannels is determined by the pseudopod length asymmetry, while the asymmetric hydraulic resistance serves only to bias the direction of the length asymmetry. It is unclear how cells might be able to compare the lengths of the two pseudopods. Furthermore, the cross-sections of the two directions of the bifurcation are equal, thus the cytoplasmic volume of each pseudopod is directly linked to the length of each pseudopod. As a result, it is unclear whether the cell is responding to differences in pseudopod length or volume. One potential mechanism for measuring length would be the response to a diffusible signal that is released from the back at a certain time. The time it would take this molecule to diffuse to the front of the leading edge depends only on the length of the leading edge. Meanwhile, it is possible that the pseudopod with more volume would have a larger store of some limited signaling molecule important for pseudopod extension. To differentiate between these two potential mechanisms, cells could be loaded into bifurcating microchannels, in which the two directions of the bifurcation have different cross-sectional areas. As a result, two pseudopods of equal volume would extend for

different lengths down the different directions of the bifurcating channels. The ultimate

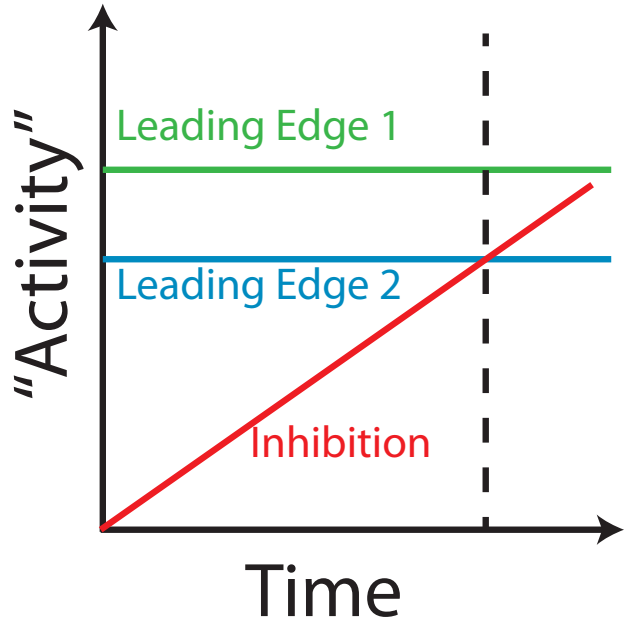

Figure 4-2 | Model of differential leading edge activity. In this model, each leading edge in the bifurcation has a different level of activity. This could result from active sensing of force generation, or from passive regulation by the external environment. As the leading edges continue to extend into the bifurcation, a global inhibitory signal increases. This could be an increase in RhoA activation due to the presence of two leading edges, or a gradual increase in membrane tension. It is also possible that depletion of some limited substrate would produce a similar effect. Whatever the signal, at some point in time, the "activity" of the inhibitory signal becomes strong enough to cancel the activity at one of the leading edges.

direction of migration could then be compared to both the difference in length and the difference in volume independently.

A further possibility is that the cell is not actually measuring the pseudopod length, but rather the difference in activity of some molecule between each pseudopod. This would imply that the length asymmetry is merely a result of this underlying process. One model of how this could occur is that over time as the cell extends both pseudopods farther, a background inhibitory signal globally increases in strength. At some point, the global signal has grown large enough that it is able to completely cancel one of the pseudopods (Figure 4-2). Once this occurs, the global signal ceases to increase in strength, leaving only the longer, or "more active", pseudopod, retracting the shorter, or "less active" pseudopod. Although this is an intriguing model, more study is necessary to identify whether such an inhibitory signal exists.

Due to their important role in actin-mediated protrusions, the Rho family

GTPases, Rac1 and CDC42 are appealing candidates for such a signal. As was mentioned above with regards to force sensing, activation of these GTPases could potentially be sensitive to the forces exerted by the cell. However, a complicating factor is the fact that F-actin-dependent feedback loops have been identified in the activation of Rho family GTPases [38, 39]. Thus it would be difficult to determine whether any observed differential activation is the direct determinant of ultimate direction of migration, or if it is merely the result of differential activation of another portion of the pathway. I believe that discriminating between the processes of force sensing and directional decision-making in confined microchannels will require advancements in experimental capabilities to expose cells to well controlled dynamic changes in external force. Exposing cells to sudden changes in the external forces and measuring the cellular response to these changes will help to separate the processes of force sensing from passively biased migration. However, in order to achieve robust control of hydraulic forces at the piconewton scale in confined microchannels requires the ability to regulate pressures with millipascal precision. This scale of pressure is equivalent to the pressure generated by a column of water only a few microns high. This represents a significant design challenge.

4.1.3 Timing of Retraction of Losing Leading Edge

The final step in the process of directional decision-making in the bifurcating microchannels is the signaling to initiate retraction of one of the pseudopods. Our data suggests that this timing might depend on the distance of the back of the cell from the bifurcation. Although there is much evidence that signaling at the front and back of a polarized cells is connected, it is unclear how the pathways involved could affect one

pseudopod more than the other, and so dramatically only at a specific time. Recently, it has been shown that membrane tension might play a role in localizing the signaling at the front [60]. It was also shown that a high baseline tension resulted in a reduced ability of the cell to polarize in response to chemokine. It is possible that tension could similarly play a role in the retraction timing. It is believed that the uropod is a stiff structure, with strong connections between the membrane and the cortical acto-myosin at the back of the cell. It is feasible that as this region approaches the bifurcation and starts to bend around the corner of the bifurcation, the rigidity of the cortex causes a large increase in membrane tension. This tension could be rapidly transmitted to both leading edges producing a negative signal for pseudopod extension.

Testing such a hypothesis would be very challenging. Visualizing changes in membrane tension is extremely difficult and methods to alter membrane tension are likely to affect many other pathways. One potential approach would be to alter the curvature of the corner of the bifurcation. A more gradual change in direction might produce a smaller stress on the cortical acto-myosin, resulting in a decreased change in membrane tension, allowing for the back of the cell to approach closer to the bifurcation junction prior to initiating a retraction signal.

Another potential mechanism relies on the propagating wave characteristics of the WAVE complex [68, 69]. It is possible that the waves generated in each pseudopod share a common origin, which could be in the body of the cell, in proximity to the rear of the cell. When the majority of the cell has yet to enter the bifurcation junction, this origin could produce a single propagating wave, which is able to split to each leading edge. However, as the back of the cell approaches close to the bifurcation, it is conceivable

that at come point, it is no longer possible for waves generated at the origin to reach both pseudopods. As a result, WAVE activity in one pseudopod would be turned off, allowing for the elements of the “backness” pathway to take over and initiate retraction. Measuring the spatiotemporal dynamics of WAVE activity and actin polymerization using TIRF microscopy would provide insight into whether such a mechanism is employed by the cells.

4.2 Cytoskeletal Memory in Confined Microchannels

As I move now to a discuss of the results of cellular responses to chemotactic cues, it is important to reiterate that the experimental microchannel system used for this study took advantage of two key features. First, the system allows for extremely fast and precise changes of the external chemical environment, providing the ability to study the dynamics of polarization and depolarization in response to well-quantified stimuli. Second, the ability to expose only two sides of a cell to given concentrations of chemokine allows for the study of how unpolarized cells respond to competing chemical stimuli. As a result of these features, we were able to identify a cytoskeletal memory which provides a directional bias as well as potentially enhancing persistence of a polarized cell. Further study of this phenomenon should focus on understanding the molecular connection between memory and polarization, as well as how the cytoskeletal memory might play a role in the interplay between dynamicity and directional persistence.

4.2.1 Dynamicity and Persistence

In the 1950s, while at Vanderbilt University, David Rogers recorded a video of a neutrophil crawling after a bacterium on a glass slide, on which a sample of whole blood

had been placed. This movie is still shown today to demonstrate a remarkable persistence of morphological polarization, while maintaing the ability to quickly and drastically change directions. Two general features of chemotactic migration are evident from this movie, namely persistence and dynamicity. Persistence can be thought of as the ability of a cell to maintain its direction of polarization despite competing cues. Meanwhile, dynamicity is the ability of the cell to quickly react to sudden changes in the chemical environment, such as the sudden change of direction of a moving bacterium.

As was discussed previously, it is believed that the ability to achieve the striking polarization observed in chemotactic cells is highly dependent on nonlinear signaling elements, such as positive feedback loops and mutual antagonism of the “frontness” and “backness” signaling modules. Many studies have shown that interrupting these nonlinear elements of the pathway affects either the magnitude of the polarization or the ability to maintain a unidirectional polarization. However, much less is known about how the system responds if these elements are instead enhanced. It is also not well-known how sensitive the machinery is to the strength of these nonlinear elements. For example, how would the polarization of a cell be affected if an additional positive feedback loop were introduced to further enhance PIP3 production, or Rac1 activation? It is possible that such an enhancement would result in a polarization of the cell that could not be turned off, or reoriented, causing the cell to continue migrating in the same direction even after a chemical cue has been removed.

Conversely, it is also possible enhancing the leading edge polarization could result in an impaired ability to polarize. Considering the results published by Xu et al. [19] and others, it appears that proper polarization is dependent on the activation of an

antagonistic pathway to properly localize the leading edge protrusions. Interestingly it

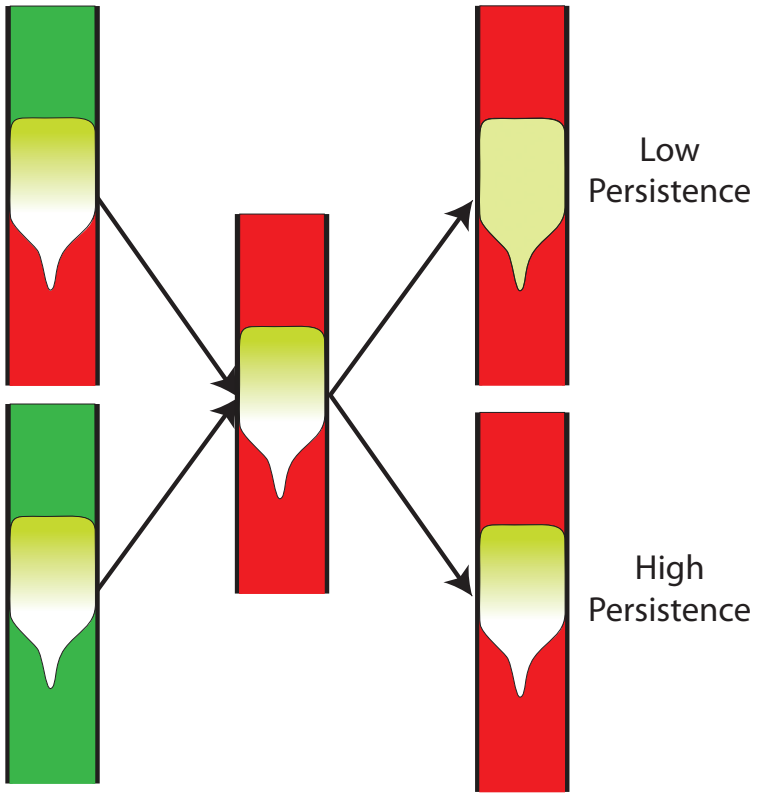

Figure 4-3 | Forced relaxation of polarization. Cells would be allowed to initially polarize in either a uniform concentration or a concentration difference. The chemokine would then be removed and the dynamics of cell polarization can be measured. In a situation where a cell would have a low persistence, this would be observed by the rapid decay of leading edge polarization. Conversely, if a cell was highly persistent, this would be observed by either a failure to depolarize, or by a significantly slower decay of the polarization.

has been shown that chemotactic cells exhibit an ability to buffer activation of the antagonistic “frontness” and “backness” pathways to ensure comparable signaling strength [58]. It is appealing to think that evolution might have selected for a cytoskeletal memory element, like the one that we have observed, as a way to buffer the positive feedback and antagonism elements to maintain a polarization network capable of both directional persistence and dynamicity.

The microfluidic system described in the previous chapter provides a unique opportunity to controllably address both of these phenomena. First, to test the persistence, cells would be allowed to enter into and migrate within microchannels, either under a chemokine concentration difference or uniform concentration. Once the cells have migrated a certain distance, the chemokine could then be washed out and

the amount of time it takes a cell to depolarize can be measured. Presumably an

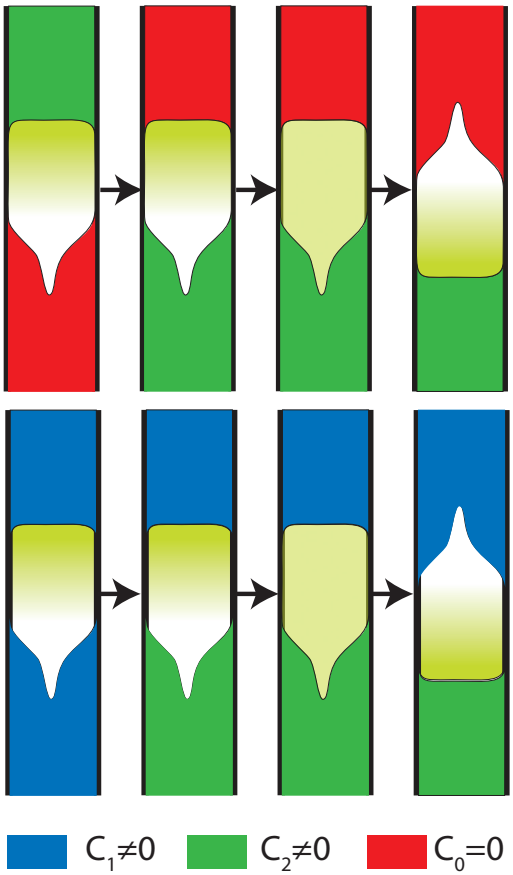

Figure 4-4 | Dynamics of forced reorientation. Cells would be allowed to initially polarize in either a uniform concentration or a concentration difference. After a period of time, the direction of the chemical difference would then be flipped (top row) or the concentration at the back of the cell would be increased, holding the concentration at the front of the cell constant. The dynamics of depolarization and subsequent reorientation of the polarization could be measured. This system would also provide the ability to test the strength of an induced persistence. It is conceivable that for concentration differences of small enough magnitude or for strong enough persistence, a cell would fail to reorient following the addition of an opposing concentration difference.

increase or decrease in persistence would be evidenced by a subsequent increase or decrease in this measured time. Meanwhile, the dynamicity can be assessed through a similar experiment. In this case, however, instead of washing out the chemokine, the cell would either be exposed to a sudden reversal of the chemical concentration difference, or to the sudden addition of a chemical difference on top of a baseline uniform concentration. The amount of time it takes the cell to subsequently flip directions can be measured, provided it even changes directions.

While measuring the persistence and dynamicity is relatively straightforward, controllably and precisely altering either one is quite complicated. Small molecule inhibitors such as the ROCK inhibitor Y27632, blebbistatin and microtubule inhibitors

are appealing for this purpose, as they do not seem to affect the ability of the cell to polarize, but rather seem to prevent the cell from properly localizing a pseudopod and making the back and sides of the cell more sensitive to external chemokine stimulation. However, in addition to the activity, it is also important to understand how the localization of these molecules affect both dynamicity and persistence. To address this, one could utilize one of the inducible dimerization systems described earlier. This approach would allow one to, for example, target a cytoplasmic constitutively active RhoA to the leading edge of a polarized cell. Similarly, one could also target a constitutively active WASp to the leading edge, introducing an additional, artificial positive feedback loop to further promote actin polymerization. In the first case, I would expect that targeting a large amount of constitutively active RhoA would result in cells that could only transiently polarize, if at all. If only a small amount of RhoA is targeted, however, I expect that cells would still be able to establish and maintain polarization but would depolarize significantly faster in response to the removal of a stimulus, as compared to wild-type cells. In contrast, I would expect targeting of molecules such as WASp and other leading edge activators would result in a cell that would exhibit an extremely persistent polarization, and might even fail to depolarize in response to chemokine removal, provided the targeting is strong enough.

Finally, it is important to understand how these phenomena of dynamicity and persistence present themselves in an unconfined environment, where the cell is not limited to one-dimensional motion. To achieve this, one could utilize microfluidic systems which generate stable gradients and allow for controllable, fast switching of the gradient [86]. Alternatively, the use of photocleavable chemokine analogs would allow one to

generate well-controlled stimuli in both space and time. In either case, the amount of time it takes for the cell to respond to the sudden stimulus can be quantified. Although this complex environment does increase the difficulty in interpreting these measurements, comparing the effect of perturbations in an open environment to the corresponding perturbation in a confined microchannel could help to elucidate the detailed processes underlying the ability of cells to navigate complex chemical environments.

There are many points of the chemotactic polarization signaling network that likely play a role in both persistence and dynamicity. Thus, understanding the effect of cytoskeletal memory on both of these phenomena and how it might be able to maintain a balance between the two requires first understanding how the cytoskeletal memory is connected to the network of pathways regulating polarization.

4.2.2 Memory and Polarization

We have identified two cytoskeletal elements which appear to play a role in a long-lived directional memory of a chemotactic cell, namely microtubules and the membrane-actin linker moesin. It has been shown that moesin interacts with microtubules *in vivo* [146] and is able to regulate both the localization and stability of microtubules. However, it is unclear how these two might interact together to provide memory. Although both are necessary for directional memory, it is possible that one functions as a scaffold, regulating the localization of the second, while the second somehow signals to the polarization network. It is also possible that both serve both functions, acting both to localize the other and signal to the polarization.

To address the question of which of the molecules provides a scaffold for the

other, it will be necessary to visualize the localization of each of these elements when

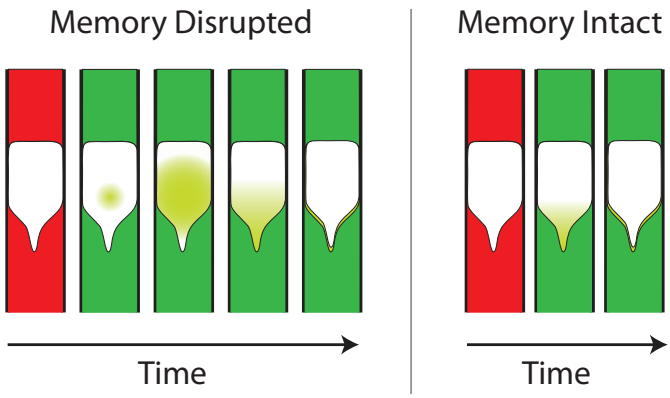

Figure 4-5 | Effect of memory on spatiotemporal dynamics of RhoA activity. Cells would be exposed to forced depolarization-polarization cycle as described in the previous chapter. Upon reintroduction of chemokine (green), the activity of RhoA could be measured. In cells where the memory has been disrupted, one might expect to see RhoA activity occur first in the cytoplasm, later spreading to the sides and rear. Meanwhile, when the memory is unperturbed, one might expect to see RhoA activity reappear first in close proximity to the previous uropod.

the other is inhibited. If one of the molecules is able to remain localized despite inhibition of the second, this would be strong evidence that the first is providing a scaffold. This does not, however, preclude the ability of the first to also signal to the polarization network.

Both microtubules and moesin have been shown to localize to the rear of a polarized chemotactic cell [143, 169]. In addition, both molecules have been shown to play a role in RhoA signaling [147, 170]. Specifically, microtubules are thought to bind a Rho GEF, GEF-H1 [148], and could thus target this GEF to the back of the cell, thereby enhancing RhoA activity. Meanwhile, it has been well demonstrated that moesin activation occurs downstream of RhoA and ROCK signaling. However, it has been reported that ezrin, another member of the ERM family and very similar to moesin, is able to recruit several Rho family GEFs. This recruitment is dependent on the activation of ezrin. Given this evidence, the most likely point of interaction between the cytoskeletal memory and the polarization is through the regulation of RhoA activity. To test such a connection, one could visualize the spatio-temporal dynamics of RhoA activation during the relaxation and activation cycles of the dynamic experiment

described in the previous chapter, both in the absence and presence of microtubule and moesin inhibition. I would expect that without either inhibitor, one would observe preferential activation of RhoA at the membrane in the region of the cell that was previously the uropod. In contrast, when either inhibitor is used, RhoA activation might initially occur only in the cytoplasm, and later localize to one side of the cell or the other, similar to what has been observed when naive cells are exposed to chemokine [45].

4.3 Understanding Cellular Signaling in the Context of Competing Stimuli

In addition to the novel phenomena described, one of the important aspects featured by the body of experiments in this work is the design and use of systems to controllably expose cells to competing signals. Exposing cells to competing stimuli of the same type can provide additional information about how cells are able to interpret their external environment for directional cues, which cannot be obtained by exposing cells to only a single stimulus. Specifically, in the bifurcating microchannels, without presenting the cells with a "choice" of different fluidic resistances, it would not have been possible to identify the ability of piconewton scale forces to bias the direction of cellular migration. In addition, the induced formation of two pseudopods allowed us to identify that cells can resolve the conflict of multiple pseudopods through signaling other than the canonical "frontness" chemotactic pathways. Meanwhile, cells in straight microchannels were exposed to various static chemical environments, in which both front and back were stimulated by equal concentrations of chemokine. Observing the cellular responses to these competing stimuli elucidated an unexpected directional bias, which was later identified as a directional memory stored in polarized cytoskeletal elements.

Exposing cells to competing stimuli of different types can be equally as

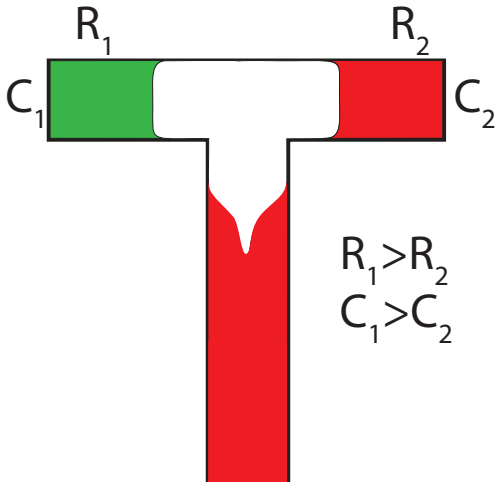

Figure 4-6 | Competing physical and chemical cues. Bifurcating microchannels of asymmetric hydraulic resistances could be fabricated so that each branch of the bifurcation leads to a separate reservoir. The reservoir to which the higher resistance branch connects could be held at one concentration, while the low resistance branch could be held at either no chemokine or a lower concentration of chemokine. Varying both the baseline resistance and resistance difference/ratio as well as the baseline concentration and concentration difference would provide a system to quantitatively asses the competition between physical and chemical cues.

informative as to how cells are able to navigate the complex environments in which they are found. We were able to achieve such a competition in the bifurcating microchannels. Through laser-induced activation of photocleavable chemokine, we were able to demonstrate that hydraulic resistance and chemokine are capable of generating competing directional cues. This suggested a possible mechanism by which cells might avoid getting trapped in areas of extremely dense matrix, and thus ensure efficient trafficking of the cells to loci of chemotactic signaling. Verifying the physiological relevance of this phenomenon will require a further quantitative characterization of the competition between hydraulic and chemical inputs is needed. One approach would be to generate a bifurcating geometry of different hydraulic resistances that lead to separate reservoirs. The higher resistance branch could then be exposed to a certain concentration of chemokine, while the lower resistance branch would not be exposed to chemokine. Varying both the relative resistances and the chemokine concentration used the relative strengths of these two directional inputs could be determined. In addition, this would provide a system to study the molecular events underlying the resolution of

such a competition. Similar systematic quantitative studies of the competition between additional directional signals such as shear stress or substrate stiffness will continue improve our understanding of how cells are able to navigate complex environments. It is appealing to think that an immune cell might incorporate information from all of these directional cues in order to avoid regions of dense tissue, which would likely have an increased stiffness, or to orient adhesive forces in regions of high interstitial flow in order to maintain sufficient adhesion for migration, such that it could reach the site of an infection as efficiently as possible.

References

1. Bardwell, L., *A walk-through of the yeast mating pheromone response pathway.* Peptides, 2004. **25**(9): p. 1465-76.
2. Slaughter, B.D., et al., *Dual modes of cdc42 recycling fine-tune polarized morphogenesis.* Developmental Cell, 2009. **17**(6): p. 823-35.
3. Slaughter, B.D., S.E. Smith, and R. Li, *Symmetry breaking in the life cycle of the budding yeast.* Cold Spring Harbor Perspectives in Biology, 2009. **1** (3): p. a003384.
4. Park, H.-O. and E. Bi, *Central roles of small GTPases in the development of cell polarity in yeast and beyond.* Microbiol Mol Biol Rev, 2007. **71**(1): p. 48-96.
5. Willard, S.S. and P.N. Devreotes, *Signaling pathways mediating chemotaxis in the social amoeba, Dictyostelium discoideum.* European journal of cell biology, 2006. **85**(9-10): p. 897-904.
6. Marín, O., et al., *Guiding neuronal cell migrations.* Cold Spring Harbor Perspectives in Biology, 2010. **2**(2): p. a001834.
7. Seppä, H., et al., *Platelet-derived growth factor in chemotactic for fibroblasts.* The Journal of Cell Biology, 1982. **92**(2): p. 584-8.
8. Condeelis, J., R.H. Singer, and J.E. Segall, *The great escape: when cancer cells hijack the genes for chemotaxis and motility.* Annu Rev Cell Dev Biol, 2005. **21**: p. 695-718.
9. Liu, X., et al., *Bidirectional regulation of neutrophil migration by mitogen-activated protein kinases.* Nat Immunol, 2012. **13**(5): p. 457-64.
10. McCann, C.P., et al., *Cell speed, persistence and information transmission during signal relay and collective migration.* J Cell Sci, 2010. **123**(Pt 10): p. 1724-31.
11. Rappel, W.-J. and W.F. Loomis, *Eukaryotic chemotaxis.* Wiley Interdiscip Rev Syst Biol Med, 2009. **1**(1): p. 141-9.
12. Parent, C.A. and P.N. Devreotes, *Molecular genetics of signal transduction in Dictyostelium.* Annu Rev Biochem, 1996. **65**: p. 411-40.
13. Zhang, N., Y. Long, and P.N. Devreotes, *Ggamma in dictyostelium: its role in localization of gbetagamma to the membrane is required for chemotaxis in shallow gradients.* Mol Biol Cell, 2001. **12**(10): p. 3204-13.
14. Lilly, P., et al., *A G-protein beta-subunit is essential for Dictyostelium development.* Genes Dev, 1993. **7**(6): p. 986-95.
15. Brzostowski, J.A., C. Johnson, and A.R. Kimmel, *Galpha-mediated inhibition of developmental signal response.* Curr Biol, 2002. **12**(14): p. 1199-208.
16. Neptune, E. and H. Bourne, *Receptors induce chemotaxis by releasing the betagamma subunit of Gi, not by activating Gq or Gs.* Proc Natl Acad Sci USA, 1997. **94**(26): p. 14489-14494.
17. Goldman, D.W., et al., *Pertussis toxin inhibition of chemotactic factor-induced calcium mobilization and function in human polymorphonuclear leukocytes.* J Exp Med, 1985. **162**(1): p. 145-56.

18. Servant, G., et al., *Dynamics of a chemoattractant receptor in living neutrophils during chemotaxis.* Mol Biol Cell, 1999. **10**(4): p. 1163-78.
19. Xu, J., et al., *Divergent signals and cytoskeletal assemblies regulate self-organizing polarity in neutrophils.* Cell, 2003. **114**(2): p. 201-14.
20. Parent, C.A. and P.N. Devreotes, *A cell's sense of direction.* Science, 1999. **284**(5415): p. 765-70.
21. Servant, G., et al., *Polarization of chemoattractant receptor signaling during neutrophil chemotaxis.* Science, 2000. **287**(5455): p. 1037-40.
22. Ferguson, K.M., et al., *Structural basis for discrimination of 3-phosphoinositides by pleckstrin homology domains.* Mol Cell, 2000. **6**(2): p. 373-84.
23. Lemmon, M.A. and K.M. Ferguson, *Signal-dependent membrane targeting by pleckstrin homology (PH) domains.* Biochem J, 2000. **350 Pt 1**: p. 1-18.
24. Bourne, H.R. and O. Weiner, *A chemical compass.* Nature, 2002. **419** (6902): p. 21.
25. Wang, F., et al., *Lipid products of PI(3)Ks maintain persistent cell polarity and directed motility in neutrophils.* Nat Cell Biol, 2002. **4**(7): p. 513-8.
26. Rickert, P., et al., *Leukocytes navigate by compass: roles of PI3Kgamma and its lipid products.* Trends in Cell Biology, 2000. **10**(11): p. 466-73.
27. Brock, C., et al., *Roles of G beta gamma in membrane recruitment and activation of p110 gamma/p101 phosphoinositide 3-kinase gamma.* The Journal of Cell Biology, 2003. **160**(1): p. 89-99.
28. Vadas, O., et al., *Molecular determinants of PI3Kγ-mediated activation downstream of G-protein-coupled receptors (GPCRs).* Proc Natl Acad Sci USA, 2013. **110**(47): p. 18862-7.
29. Sasaki, A.T. and R.A. Firtel, *Regulation of chemotaxis by the orchestrated activation of Ras, PI3K, and TOR.* European journal of cell biology, 2006. **85**(9-10): p. 873-95.
30. Sasaki, A.T., et al., *Localized Ras signaling at the leading edge regulates PI3K, cell polarity, and directional cell movement.* The Journal of Cell Biology, 2004. **167**(3): p. 505-18.
31. Chen, L., et al., *PLA2 and PI3K/PTEN pathways act in parallel to mediate chemotaxis.* Developmental Cell, 2007. **12**(4): p. 603-14.
32. van Haastert, P.J.M., I. Keizer-Gunnink, and A. Kortholt, *Essential role of PI3-kinase and phospholipase A2 in Dictyostelium discoideum chemotaxis.* The Journal of Cell Biology, 2007. **177**(5): p. 809-16.
33. Srinivasan, S., et al., *Rac and Cdc42 play distinct roles in regulating PI (3,4,5)P3 and polarity during neutrophil chemotaxis.* The Journal of Cell Biology, 2003. **160**(3): p. 375-85.
34. Li, Z., et al., *Directional sensing requires G beta gamma-mediated PAK1 and PIX alpha-dependent activation of Cdc42.* Cell, 2003. **114**(2): p. 215-27.
35. Kunisaki, Y., et al., *DOCK2 is a Rac activator that regulates motility and polarity during neutrophil chemotaxis.* The Journal of Cell Biology, 2006. **174**(5): p. 647-52.

36. Zhelev, D.V. and A. Alteraifi, *Signaling in the motility responses of the human neutrophil.* Annals of biomedical engineering, 2002. **30**(3): p. 356-70.
37. Wilson, K., et al., *Mechanisms of leading edge protrusion in interstitial migration.* Nat Commun, 2013. **4**: p. 2896.
38. Weiner, O.D., et al., *A PtdInsP(3)- and Rho GTPase-mediated positive feedback loop regulates neutrophil polarity.* Nat Cell Biol, 2002. **4**(7): p. 509-13.
39. Castro-Castro, A., et al., *Coronin 1A promotes a cytoskeletal-based feedback loop that facilitates Rac1 translocation and activation.* EMBO J, 2011. **30**(19): p. 3913-27.
40. Zondag, G.C., et al., *Oncogenic Ras downregulates Rac activity, which leads to increased Rho activity and epithelial-mesenchymal transition.* The Journal of Cell Biology, 2000. **149**(4): p. 775-82.
41. Sander, E.E., et al., *Rac downregulates Rho activity: reciprocal balance between both GTPases determines cellular morphology and migratory behavior.* The Journal of Cell Biology, 1999. **147**(5): p. 1009-22.
42. Orchard, R.C., et al., *Identification of F-actin as the dynamic hub in a microbial-induced GTPase polarity circuit.* Cell, 2012. **148**(4): p. 803-15.
43. Hildebrandt, J.D., et al., *Characterization by two-dimensional peptide mapping of the gamma subunits of Ns and Ni, the regulatory proteins of adenylyl cyclase, and of transducin, the guanine nucleotide-binding protein of rod outer segments of the eye.* J Biol Chem, 1985. **260**(27): p. 14867-72.
44. Hildebrandt, J.D., et al., *The membrane-bound spermatozoal adenylyl cyclase system does not share coupling characteristics with somatic cell adenylyl cyclases.* Endocrinology, 1985. **116**(4): p. 1357-66.
45. Wong, K., et al., *Neutrophil polarization: spatiotemporal dynamics of RhoA activity support a self-organizing mechanism.* Proc Natl Acad Sci USA, 2006. **103**(10): p. 3639-44.
46. Li, Z., et al., *Regulation of PTEN by Rho small GTPases.* Nat Cell Biol, 2005. **7**(4): p. 399-404.
47. Funamoto, S., et al., *Spatial and temporal regulation of 3-phosphoinositides by PI 3-kinase and PTEN mediates chemotaxis.* Cell, 2002. **109**(5): p. 611-23.
48. Iijima, M. and P. Devreotes, *Tumor suppressor PTEN mediates sensing of chemoattractant gradients.* Cell, 2002. **109**(5): p. 599-610.
49. Riento, K. and A.J. Ridley, *Rocks: multifunctional kinases in cell behaviour.* Nat Rev Mol Cell Bio, 2003. **4**(6): p. 446-56.
50. Laevsky, G. and D.A. Knecht, *Cross-linking of actin filaments by myosin II is a major contributor to cortical integrity and cell motility in restrictive environments.* J Cell Sci, 2003. **116**(Pt 18): p. 3761-70.
51. Iijima, M., et al., *Novel mechanism of PTEN regulation by its phosphatidylinositol 4,5-bisphosphate binding motif is critical for chemotaxis.* J Biol Chem, 2004. **279**(16): p. 16606-13.

52. Van Keymeulen, A., et al., *To stabilize neutrophil polarity, PIP3 and Cdc42 augment RhoA activity at the back as well as signals at the front.* The Journal of Cell Biology, 2006. **174**(3): p. 437-45.
53. Sanz-Moreno, V., et al., *Rac activation and inactivation control plasticity of tumor cell movement.* Cell, 2008. **135**(3): p. 510-23.
54. Krugmann, S., et al., *ARAP3 is a PI3K- and rap-regulated GAP for RhoA.* Curr Biol, 2004. **14**(15): p. 1380-4.
55. Krugmann, S., et al., *Identification of ARAP3, a novel PI3K effector regulating both Arf and Rho GTPases, by selective capture on phosphoinositide affinity matrices.* Mol Cell, 2002. **9**(1): p. 95-108.
56. Gómez-Móuton, C., et al., *Segregation of leading-edge and uropod components into specific lipid rafts during T cell polarization.* Proc Natl Acad Sci USA, 2001. **98**(17): p. 9642-7.
57. Filic, V., et al., *A dual role for Rac1 GTPases in the regulation of cell motility.* J Cell Sci, 2012. **125**(Pt 2): p. 387-98.
58. Wang, Y., et al., *Identifying network motifs that buffer front-to-back signaling in polarized neutrophils.* Cell Rep, 2013. **3**(5): p. 1607-16.
59. Ku, C.-J., et al., *Network crosstalk dynamically changes during neutrophil polarization.* Cell, 2012. **149**(5): p. 1073-83.
60. Houk, A.R., et al., *Membrane tension maintains cell polarity by confining signals to the leading edge during neutrophil migration.* Cell, 2012. **148** (1-2): p. 175-88.
61. Iglesias, P.A. and P.N. Devreotes, *Navigating through models of chemotaxis.* Curr Opin Cell Biol, 2008. **20**(1): p. 35-40.
62. Jilkine, A. and L. Edelstein-Keshet, *A comparison of mathematical models for polarization of single eukaryotic cells in response to guided cues.* PLoS Comput Biol, 2011. **7**(4): p. e1001121.
63. Zigmond, S.H., *Ability of polymorphonuclear leukocytes to orient in gradients of chemotactic factors.* The Journal of Cell Biology, 1977. **75**(2 Pt 1): p. 606-16.
64. Levchenko, A. and P.A. Iglesias, *Models of eukaryotic gradient sensing: application to chemotaxis of amoebae and neutrophils.* Biophysical Journal, 2002. **82**(1 Pt 1): p. 50-63.
65. Ma, L., et al., *Two complementary, local excitation, global inhibition mechanisms acting in parallel can explain the chemoattractant-induced regulation of PI(3,4,5)P3 response in dictyostelium cells.* Biophysical Journal, 2004. **87**(6): p. 3764-74.
66. Xiong, Y., et al., *Cells navigate with a local-excitation, global-inhibition-biased excitable network.* Proc Natl Acad Sci USA, 2010. **107**(40): p. 17079-86.
67. Millius, A., et al., *Neutrophils establish rapid and robust WAVE complex polarity in an actin-dependent fashion.* Curr Biol, 2009. **19**(3): p. 253-9.
68. Weiner, O.D., et al., *An actin-based wave generator organizes cell motility.* PLoS Biol, 2007. **5**(9): p. e221.

69. Weiner, O.D., et al., *Hem-1 complexes are essential for Rac activation, actin polymerization, and myosin regulation during neutrophil chemotaxis.* PLoS Biol, 2006. **4**(2): p. e38.
70. Levine, H., D.A. Kessler, and W.-J. Rappel, *Directional sensing in eukaryotic chemotaxis: a balanced inactivation model.* Proc Natl Acad Sci USA, 2006. **103**(26): p. 9761-6.
71. Narang, A., *Spontaneous polarization in eukaryotic gradient sensing: a mathematical model based on mutual inhibition of frontness and backness pathways.* J Theor Biol, 2006. **240**(4): p. 538-53.
72. Berzat, A. and A. Hall, *Cellular responses to extracellular guidance cues.* EMBO J, 2010. **29**(16): p. 2734-45.
73. Onsum, M. and C.V. Rao, *A mathematical model for neutrophil gradient sensing and polarization.* PLoS Comput Biol, 2007. **3**(3): p. e36.
74. Wu, J., X. Wu, and F. Lin, *Recent developments in microfluidics-based chemotaxis studies.* Lab Chip, 2013. **13**(13): p. 2484-99.
75. Irimia, D., *Microfluidic technologies for temporal perturbations of chemotaxis.* Annual review of biomedical engineering, 2010. **12**: p. 259-84.
76. Irimia, D., D.A. Geba, and M. Toner, *Universal microfluidic gradient generator.* Anal Chem, 2006. **78**(10): p. 3472-7.
77. Li Jeon, N., et al., *Neutrophil chemotaxis in linear and complex gradients of interleukin-8 formed in a microfabricated device.* Nat Biotech, 2002. **20** (8): p. 826-830.
78. Jeon, N., et al., *Generation of solution and surface gradients using microfluidic systems.* Langmuir, 2000. **16**(22): p. 8311-8316.
79. Dertinger, S., et al., *Generation of gradients having complex shapes using microfluidic networks.* Anal. Chem, 2001.
80. Herzmark, P., et al., *Bound attractant at the leading vs. the trailing edge determines chemotactic prowess.* Proc Natl Acad Sci USA, 2007. **104**(33): p. 13349-54.
81. Ambravaneswaran, V., et al., *Directional decisions during neutrophil chemotaxis inside bifurcating channels.* Integrative biology : quantitative biosciences from nano to macro, 2010. **2**(11-12): p. 639-47.
82. Irimia, D., et al., *Polar stimulation and constrained cell migration in microfluidic channels.* Lab Chip, 2007. **7**(12): p. 1783-90.
83. Lautenschläger, F. and M. Piel, *Microfabricated devices for cell biology: all for one and one for all.* Curr Opin Cell Biol, 2013. **25**(1): p. 116-24.
84. Haessler, U., et al., *An agarose-based microfluidic platform with a gradient buffer for 3D chemotaxis studies.* Biomed Microdevices, 2009. **11**(4): p. 827-35.
85. Irimia, D. and M. Toner, *Cell handling using microstructured membranes.* Lab Chip, 2006. **6**(3): p. 345-52.
86. Irimia, D., et al., *Microfluidic system for measuring neutrophil migratory responses to fast switches of chemical gradients.* Lab Chip, 2006. **6**(2): p. 191-8.

87. Hamza, B., et al., *Retrotaxis of human neutrophils during mechanical confinement inside microfluidic channels.* Integrative biology : quantitative biosciences from nano to macro, 2014. **6**(2): p. 175-83.
88. Butler, K.L., et al., *Burn injury reduces neutrophil directional migration speed in microfluidic devices.* PLoS ONE, 2010. **5**(7): p. e11921.
89. Samadani, A., J. Mettetal, and A. van Oudenaarden, *Cellular asymmetry and individuality in directional sensing.* Proc Natl Acad Sci USA, 2006. **103** (31): p. 11549-54.
90. Pirrung, M.C., et al., *Caged chemotactic peptides.* Bioconjug Chem, 2000. **11**(5): p. 679-81.
91. Kress, H., et al., *Cell stimulation with optically manipulated microsources.* Nat Methods, 2009. **6**(12): p. 905-9.
92. Karunarathne, W.K.A., et al., *Optical control demonstrates switch-like PIP3 dynamics underlying the initiation of immune cell migration.* Proc Natl Acad Sci USA, 2013. **110**(17): p. E1575-83.
93. Wu, Y.I., et al., *A genetically encoded photoactivatable Rac controls the motility of living cells.* Nature, 2009. **461**(7260): p. 104-8.
94. Levskaya, A., et al., *Spatiotemporal control of cell signalling using a light-switchable protein interaction.* Nature, 2009.
95. Toettcher, J., et al., *Light-based feedback for controlling intracellular signaling dynamics.* Nat Methods, 2011.
96. Inoue, T., et al., *An inducible translocation strategy to rapidly activate and inhibit small GTPase signaling pathways.* Nat Methods, 2005. **2**(6): p. 415-8.
97. Bayle, J.H., et al., *Rapamycin analogs with differential binding specificity permit orthogonal control of protein activity.* Chem Biol, 2006. **13**(1): p. 99-107.
98. Umeda, N., et al., *A photocleavable rapamycin conjugate for spatiotemporal control of small GTPase activity.* J Am Chem Soc, 2011. **133**(1): p. 12-4.
99. Tse, J.R. and A.J. Engler, *Stiffness gradients mimicking in vivo tissue variation regulate mesenchymal stem cell fate.* PLoS ONE, 2011. **6**(1): p. e15978.
100. Engler, A.J., et al., *Matrix elasticity directs stem cell lineage specification.* Cell, 2006. **126**(4): p. 677-89.
101. Kitagawa, Y., et al., *Effect of mechanical deformation on structure and function of polymorphonuclear leukocytes.* J Appl Physiol, 1997. **82**(5): p. 1397-405.
102. Lo, C.M., et al., *Cell movement is guided by the rigidity of the substrate.* Biophysical Journal, 2000. **79**(1): p. 144-52.
103. Isenberg, B.C., et al., *Vascular smooth muscle cell durotaxis depends on substrate stiffness gradient strength.* Biophysical Journal, 2009. **97**(5): p. 1313-22.
104. Raab, M., et al., *Crawling from soft to stiff matrix polarizes the cytoskeleton and phosphoregulates myosin-II heavy chain.* The Journal of Cell Biology, 2012. **199**(4): p. 669-83.

105. Jiang, G., et al., *Rigidity sensing at the leading edge through alphavbeta3 integrins and RPTPalpha.* Biophysical Journal, 2006. **90**(5): p. 1804-9.
106. Décave, E., et al., *Shear flow-induced motility of Dictyostelium discoideum cells on solid substrate.* J Cell Sci, 2003. **116**(Pt 21): p. 4331-43.
107. Dalous, J., et al., *Reversal of cell polarity and actin-myosin cytoskeleton reorganization under mechanical and chemical stimulation.* Biophysical Journal, 2008. **94**(3): p. 1063-74.
108. Polacheck, W.J., et al., *Mechanotransduction of fluid stresses governs 3D cell migration.* Proc Natl Acad Sci USA, 2014. **111**(7): p. 2447-52.
109. Chen, C.S., *Mechanotransduction - a field pulling together?* J Cell Sci, 2008. **121**(Pt 20): p. 3285-92.
110. Choquet, D., D.P. Felsenfeld, and M.P. Sheetz, *Extracellular matrix rigidity causes strengthening of integrin-cytoskeleton linkages.* Cell, 1997. **88**(1): p. 39-48.
111. Stefanoni, F., et al., *A numerical model for durotaxis.* J Theor Biol, 2011. **280**(1): p. 150-8.
112. Krzyszczyk, P. and C.W. Wolgemuth, *Mechanosensing can result from adhesion molecule dynamics.* Biophysical Journal, 2011. **101**(10): p. L53-5.
113. Bruinsma, R., *Theory of force regulation by nascent adhesion sites.* Biophysical Journal, 2005. **89**(1): p. 87-94.
114. Lara Rodriguez, L. and I.C. Schneider, *Directed cell migration in multi-cue environments.* Integr Biol (Camb), 2013. **5**(11): p. 1306-23.
115. Jannat, R.A., et al., *Neutrophil adhesion and chemotaxis depend on substrate mechanics.* J Phys Condens Matter, 2010. **22**(19): p. 194117.
116. Kidoaki, S. and H. Sakashita, *Rectified cell migration on saw-like micro-elastically patterned hydrogels with asymmetric gradient ratchet teeth.* PLoS ONE, 2013. **8**(10): p. e78067.
117. Wong, S., et al., *Preparation of a micropatterned rigid-soft composite substrate for probing cellular rigidity sensing.* Methods Cell Biol, 2014. **121**: p. 3-15.
118. Le Berre, M., et al., *Geometric friction directs cell migration.* Phys Rev Lett, 2013. **111**(19): p. 198101.
119. Swaney, K.F., C.-H. Huang, and P.N. Devreotes, *Eukaryotic chemotaxis: a network of signaling pathways controls motility, directional sensing, and polarity.* Annu Rev Biophys, 2010. **39**: p. 265-89.
120. Insall, R.H., *Understanding eukaryotic chemotaxis: a pseudopod-centred view.* Nat Rev Mol Cell Bio, 2010.
121. Parent, C.A., *Making all the right moves: chemotaxis in neutrophils and Dictyostelium.* Current Opinion in Cell Biology, 2004. **16**(1): p. 4-13.
122. Fuller, D., et al., *External and internal constraints on eukaryotic chemotaxis.* Proc Natl Acad Sci USA, 2010.
123. Kay, R.R., et al., *Changing directions in the study of chemotaxis.* Nat Rev Mol Cell Bio, 2008. **9**(6): p. 455-63.

124. Nicolas, A., B. Geiger, and S.A. Safran, *Cell mechanosensitivity controls the anisotropy of focal adhesions.* Proc Natl Acad Sci USA, 2004. **101**(34): p. 12520-5.
125. Harland, B., S. Walcott, and S.X. Sun, *Adhesion dynamics and durotaxis in migrating cells.* Phys Biol, 2011. **8**(1): p. 015011.
126. Shah, J.V., et al., *Dynamics of centromere and kinetochore proteins; implications for checkpoint signaling and silencing.* Curr Biol, 2004. **14**(11): p. 942-52.
127. Lämmermann, T., et al., *Rapid leukocyte migration by integrin-independent flowing and squeezing.* Nature, 2008. **453**(7191): p. 51-5.
128. Scherber, C., et al., *Epithelial cell guidance by self-generated EGF gradients.* Integrative biology : quantitative biosciences from nano to macro, 2012. **4**(3): p. 259-69.
129. Breitman, T.R., S.E. Selonick, and S.J. Collins, *Induction of differentiation of the human promyelocytic leukemia cell line (HL-60) by retinoic acid.* Proc Natl Acad Sci USA, 1980. **77**(5): p. 2936-40.
130. Hauert, A.B., et al., *Differentiated HL-60 cells are a valid model system for the analysis of human neutrophil migration and chemotaxis.* The International Journal of Biochemistry & Cell Biology, 2002. **34**(7): p. 838-54.
131. Hebert, B., S. Costantino, and P.W. Wiseman, *Spatiotemporal image correlation spectroscopy (STICS) theory, verification, and application to protein velocity mapping in living CHO cells.* Biophysical Journal, 2005. **88** (5): p. 3601-14.
132. Fuerstman, M.J., et al., *The pressure drop along rectangular microchannels containing bubbles.* Lab Chip, 2007. **7**(11): p. 1479-89.
133. Zhang, S., P.G. Charest, and R.A. Firtel, *Spatiotemporal regulation of Ras activity provides directional sensing.* Curr Biol, 2008. **18**(20): p. 1587-93.
134. Morgenstern, J.P. and H. Land, *Advanced mammalian gene transfer: high titre retroviral vectors with multiple drug selection markers and a complementary helper-free packaging cell line.* Nucleic Acids Res, 1990. **18**(12): p. 3587-96.
135. Chung, S.H. and R.A. Kennedy, *Forward-backward non-linear filtering technique for extracting small biological signals from noise.* J Neurosci Methods, 1991. **40**(1): p. 71-86.
136. Zigmond, S.H. and S.J. Sullivan, *Sensory adaptation of leukocytes to chemotactic peptides.* The Journal of Cell Biology, 1979. **82**(2): p. 517-27.
137. Zigmond, S.H., *Mechanisms of sensing chemical gradients by polymorphonuclear leukocytes.* Nature, 1974. **249**(456): p. 450-2.
138. Zigmond, S.H. and J.G. Hirsch, *Leukocyte locomotion and chemotaxis. New methods for evaluation, and demonstration of a cell-derived chemotactic factor.* J Exp Med, 1973. **137**(2): p. 387-410.
139. Gardiner, E.M., et al., *Spatial and temporal analysis of Rac activation during live neutrophil chemotaxis.* Curr Biol, 2002. **12**(23): p. 2029-34.
140. Zicha, D., G. Dunn, and A. Brown, *A new direct-viewing chemotaxis chamber.* J Cell Sci, 1991. **99 (Pt 4)**: p. 769-75.

141. Lin, F., et al., *Generation of dynamic temporal and spatial concentration gradients using microfluidic devices.* Lab Chip, 2004. **4**(3): p. 164-7.
142. Le Berre, M., et al., *Methods for two-dimensional cell confinement.* Methods Cell Biol, 2014. **121**: p. 213-29.
143. Eddy, R.J., L.M. Pierini, and F.R. Maxfield, *Microtubule asymmetry during neutrophil polarization and migration.* Mol Biol Cell, 2002. **13**(12): p. 4470-83.
144. Fritzsche, M., R. Thorogate, and G. Charras, *Quantitative analysis of ezrin turnover dynamics in the actin cortex.* Biophysical Journal, 2014. **106**(2): p. 343-53.
145. Herzmark, P., et al., *Bound attractant at the leading vs. the trailing edge determines chemotactic prowess.* Proceedings of the National Academy of Sciences of the United States of America, 2007. **104**(33): p. 13349-54.
146. Solinet, S., et al., *The actin-binding ERM protein Moesin binds to and stabilizes microtubules at the cell cortex.* The Journal of Cell Biology, 2013. **202**(2): p. 251-60.
147. Prag, S., et al., *Activated ezrin promotes cell migration through recruitment of the GEF Dbl to lipid rafts and preferential downstream activation of Cdc42.* Mol Biol Cell, 2007. **18**(8): p. 2935-48.
148. Krendel, M., F.T. Zenke, and G.M. Bokoch, *Nucleotide exchange factor GEF-H1 mediates cross-talk between microtubules and the actin cytoskeleton.* Nat Cell Biol, 2002. **4**(4): p. 294-301.
149. Takesono, A., et al., *Microtubules regulate migratory polarity through Rho/ROCK signaling in T cells.* PLoS ONE, 2010. **5**(1): p. e8774.
150. Jannat, R.A., M. Dembo, and D.A. Hammer, *Traction forces of neutrophils migrating on compliant substrates.* Biophysical Journal, 2011. **101**(3): p. 575-84.
151. Burton, K., J.H. Park, and D.L. Taylor, *Keratocytes generate traction forces in two phases.* Mol Biol Cell, 1999. **10**(11): p. 3745-69.
152. Lee, J., et al., *Traction forces generated by locomoting keratocytes.* The Journal of Cell Biology, 1994. **127**(6 Pt 2): p. 1957-64.
153. Usami, S., et al., *Locomotion forces generated by a polymorphonuclear leukocyte.* Biophysical Journal, 1992. **63**(6): p. 1663-6.
154. Footer, M.J., et al., *Direct measurement of force generation by actin filament polymerization using an optical trap.* Proc Natl Acad Sci USA, 2007. **104**(7): p. 2181-6.
155. VanBuren, P., et al., *Smooth muscle myosin: a high force-generating molecular motor.* Biophysical Journal, 1995. **68**(4 Suppl): p. 256S-258S; 258S-259S.
156. Parekh, S.H., et al., *Loading history determines the velocity of actin-network growth.* Nat Cell Biol, 2005. **7**(12): p. 1219-23.
157. Galbraith, C.G. and M.P. Sheetz, *A micromachined device provides a new bend on fibroblast traction forces.* Proc Natl Acad Sci USA, 1997. **94**(17): p. 9114-8.

158. Bendix, P.M., et al., *A quantitative analysis of contractility in active cytoskeletal protein networks.* Biophysical Journal, 2008. **94**(8): p. 3126-36.
159. Hawkins, R., et al., *Pushing off the walls: a mechanism of cell motility in confinement.* Phys Rev Lett, 2009. **102**(5): p. 058103.
160. Csucs, G., et al., *Microcontact printing of novel co-polymers in combination with proteins for cell-biological applications.* Biomaterials, 2003. **24**(10): p. 1713-20.
161. Sui, G., et al., *Solution-phase surface modification in intact poly (dimethylsiloxane) microfluidic channels.* Anal Chem, 2006. **78**(15): p. 5543-51.
162. Buckley, C.D., et al., *Cell adhesion: more than just glue (review).* Mol Membr Biol, 1998. **15**(4): p. 167-76.
163. Rainger, G.E., et al., *Cross-talk between cell adhesion molecules regulates the migration velocity of neutrophils.* Curr Biol, 1997. **7**(5): p. 316-25.
164. de Kreuk, B.-J. and P.L. Hordijk, *Control of Rho GTPase function by BAR-domains.* Small GTPases, 2012. **3**(1): p. 45-52.
165. Watanabe, T., J. Noritake, and K. Kaibuchi, *Regulation of microtubules in cell migration.* Trends in Cell Biology, 2005. **15**(2): p. 76-83.
166. Niggli, V., *Microtubule-disruption-induced and chemotactic-peptide-induced migration of human neutrophils: implications for differential sets of signalling pathways.* J Cell Sci, 2003. **116**(Pt 5): p. 813-822.
167. Wittmann, T. and C.M. Waterman-Storer, *Cell motility: can Rho GTPases and microtubules point the way?* J Cell Sci, 2001. **114**(Pt 21): p. 3795-803.
168. Jensen, M.B., et al., *Membrane curvature sensing by amphipathic helices: a single liposome study using α-synuclein and annexin B12.* J Biol Chem, 2011. **286**(49): p. 42603-14.
169. Rossy, J., et al., *Ezrin/moesin in motile Walker 256 carcinosarcoma cells: signal-dependent relocalization and role in migration.* Experimental Cell Research, 2007. **313**(6): p. 1106-20.
170. D'Angelo, R., et al., *Interaction of ezrin with the novel guanine nucleotide exchange factor PLEKHG6 promotes RhoG-dependent apical cytoskeleton rearrangements in epithelial cells.* Mol Biol Cell, 2007. **18** (12): p. 4780-93.
171. Stephens, L., L. Milne, and P. Hawkins, *Moving towards a better understanding of chemotaxis.* Curr Biol, 2008. **18**(11): p. R485-94.